The Role of the IKKα Kinase in Atherosclerosis

Von der Fakultät für Mathematik, Informatik und Naturwissenschaften der RWTH Aachen University zur Erlangung des akademischen Grades einer Doktorin der Naturwissenschaften genehmigte Dissertation

vorgelegt von

Dipl.-Biol. Pathricia Veronica Tilstam

Aus Brännkyrka (Stockholm), Schweden

Berichter: Universitätsprofessor Dr.rer.nat. Jürgen Bernhagen

Universitätsprofessorin Dr.phil.nat. Gabriele Pradel

Tag der mündlichen Prüfung: 03.02.2015

Diese Dissertation ist auf den Internetseiten der Hochschulbibliothek online verfügbar.

THE RESULTS OF THIS WORK HAVE BEEN PARTLY PUBLISHED IN:

Tilstam PV, Gijbels MJ, Cudejko C, Asare Y, Theelen W, Zhou B, Döring Y, Drechsler M, Pawig L, Simsekyilmaz S, Koenen RR, de Winther MP, Lawrence T, Bernhagen J, Zernecke A, Weber C, Noels H. *Bone marrow-specific knock-in of a non-activatable Ikkα kinase mutant influences haematopoiesis but not atherosclerosis in Apoe-deficient mice.* PlosOne, 2014 Feb 3;9(2):e87452. doi: 10.1371/journal.pone.0087452. eCollection 2014

Dedicated To

Annette & Ulf Tilstam

Content

Content

Content

Abbreviations

Ago	Argonaute
Ala	Alanine
Ap-1	Activator protein 1
Apoe	Apolipoprotein E
APC	Allophycocyanin
APC-Cy7	Allophycocyanin-cyanine 7
BAFF	B-cell activating factor
BAFFR	BAFF receptor
BCA	Brachiocephalic artery
BM	Bone marrow
B$_{regs}$	Regulatory B-cells
BSA	Bovine serum albumin
CBA	Cytometric bead assay
CC	Coiled-coil domains
CCL	CC chemokine ligand
CD	Cluster of differentiation
cDC	Conventional dendritic cell
cDNA	Complementary DNA
CD40L	Cd40 ligand
Chuk	Conserved helix-loop-helix ubiquitous kinase
cIAP	Calf intestinal alkaline phosphatase
CLP	Common lymphoid progenitor cell
CMP	Common myeloid progenitor cell
CVD	Cardiovascular disease
CytD	Cytochalasin D
CXCR7	Chemokine (C-X-C motif) receptor 7
CXCL19	Chemokine (C-X-C motif) ligand 19
Cy3	Cyanine 3

Abbreviations

DAPI	4',6-diamindino-2-phenylindole
DC	Dendritic cell
DiL	1,10-dioctadecyl-3,3,3030-tetramethylindocyanide percholorate
DMSO	Dimethyl sulfoxide
DNA	Deoxyribonucleic acid
EC	Endothelial cell
ECA	External carotid artery
EDTA	Ethylenediaminetetraacetic acid
EEL	External elastica lamina
ELISA	Enzyme-linked immunosorbent assay
eNOS	Endothelial NO synthase
EVG	Elastic van Gieson
FACS	Fluorescence-activated cell sorting
FADD	Fas-associated protein with death domain
FITC	Fluorescein isothiocyanate
FSC	Forward scatter
FMO	Fluorescence minus one
Gapdh	Glyceraldehyde 3-phosphate dehydrogenase
G-CSF	Granulocyte colony-stimulating factor
GPCR	G protein-coupled receptor
GM-CSF	Granulocyte monocyte colony-stimulating factor
gMFI	Geometric mean fluorescence intensity
Gr-1	Granulocyte antigen 1
h	Hour
H3	Histone 3
HAoEC	Human aortic endothelial cell
HBSS	Hank's balanced solution
HDL	High density lipoprotein
HFD	High-fat diet

HPC	Haematopoietic progenitor cell
Hprt	Hypoxanthine-guanine phosphoribosyltransferase
HRP	Horseradish peroxidase
HSC	Haematopoietic stem cell
Hz	Hertz
ICA	Internal carotid artery
ICAM-1	Intracellular adhesion molecule
IEL	Inner elastic lamina
IFN-γ	Interferon γ
IgG	Immunoglobulin G
IL-1/2/4/6/8/12/17	Interleukin-1/2/4/6/8/12/17
IκBα	Inhibitor of kappa B - α
IKKα/IKKβ	IκB kinase-α/ IκB kinase-β
IRF 3/7	Interferon regulatory factor 3/7
KD	Kinase domain
kDa	Kilo-dalton
Klf-2	Krüppel-like factor 2
LCA	Left carotid artery
LCM	L929 conditioned medium
LDL	Low density lipoprotein
LN	Lymph nodes
LPS	Lipopolysaccharide
LT-β	Lymphotoxin-β
LZ	Leucine zipper domain
Mac2	Macrophage galactose-specific lectin-2 (Galectin-3)
MCP-1/CCL2	Monocyte chemoattractant protein-1
min	Minute
miR	MicroRNA
MMP-3/9/13	Matrix metalloproteinase-3/9/13

Abbreviations

MOD	Minimal oligomerization domain
mRNA	Messenger RNA
NBD	NEMO-binding domain
ND	No dietary condition
NEMO	NF-κB essential modulator
NET	Neutrophil extracellular traps
NF-κB	Nuclear factor kappa B
Nik	NF-κB inducing kinase
NK	Natural killer
nm	nanometer
NO	Nitric oxide
Nrf2	NF-E2-related factor 2
OA	Occipital artery
oxLDL	oxidized LDL
PACT	Protein activator of PKR
PBS	Phosphate buffered saline
PCR	Polymerase chain reaction
pDC	Plasmacytoid dendritic cell
PE	Phycoerythrin
PE-Cy7	Phycoerythrin-cyanine 7
PFA	Paraformaldehyde
P-IKKα	Phosphorylated (activated) IKKα
pri-miR	Primary microRNA transcript
qRT-PCR	Quantitative real time PCR
Rag	Recombinant activating gene
RANTES	Regulated on activation normal T cell expressed and secreted
RCA	Right carotid artery
Rip-1	Receptor-interacting protein 1
RISC	RNA-induced silencing complex

v

RNA	Ribonucleic acid
SEM	Standard error of mean
SDD	Scaffold/dimerization domain
Sma	Smooth muscle actin
Smad 2/3/4	Sma- and Mad-related protein 2/3/4
SMC	Smooth muscle cell
SSC	Side scatter
STA	Superior thyroid artery
STAT1	Signal transducers and activators of transcription-1
TAX1BP1	Tax1-binding protein 1
TF	Tissue factor
TGFβ	Transforming growth factor-β
Th	T helper cells
TNFα	Tumor necrosis factor alpha
TNFR1	Tumor necrosis factor receptor 1
TRAIL	TNF-related apoptosis-inducing ligand
TRAF 3/2	TNF receptor associated factor 3/2
T_{regs}	Regulatory T-cells
ULD	Ubiquitin-like domain
Vcam-1	Vascular cell adhesion molecule-1
VLDL	Very low density lipoprotein
VSMCs	Vascular smooth muscle cells
WHO	World health organization
WT	Wild type
ZF	Zinc finger domain

1. Introduction

1.1 Cardiovascular disease - mortality and risk factors

Cardiovascular disease (CVD) is the main cause of death in western societies. According to the World Health Organization (WHO) CVD is the number one cause of death globally: more people die annually from CVD than from any other cause and the number of people dying from CVD, mainly heart disease and stroke, will increase to reach 23.3 million by 2030[1,2]. CVD is projected to remain the single leading cause of death[2]. The term CVD covers a wide array of disorders, including diseases of the vascular system supplying blood to the heart, brain and other vital organs, damages to the heart muscle and heart valves, malformations of the heart structure and diseases such as deep vein thrombosis[3].

Risk factors for CVD are unhealthy diet, physical inactivity, tobacco use and harmful use of alcohol. The effects of unhealthy diet and physical inactivity may show up in individuals as a raise in blood pressure, blood glucose and blood lipids, in addition to overweight and obesity. These "intermediate risks factors" can be measured in primary care facilities and indicate an increased risk of developing a heart attack, stroke, heart failure and other complications such as deep vein thrombosis or pulmonary embolism[4]. However, there is an urgent need for new medications treating acute CVDs like myocardial infarction and ischemic stroke. Therefore, it is very important for the future to investigate the underlying mechanisms of these pathologies and to devise new therapeutical treatments to prevent and cure CVD.

Heart attacks and strokes are usually acute events and are mainly caused by a blockage that prevents blood from flowing to the heart or brain. The most common reason for this is a build-up of fatty deposits on the inner walls of the blood vessels, which supply the heart or brain. Strokes can also be caused by bleeding from a blood vessel in the brain or from blood clots[5].

The underlying pathophysiology leading to these cardio- and cerebrovascular incidents is called atherosclerosis. It is defined as an inflammatory fibro-proliferative response to various forms of endothelial injury, which develops mainly at sites of disturbed blood flow such as at bifurcations[6].

1.2   Atherosclerosis

1.2.1 Pathogenesis of atherosclerosis

Blood vessels are constructed in three main layers, so-called tunics (Figure 1). The innermost layer (tunica interna, tunica intima or shortly intima) is comprised of endothelial cells on the luminal side, extracellular connective tissue matrix (proteoglycans and collagen) and the inner elastic lamina (IEL) at the medial end. Below the IEL follows the middle layer, the so-called tunica media (or shortly media). It consists of vascular smooth muscle cells (VSMCs) embedded in interstitial extracellular matrix. Last the vessel is enclosed by the tunica adventitia or tunica externa (shortly adventitia), which is composed mainly of collagen with interspersed fibroblasts and SMCs and is supported by the external elastica lamina (EEL)[7,8].
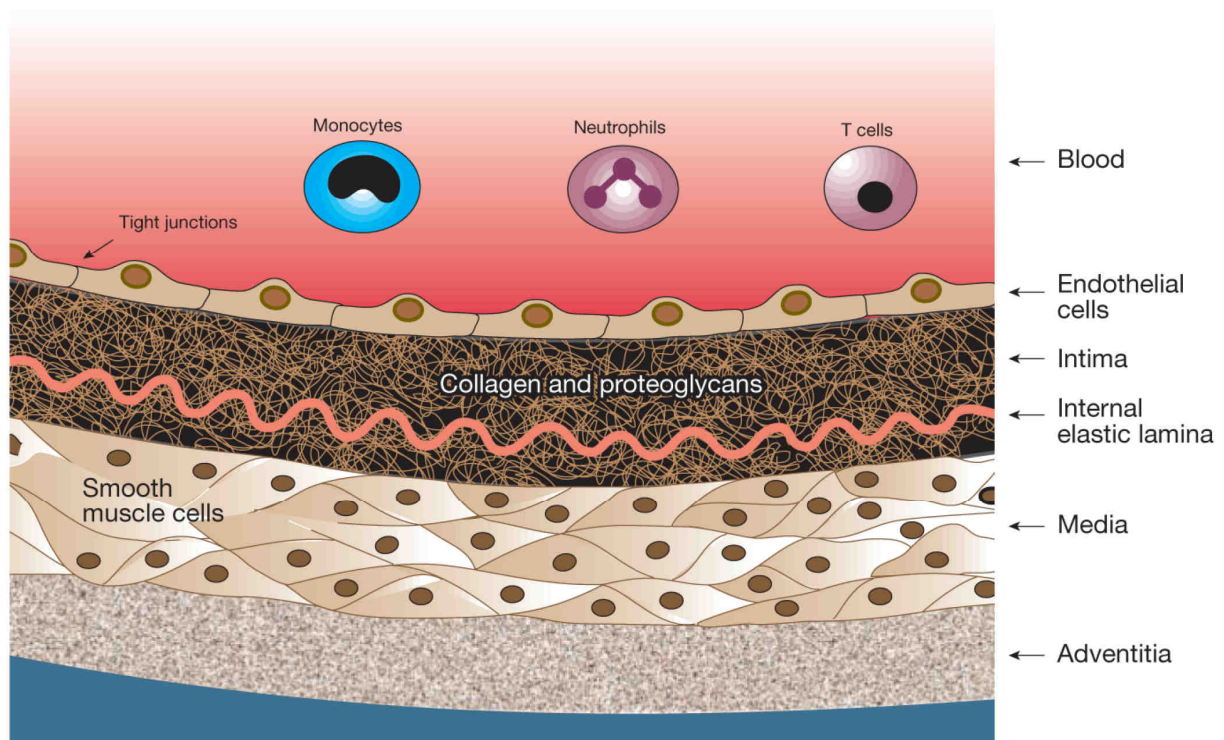
Figure 1: Structure of an artery. A blood vessel is composed of three different layers. The intima, also called the tunica interna, carries endothelial cells on the luminal side and the internal elastic lamina on the peripheral side. The second layer (media or tunica media) consists of SMCs and the outer layer (adventitia, tunica externa) is built up of connective tissue with interspersed fibroblasts and SMCs. (Figure from Lusis A.J.[8])

Introduction

Atherosclerosis is thought to be initiated by damage of the endothelium, resulting in dysfunction and activation of endothelial cells[9]. Cardiovascular risk factors such as hyperlipidemia, smoking, hypertension and oxidative stress cause endothelial dysfunction[10]. Also, endogenous cytokines or disturbed flow in areas predisposed to atherosclerosis, as e.g. at bifurcations, lead to endothelial cell activation[11,12]. Nitric oxide (NO) is an important mediator in endothelial cells and fulfills multiple functions in the context of vascular reactivity and atherosclerosis. It mediates endothelium-dependent vasodilation by opposing the effects of endothelium-derived vasoconstrictors such as angiotensin II and endothelin. Furthermore, it inhibits platelet aggregation and adherence on the endothelium and with leukocyte infiltration. Also, NO interferes with SMC proliferation and prevents the oxidation of low-density lipoprotein (LDL)[9,13]. The loss of nitric oxide (NO) is not only defined as a hallmark for endothelial dysfunction but it leads as well to increased endothelial activation. Once endothelial cells are activated, they express adhesion molecules such as E-selectin, P-selectin, vascular cell adhesion molecule-1 (VCAM-1) and the chemokine monocyte chemoattractant protein-1 (MCP-1)[10].

Endothelial dysfunction and activation trigger atherogenesis as they permit the subendothelial accumulation of LDL and inflammatory cells (T-cells, monocytes)[10,14]. Once the LDL particles have entered the intima they are susceptible to oxidation by reactive oxygen species or enzymes as e.g. myeloperoxidase released from inflammatory cells. Oxidized lipids and LDL (oxLDL) trigger the further activation of endothelial cells, leading to enhanced expression of adhesion molecules and increased secretion of chemokines attracting more immune cells to infiltrate the vessel wall. Leukocyte invasion occurs through rolling over the endothelium, adhesion and transmigration through the endothelium into the intima (Figure 2b). The first cells to adhere and enter are monocytes, which then subsequently differentiate into macrophages. Macrophages are crucial players in atherosclerotic lesions, contributing to atherogenesis[14]. They take up oxLDL accumulating in the lesions and produce crucial pro-inflammatory markers sustaining plaque progression. Early lesion formations mainly contain monocyte-derived-macrophage-like-foam cells in addition to T-cells, and are therefore called "fatty streaks" (Figure 2b)[14,15].

The progression into more complex lesions is stimulated by the continuous accumulation of immune cells and the development of a necrotic core. Lipid

3

overloading eventually triggers macrophage death and the formation of necrotic cores, a hallmark of progressed lesions. The release of foam cell content leads to further accumulation of extracellular lipids and pro-inflammatory cytokines, which sustain inflammation. VSMCs migrate from the adventitia and media to the intima, where they proliferate and together with collagen fibers form a fibrous cap covering the atherosclerotic lesion. Although the fibrous cap stabilizes the plaque, it causes as well augmentation of the atherosclerotic bulk, which now protrudes into the lumen of the artery[7,16] (Figure 2c). Progressed plaques can be classified into different categories according to their lesion content. While a plaque with a large necrotic core, high levels of inflammatory cells and a thin fibrous cap is called an unstable plaque, a plaque with a thicker fibrous cap, less inflammatory cells and a smaller necrotic core is classified as a stable plaque. Unstable plaques are more prone to rupture. This will trigger thrombus formation (Figure 2d), which can occlude the lumen and cause myocardial infarction or stroke[17].

Introduction
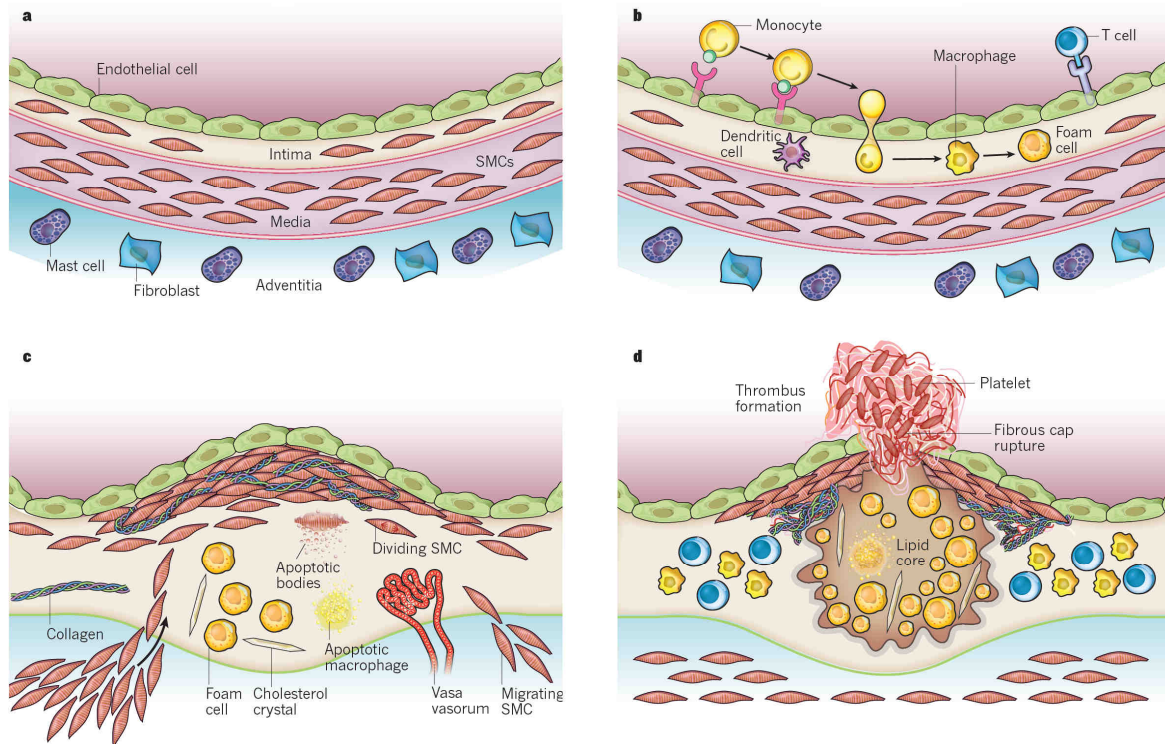
Figure 2: Initiation and progression of atherosclerosis. (a) Under normal conditions the artery consists of three layers: the intima with an endothelial cell cover on the luminal side, the media and the surrounding adventitia. (b) Under pro-inflammatory conditions endothelial cell dysfunction and activation lead to increased permeability and expression of adhesion molecules. These adhesion molecules help leukocytes such as T-cells and monocytes to adhere to the activated endothelium, which is followed by their transmigration into the intima. Once in the intima, monocytes differentiate into macrophages, which accumulate lipids and transform into foam cells, which make up fatty streaks. (c) Continued leukocyte influx and deposition of cholesterol crystals further stimulate atheroprogression. Cytokines produced in the plaque, as e.g. PDGF-beta, trigger the migration of SMCs into the plaque giving rise to a fibroproliferative progression of the lesion. Together with collagen fibres, these SMCs form a protective fibrous cap covering the plaque. (d) Apoptosis of macrophage foam cells and other plaque cells result in the formation of a necrotic core composed of dead cell material and accumulated lipids. The thickness of the protective fibrous cap can with time decrease due to matrix degradation by proteases, making the plaque unstable and prone to plaque rupture. Once a plaque has ruptured, the lesion content is released, the coagulation system gets activated and a thrombus is formed, which can occlude the artery and lead to heart attack or stroke. (Figure from Libby P. et al.[18])

Many immune cells, both from the innate as well as the adaptive immune system, are involved in the development and progression of atherosclerosis[14,15,19]. As mentioned before, monocytes are the first cells to adhere to the endothelium and transmigrate into the intima, where they differentiate into macrophages. Macrophages are highly versatile cells, taking on many different phenotypes. M1 (classically activated macrophages) and M2 macrophages (non-classically activated macrophages) are suggested to play opposite roles during inflammation, but both are present in atherosclerotic lesions. M1 macrophages can be found in plaque

5

shoulders, which are predilection sites for rupture[20], and can release elevated levels of tumor necrosis factor-α (TNFα), IL-1β and IL-6 cytokines, which have been attributed to further activate endothelial and smooth muscle cells, thus driving atherosclerotic progression[21]. On the contrary, M2 cells were shown to induce differentiation of atheroprotective regulatory T-cells[22] and are rather found far from the lipid core, in more stable zones of the lesion, suggesting atheroprotective functions[23]. Furthermore, M2 macrophages produce anti-inflammatory cytokines IL-4, IL-13, and IL-10, which through their immunosuppressive effects on T-cell and macrophage activation, may lead to decreased endothelial cell and smooth muscle cell activation[21]. Additionally, M2 macrophages have been involved in promoting angiogenesis, tissue remodeling and repair[24].

Neutrophils are involved in the initiation and progression of atherosclerosis[14]. Hyperlipidemia increases the number of circulating neutrophils and with help of specific chemokine receptors, such as CCR1, CCR2, CCR5 and CXCR2, they infiltrate the lesion[25]. Early neutrophil inflammatory signals attract and recruit monocytes into the plaque and apoptotic neutrophils sustain monocyte recruitment[26]. Neutrophil activation triggers the formation of NETs, which are neutrophil extracellular traps. Such NETs have been shown to promote atheroprogression and thrombus growth[27,28]. All together neutrophils have been suggested to drive the initiation and progression of atherosclerosis by providing chronic inflammatory triggers[29].

Together with macrophages, T-cells can be found already in early lesions. They can be subdivided into different subtypes, which are all involved in atherosclerosis. CD4$^+$ T-cells can be divided into at least four types of T helper (Th) cells: Th1, Th2, Th17 and regulatory T-cells (T$_{reg}$). Th1 cells produce high levels of IFN-γ and mediate cellular immune responses that are atherogenic. For example, IFN-γ activates monocytes/macrophages and dendritic cells. Furthermore, IFN-γ inhibits SMC proliferation and collagen production, which subsequently leads to the formation of unstable plaques prone to rupture[30]. Also Th17 cells have been demonstrated to be critical in atherosclerotic plaque progression, as they release the pro-inflammatory cytokine IL-17, which has been shown to exacerbate atherosclerotic lesion development[31]. Th2 cells are hardly found in atherosclerotic lesions and their role in atherogenesis has been debated. One study observed a

decrease in atherosclerotic lesion formation upon deficiency of IL-4, the prototypic Th2-related cytokine, suggesting a potentially proatherogenic role of IL-4 and Th2 cells[32]. In contrast, another study showed that Th2 cells antagonize the proatherogenic effect of Th1 cells by downregulating IFN-γ production by Th1 cells through IL4[33]. Thus, the role of Th2 cells in atherogenesis remains controversial and might be dependent on the stage of the atherosclerotic process and/or anatomic location of the lesion. Finally, T_{regs} exert important immunoregulatory functions in atherosclerosis by controlling Th1 and Th2 immune responses and have been attributed an atheroprotective function[34].

Dendritic cells (DCs) are specialized antigen-presenting cells that are required for the activation of naive T-cells and the development of antigen-specific T-cell-mediated immune responses. DCs are already present in the intima before atherosclerotic lesion development[35] and play a crucial pathogenic role in all stages of the atherosclerotic process. At early stages of lesion development, DCs accumulate in large numbers within the intima of atherosclerosis-susceptible regions. Their continued accumulation during lesion development is correlated with lesion progression and inflammation[36]. Plasmacytoid dendritic cells (pDCs), which are a distinct set of DCs producing large amounts of IFN- type 1, were found at plaque shoulder regions. An atheroprogressive role of pDCs was revealed through its effector cytokine IFNγ, which increased macrophage accumulation in atherosclerotic lesions[37]. Also, pDCs induce an up-regulation of the molecule TRAIL on T-cells. TRAIL-expressing T-cells effectively kill plaque-resident cells, weakening the lesion content and rendering the plaque vulnerable[38]. On the other hand, pDCs were also shown to have atheroprotective properties[39].

B-cells are involved as well in all stages of atherosclerosis[40] and can be divided into 3 subtypes: B1 and B2 B-cells and regulatory B-cells (B_{regs}). B1 B-cells have been demonstrated to protect from atherosclerosis, while B2 B-cells have an atherogenic effect and aggravate atherosclerosis. B_{regs} produce IL-10, and therefore it has been suggested that they might have a protective role similarly to T_{regs}, although the direct role of B_{regs} still remains to be studied[41].

In summary atherosclerosis is a complex disease modulated by various risk factors and involving different immune cell types[42,43]. Although many processes have

been identified to trigger the initiation and progression of atherosclerosis, many questions on detailed mechanisms are still un-answered. Being the leading pathology to heart attack and stroke, a greater understanding of this disease is vital for the development of new therapies.

1.2.2 Haemodynamic forces in atherosclerosis

As mentioned in the previous chapter, haemodynamic forces are one of the mechanisms triggering endothelial activation and changes of the endothelial phenotype, subsequently leading to the initiation of atherosclerosis[12,44,45]. Atherosclerotic lesions mainly develop at predilections sites along the arterial tree, which are exposed to disturbed flow[6]. These regions are e.g. the inner curvature of the aortic arch and branching points along the aorta as well as bifurcations e.g. in the brachiocephalic artery, as shown in Figure 3. In contrast, in straight parts of the arterial tree, blood flow is laminar and wall shear stress is high. Laminar flow and high shear stress both are considered to be atheroprotective, whereas low shear stress associated with disturbed flow pre-activates the endothelium and is described as pro-atherogenic[46].
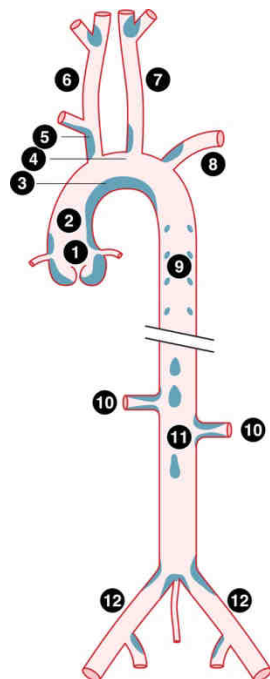
Figure 3: Atherosclerosis mainly develops at regions with disturbed blood flow. Schematic drawing of the arterial tree, indicated in blue the areas, where atherosclerotic plaques are prone to develop. 1) aortic sinus 2) ascending aorta 3) inner curvature of aortic arch 4) outer curvature of aortic arch 5) innominate or brachiocephalic artery 6) right common carotid artery 7) left common carotid artery 8) left subclavian artery 9) thoracic aorta 10) renal artery 11) abdominal aorta 12) iliac artery (Figure from Chiu J.J. et al.[6])

Vascular endothelial cells serve as important homeostatic regulators in response to chemical and mechanical forces[47]. Endothelial cells sense the wall shear stress and transmit this information as intracellular signals. Several theories have been postulated on how endothelial cells sense shear stress, which include ion channel activation, aveolae-mediated regulation of Ca^{2+}, activation of G-protein-coupled receptors and tyrosine kinase receptors, adhesive protein activation, glycocalyx elongation and bending of primary cilia[48]. These mechanosensors generate, in response to shear stress, biochemical signals that initiate complex and multiple signalling cascades[49]. The type of shear, laminar or disturbed, impacts which signal transduction pathways are initiated as well as which subsequent genes are transcribed, thereby influencing endothelial phenotype and function[48]. The pro-atherogenic effects attributed to low endothelial shear stress can be explained by the activation of pro-inflammatory transcription factors such as AP1 and NF-κB, whereas the anti-atherogenic effects of high shear stress are mediated by anti-inflammatory transcription factors like KLF2 and NRF2[50]. Furthermore, haemodynamic forces regulate as well the induction of various microRNAs (miRs), which can mediate either athero-protective or –progressive functions[51]. An insight on miRs is given in the following chapter. More details concerning the transcription factor NF-κB and its activation and involvement in atherosclerosis are given in chapter 1.3.

1.2.3 MicroRNAs in atherosclerosis

MicroRNAs (miRs) are short, highly conserved, non-coding RNAs, which play a key regulatory role in the complex network of posttranscriptional gene expression. More than 10.000 miRs have been identified to date and 940 of them in the human organism. In mammals miRs control the expression of 50% of all protein coding genes[52].

MiRs originate either from protein-independent genes being transcribed by RNA polymerase II and III or from introns of protein-coding genes. The primary transcript, so called pri-miRs, remains in the nucleus and undergoes cleavage, mediated by Drosha, an RNase III enzyme, and DGCR8 as a cofactor, to form a ~60-70 nucleotide long hairpin structure, known as pre-miR. Pre-miRs are exported through the nuclear pore complexes into the cytoplasm by binding to Exportin-5–Ran-GTP. Once in the cytoplasm, the pre-miR is further processed into mature miR by another

RNase III enzyme known as Dicer, which forms a multi-protein complex together with TRBP, PACT and an Argonaute (Ago) protein. The Dicer produces a miR duplex, consisting of a passenger and a guide strand. While the passenger strand is cleaved off and mostly degraded, the guide strand assembles with proteins of the Ago family, a process that shapes the effector RNA-induced silencing complex (RISC)[52,53]. This RISC complex then induces translational repression or mRNA degradation of the target mRNA through binding of the miR to this target (Figure 4).
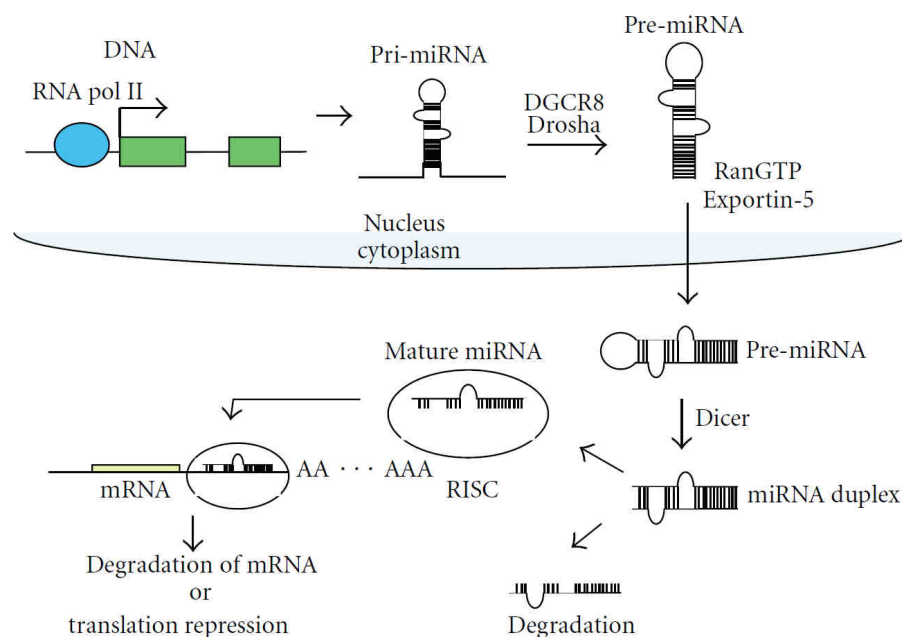
Figure 4: Biogenesis of microRNA (miR). Primary miRNA (pri-miRNA) is transcribed by RNA polymerase II and then cleaved by the Drosha/DGCR8 complex into a hairpin forming pre-miRNA. Pre-miRNA is transported out of the nucleus into the cytoplasm with the help of RanGTP and Exportin-5, where it is processed into a miRNA duplex form by Dicer. One of the duplex strands is incorporated into RISC (guide strand), while the other strand (passenger strand) is mostly degraded. MiRNA binds to the 3´UTR region of the target mRNA, leading to translational repression or mRNA degradation. (Figure from Yamakuchi M.[54])

An individual miR is capable of targeting hundreds of mRNAs and a single mRNA can be regulated by multiple miRs. MiRs target mRNAs by complementary sequence in the 3´UTR regions using basic base-pairing. The gene regulation takes place by the down-regulation of the respective mRNA, either by mRNA translational repression or mRNA cleavage[54].

Altered miR expression patterns have been implicated in various disease states, including cancer and cardiovascular disease[55,56]. As mentioned shortly in the

previous chapter, miRs were found in atherosclerotic lesions and changes in haemodynamic forces result in altered expression of miRs in endothelial cells[57]. In areas with high shear stress the expression of atheroprotective miRs is upregulated, whereas pro-inflammatory miRs are downregulated[58]. For example, the down-regulation of miR-92a by high shear stress increases the expression of the endothelial NO synthase (eNOS), whereas the up-regulation of miR-19a contributes to the shear stress-induced inhibition of cell proliferation[59]. Similarly, the expression of miR-10 is enhanced in atheroprotected regions, which reduces the inflammatory response of endothelial cells[50]. But miRs do not only play a key role in endothelial cell activation and phenotype[60], miRs are as well involved in the communication between cells e.g. endothelial cells and monocytes or between endothelial cells and smooth muscle cells, which is of crucial importance in atherosclerosis[61]. For example, miRs regulate the phenotype, the proliferation and migration of SMCs and control the inflammatory response in macrophages[62,63].

To summarize, miRs are important fine tuners of various biological processes in order to maintain homeostasis, but also play an important role in the context of inflammation, such as in atherosclerosis.

1.3 The transcription factor NF-κB

1.3.1 NF-κB activation pathway

As described in the previous chapter 1.2.1, atherosclerosis is an inflammatory fibro-proliferative disease, in which inflammation plays a central role in the initiation as well as the progression of atherosclerosis. Thereby, not only vascular cells undergo an inflammatory activation, but as well the circulating, adhering and infiltrating leukocytes. The transcription factor nuclear factor kappa B (NF-κB), first identified in 1986[64], has been implicated with pro-inflammatory reactions as well as with atherosclerosis[65]. The NF-κB family has five members: RelA (p65), RelB and c-Rel and the precursor proteins NF-κB1 (p105) and NF-κB2 (p100). Both of these precursor proteins need to be processed into an active NF-κB form, being p50 and p52, respectively, whereas the other family members are already present in a mature state in the cytoplasm. The NF-κB transcription factors form dimers and bind to κB sites in promoters and enhancers of a variety of genes to induce as well as repress

gene transcription[66]. All family members share a conserved central region known as the Rel homology domain, which is involved in dimerization of the NF-κB proteins, DNA binding and interaction with the inhibitory molecules IκB. The vertebrate NF-κB transcription factor is induced by over 150 different stimuli, and in turn, active NF-κB controls transcription of over 150 target genes. The range of NF-κB-inducing stimuli, include physical, physiological and oxidative stress, bacterial and viral infections, inflammatory cytokines and engagement of antigen receptors, all able to elicit NF-κB activation. NF-κB regulates the expression of inflammatory cytokines, chemokines, immunoreceptors and cell adhesion molecules. In addition, NF-κB regulates cell differentiation, proliferation and survival. Because of this large variety in functions, NF-κB has often been called a "central mediator of human immune response"[66,67].

In resting conditions NF-κB is present in the cytoplasm bound to an inhibitory protein, named inhibitor of κB (IκB), which prevents NF-κB to translocate to the nucleus. NF-κB signalling can be activated via two main pathways, the classical (canonical) or the alternative (non-canonical pathway)[68], as shown in Figure 5. While the canonical NF-κB pathway is mainly triggered by physiological pro-inflammatory stimuli such as TNF (in Figure 5 represented by TNFR1 signalling), the non-canonical pathway is activated by TNF family members such as CD40L, BAFF and lymphotoxin-β (LT-β). In the canonical pathway, receptor stimulation triggers intracellular signalling leading to activation of the IκB kinase (IKK) complex[69]. The IKK complex consists of two catalytically active kinases, IKKα and IKKβ, and one regulatory component, IKKγ (NEMO). Once the IKK complex is activated, IKKβ mediates the phosphorylation of IκB proteins on two N-terminal serine residues in an NEMO-dependent manner. This then leads to the ubiquitination and proteasomal degradation of IκB[70]. Once the NF-κB dimer, mainly p65-containing heterodimers, is released from IκB, it is already in an active state and can translocate to the nucleus and start gene transcription[66,71]. The transcriptional activity of NF-κB is regulated by post-translational modifications, including acetylation, phosphorylation and ubiquitination. These post-translational modifications are necessary to ensure a tight regulation of NF-κB activity, given the wide range of biological processes that are affected by NF-κB[72].

Whereas the canonical NF-κB pathway mainly plays a central role in inflammatory responses, the non-canonical pathway has been implicated in B-cell

maturation and lymphoid development[73]. Non-canonical NF-κB signalling is triggered by TNF family members such as LT-β and depends only on the IKKα kinase and not IKKβ or IKKγ, in contrast to the canonical NF-κB pathway[74]. In resting conditions the inhibitory protein TRAF3 is associated with the kinase NIK and mediates its ubiquitination and proteasomal degradation[75]. Upon stimulation TRAF3 gets degraded (mediated by TRAF2 and cIAP), resulting in the stabilization of NIK[76]. Stabilized NIK activates IKKα homodimers by phosphorylation and in turn active IKKα mediates the phosphorylation and proteasomal processing of the NF-κB precursor p100. This processing leads to transcriptional active p52/RelB NF-κB heterodimers[77,78] (Figure 5). To prevent exuberant NF-κB activation in response to non-canonical NF-κB stimuli, the deubiquitinase OTUD7B provides a negative feedback keeping non-canonical NF-κB activation in check by binding to TRAF3 and protecting it from degradation[79].
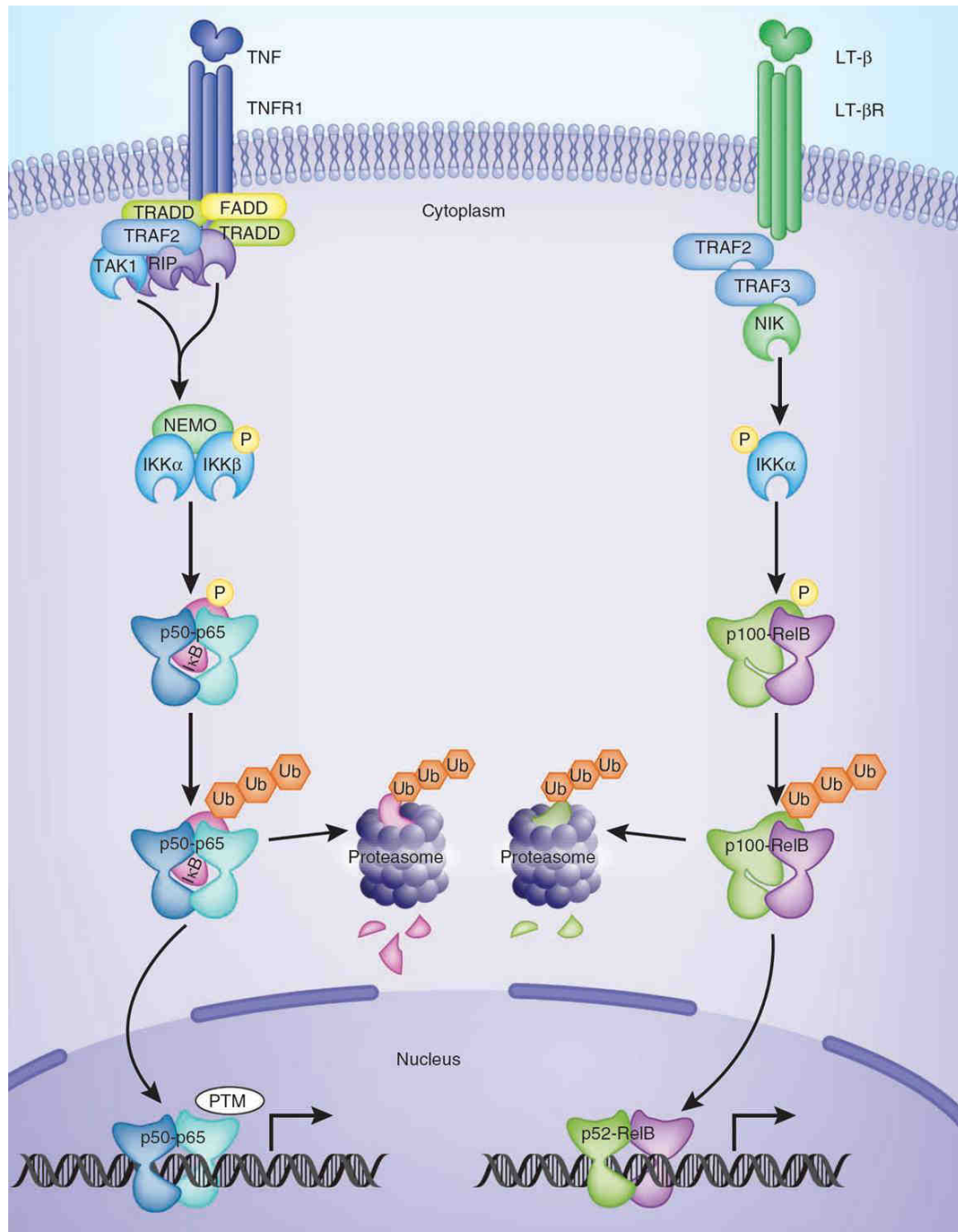
Figure 5: Signalling pathways to NF-κB activation. The transcription factor NF-κB plays a central role in inflammatory reactions. It is activated via two main pathways. Inflammatory signals such as TNF induce canonical NF-κB activation through the IKKβ/NEMO kinase complex (left side). Once the IKK complex is activated, IKKβ phosphorylates in an NEMO-dependent manner the inhibitory protein IκB, causing its ubiquitination and proteasomal degradation. Once IκB is removed, the NF-κB dimer can translocate to the nucleus and start gene transcription. The transcriptional activity of NF-κB is regulated by post-translational modifications. Non-canonical NF-κB activation on the other hand is dependent on the IKKα kinase. NIK activates IKKα homodimers, which in turn phosphorylate the NF-κB precursor p100 triggering its processing into a transcriptional active form. (Figure from Oeckinghaus, A. et al.[66])

1.3.2 NF-κB activation in atherosclerosis

NF-κB has been involved in different stages of atherosclerosis, from its initiation to plaque destabilization and rupture[65,80,81]. NF-κB expression has been found both in human atherosclerotic lesions[82], e.g. in aortas of patients suffering from coronary atherosclerosis[83], as well as in plaques from Ldl receptor (*Ldlr*)-deficient mice[84]. During initiation of atherosclerosis, endothelial cells become activated in response to various stimuli as described in the previous chapter. Once activated, endothelial cells express adhesion molecules (e.g. ICAM-1, VCAM-1, E-selectins), chemokines (e.g. MCP-1), cytokines (e.g. TNFα, IL-1, IL-6 and IL-8) and other pro-inflammatory proteins, which recruit leukocytes, help them to adhere to the endothelium and to infiltrate into the vessel wall. As many of these proteins are targets genes of NF-κB, this process involves the activation of NF-κB in endothelial cells in response to pro-inflammatory molecules such as lipopolysaccharides (LPS), TNFα, oxLDL or cytokines[65,85]. Furthermore, endothelial dysfunction activates NF-κB through impaired NO production, which has been shown to inhibit NF-κB activation by increasing the expression of IκBα[86,87]. Also, haemodynamic forces influence vascular inflammation by regulating NF-κB activation in endothelial cells[88]. For example, the up-regulation of VCAM-1 and ICAM-1, both target genes of NF-κB, have been shown to be most prominent at lesion-prone sites with altered blood flow[89]. Human aortic ECs (HAECs) exposed to low shear stress or disturbed flow conditions, showed a significant increase in NF-κB (p50 and p65) activation compared with HAECs exposed to high shear stress (laminar flow conditions)[90]. And as already described in the previous chapter, NF-κB activity is elevated at regions of the arterial tree that are exposed to disturbed blood flow, while atheroprotected regions exposed to steady flow show increased expression of the protective transcription factor KLF2 (Figure 6)[91-93].
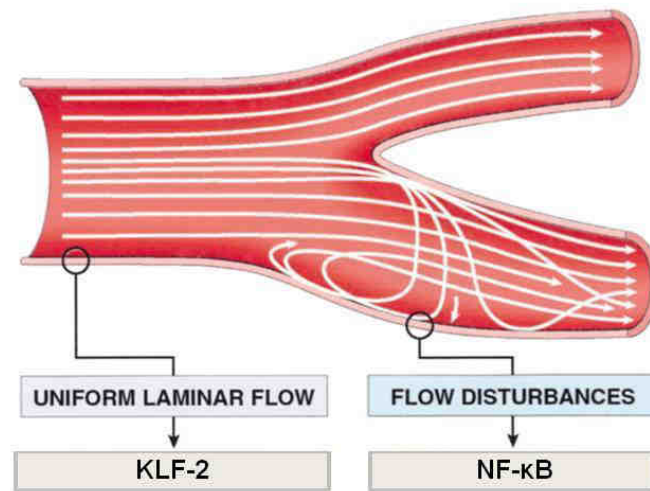
Figure 6: NF-κB and haemodynamic forces. Schematic of flow conditions in a human carotid bifurcation. The straight segment displays uniform and laminar flow and here endothelial cells are exposed to high shear stress. These areas show an athero-protected, anti-inflammatory and anti-thrombotic phenotype, which is induced by the increased expression of the transcription factor KLF2, which mainly targets atheroprotective and anti-inflammatory genes. In contrast, at the bifurcation, disturbed blood flow with flow reversal and secondary flows is typical. These areas are predisposed to atherosclerosis and the shear stress is relatively low. NF-κB activity is high in these regions leading to enhanced expression of pro-atherogenic NF-κB dependent genes (Figure adapted from Collins, T. et al.[93])

Furthermore NF-κB has been detected in advanced lesions in SMCs, macrophages and T-cells[82,94]. Canonical NF-κB activation results in the up-regulation of pro-inflammatory proteins as cytokines (e.g. TNFα, IL-6 and IL-8) and matrix metalloproteases (MMPs), but also of pro-thrombotic tissue factor (TF), most of these contributing to plaque progression and instability. Through this regulation of gene expression, NF-κB signalling sustains pro-atherogenic recruitment and activation of inflammatory cells, and induces SMC proliferation[80]. Additionally, NF-κB has been associated with plaque rupture. Patients with unstable angina and high risk of plaque rupture showed increased NF-κB activity in their leukocytes[95] and unstable plaques show higher NF-κB expression than stable plaques[96]. MMPs contribute to the destruction of extracellular matrix at shoulder regions of plaques and high MMP activity in macrophages has been associated with plaque rupture. MMP-1,-3 and -9, shown to be linked with plaque destabilization, are regulated by NF-κB[97,98].

The functions of NF-κB in atherosclerosis seem to be complex and NF-κB has been suggested as a potential therapeutic target for the treatment of atherosclerosis[85,99]. Reduced lesion formation in Apolipoprotein E (*Apoe*)-deficient

mice was observed when treated with the NF-κB inhibitor DHMEQ, which prevented the TNF-α-induced nuclear translocation of p65[100]. Recent studies showed anti-inflammatory effects after selective inhibition of cRel, such as reduced neointima formation after vascular injury upon NF-κB inhibition in SMCs[101] or decreased atherosclerotic lesion size[102]. Furthermore, myeloid deficiency of IκBα, the inhibitor of NF-κB, promoted atherosclerosis by the recruitment of leukocytes into the lesion[103]. Also, the genetic deletion of NF-κB1 in macrophages of *Ldlr*^{-/-} mice resulted in a decrease in atherosclerosis[104].

This demonstrates the potential of using NF-κB as a potential therapeutic target, but so far no drug has yet made it through clinical trials. One reason might be the complexity of NF-κB and its multiple functions in different cell types. Of note, in addition to its pro-inflammatory function, NF-κB activity in leukocytes has an important role in the resolution of inflammation through transcription of anti-inflammatory cytokines such as IL-10[105] and the suppression of pro-inflammatory IL1-β secretion[106]. Therefore, although NF-κB-suppressing strategies to interfere with its pro-inflammatory functions seem to be a valid direction in pharmaceutical treatment[81], caution has to be raised because of the important anti-inflammatory functions of NF-κB. Furthermore, as NF-κB is critical for many immune and inflammatory responses and additionally plays a central role in homeostasis, chronic inhibition and non-tissue specific inhibition would cause serious side effects. Therefore, the interest in developing selective and specific inhibitors targeting specific NF-κB signalling pathways over e.g. IKKα or IKKβ is high and could result in promising therapeutic instruments[107,108].

1.4   The IKK family

1.4.1 Introducing IKK family members

The IKK kinase complex is the core element of the NF-κB cascade. It essentially consists of two kinases (IKKα and IKKβ) and a regulatory subunit, IKKγ (also known as NEMO). The complex activated by external, inflammatory stimuli, is in charge of the phosphorylation of either the inhibitory protein IκB or the NF-κB precursor p100. These two separate NF-κB activation pathways require different subunits of the IKK

complex: while the canonical pathway depends on IKKβ and NEMO to trigger phosphorylation of IκB, the noncanonical pathway requires only IKKα for phosphorylation of p100. Several years ago, two protein kinases with structural similarities to IKKα and IKKβ were found. One was called IKK-ε or IKK-I and the other was named Tank-binding Kinase (TBK)-1, and both play a key role in the activation of IRF3 and IRF7, important for the induction of type 1 interferon (IFN-I)[109].

IKKα and IKKβ were first identified by Chen et al. (1996) and Didonato et al. (1997) with help of biochemical purification. Investigating the kinases responsible for phosphorylation of IκB proteins, they observed a complex migrating around 700-900 kDa, containing two related catalytic subunits, later called IKKα (or IKK1) and IKKβ (or IKK2)[110,111]. NEMO was identified later and although this subunit does not have a catalytic function, cell lines deficient for NEMO cannot activate NF-κB, thereby proving the important regulatory function of NEMO in activating NF-κB[112,113].

The two kinase subunits of the IKK complex, IKKα and IKKβ, have a high sequence homology (approximately 50% identity)[114]. Both are serine/threonine kinases, contain an N-terminal kinase domain (KD), α-helical scaffold/dimerization domain (SDD) and a C-terminal NEMO-binding domain (NBD)[115]. Additionally, IKKα has a nuclear localization sequence, which is possibly linked with nuclear activity[116]. Furthermore, IKKβ contains a central, conserved ubiquitin-like domain (ULD), which has been suggested to be required for kinase activity and, together with the SDD, to be involved in the exact positioning of the kinase substrate IκBα[115] (Figure 7). A similar domain was not found in IKKα. Activation of IKKα and IKKβ is based on phosphorylation of two serine residues, S176/180 for IKKα and S177/181 for IKKβ, located in the so-called activation loop[117]. These phosphorylations probably lead to a conformational change and subsequently to kinase activity. A mutation of these serine residues to alanine renders the kinases inactive[70]. Nevertheless, how signal transmission from a stimulated receptor results in phosphorylation of the IKK activation loop is still discussed. The first scenario proposed is that the IKKs phosphorylate each other by autophosphorylation facilitated by either conformational changes within the IKK complex or induced proximity through the oligomerization of multiple core IKK complexes[118]. The second theory is the existence of separate IKK complexes that target these residues. Both theories seem plausible and of course it could be feasible that both mechanisms take place independently or together[119,120].
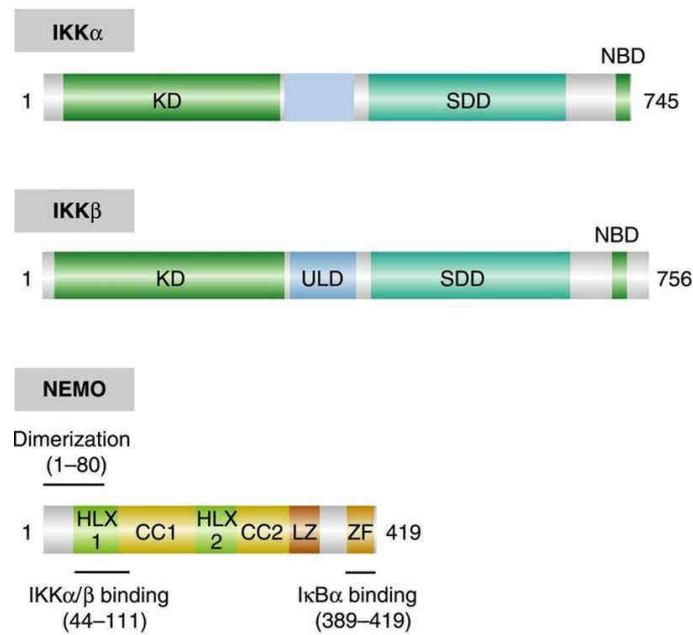
Figure 7: Domain structures of IKK complex family members. IKKα and IKKβ both have an N-terminal kinase domain (KD), α-helical scaffold/dimerization domain (SDD) and a C-terminal NEMO-binding domain (NBD). IKKβ has additionally an ubiquitin-like domain (ULD), required for kinase activity. NEMO consists of two coiled-coil domains (CC), a leucine zipper (LZ), a C-terminal zinc-finger (ZF) region and an IKKα/IKKβ binding zone located in amino acid 44-111. (Figure adapted from Hinz, M. et al.[115])

A detailed inspection of IKKβ´s crystal structure revealed that when the kinase is inactive, the activation loop adopts conformations that are incompatible with protein substrate binding, which supports the theory that phosphorylation of the serine residues of IKKβ leads to conformational change[121]. Furthermore, it has been proposed that multiple combinations of IKK subunits exist, including homodimers of IKKα or IKKβ either associated or distinct from NEMO, but most biochemical evidence indicates that the majority of cellular IKK complexes contains a core of IKKα-IKKβ-NEMO in the ratio of 1:1:2 [122].

NEMO is a regulatory non-enzymatic scaffold protein and has been suggested to be a mainly α-helical protein containing two coiled-coil domains (CC), a leucine zipper (LZ) and a C-terminal zinc-finger (ZF) region[123,124]. In addition, NEMO has a minimal oligomerization domain (MOD) and an IKKα/IKKβ binding zone located in amino acid 44-111 of NEMO (Figure 7). The MOD is an N-terminal dimerization domain that enables the formation of higher order oligomers. The ZF has been implicated in efficient IκBα binding and might direct IκBα to the ULD/SDD of IKKβ[125].

Of note, it was shown that IKK activation depends on NEMO. Exactly how NEMO regulates IKK activity is still unknown, but there is no doubt that it is a key regulator of the IKK complex, both positively and negatively[122]. It is possible that NEMO may function as a chaperone protein that brings the IKK complex to upstream polyubiquitinated kinases such as RIP-1, leading to IKK activation. However, phosphorylation of NEMO on S68, which is located in the region responsible for IKK interaction, has been shown to downregulate NF-κB activation in the presence of stimuli, providing the possibility that phosphorylation of NEMO can serve as a negative regulatory event.

1.4.2 IKKβ and NEMO in atherosclerosis

In recent years studies have focused on NF-κB and the IKK complex as potential therapeutic targets. As already mentioned in chapter 1.3.2 several studies successfully showed that blocking NF-κB could have atheroprotective, antithrombotic and anti-inflammatory effects. In terms of the IKK complex most studies chose IKKβ as their research target, due to its strong involvement in canonical NF-κB activation [126].

Kanters et al. inhibited NF-κB activity specifically in macrophages and neutrophils using bone marrow transfer from LysM-Cre[+] *Ikkβ*-floxed mice into *Ldlr*^{-/-} recipient mice. In contrast to what was expected from inhibiting NF-κB activation, they observed increased atherosclerotic plaque development, which was linked with an important anti-inflammatory role of IKKβ/ NF-κB in regulating expression of the anti-inflammatory cytokine IL-10[127].In the same direction, an anti-inflammatory role was described for IKKβ by suppression of the classically activated (or M1) macrophage phenotype[128]. However, a recent study observed, that deficiency of *Ikkβ* decreased adhesion, migration and lipid uptake in macrophages and reduced atherosclerosis in *Ldlr*^{-/-} mice[129]. These inconsistent observations regarding the pro-*vs* anti-atherogenic function of IKKβ suggest that further research is needed to define the role of macrophage IKKβ/NF-κB signalling in atherosclerosis.

Other studies showed a more pro-inflammatory and pro-thrombotic function for IKKβ. Low shear stress, which is seen as pro-atherogenic, induced both IKKα and IKKβ in HAECs, but IKKβ contributed to the majority of the IKK kinase activity[130]. Furthermore, IKKβ inhibition induced expression of endothelial thrombomodulin

,critically involved in anticoagulation, in a KLF2 manner[131]. Also, Ashida et al recently observed that upon IKKβ inhibition vascular endothelial cell permeability was increased and cell migration was decreased[132]. In relation to SMCs, IKKβ functions as a regulator of vascular inflammatory responses and atherosclerosis. *Ikkβ* deficiency specifically in SMCs rendered *Ldlr*^{-/-} mice resistant to vascular inflammation and atherosclerosis induced by high-fat feeding, again suggesting a pro-atherogenic role of IKKβ[133].

Although it has been shown how essential NEMO is in case of cell survival and as a regulator of IKK activity, so far only one study used NEMO as potential NF-κB inhibition target. Gareus and colleagues generated a mouse model with an EC-specific ablation of NEMO to interfere with IKK activation, which resulted in greatly reduced atherosclerotic lesions[134]. This again links the IKK complex and canonical NF-κB activation with pro-atherogenic functions.

Thus, NEMO/IKKβ/NF-κB signalling plays a complex role in inflammation and atherogenesis by driving pro-, but also anti-inflammatory processes and the outcome seems dependent on which cells are studied.

1.4.3 Versatile functions of IKKα

In contrast to IKKβ and NEMO the role of IKKα (IKK1/ CHUK) activity in atherosclerosis has not yet been investigated. However, IKKα exerts multiple versatile functions involved in inflammatory reactions and immune responses[115], which could influence atherogenesis.

In case of canonical NF-κB pathway, IKKβ and not IKKα is responsible for IκBα phosphorylation, but some studies have shown that IKKα has a compensatory function upon IKKβ inhibition and is able to directly phosphorylate IκBα itself[135, 136]. In addition to its compensatory function, IKKα has also been involved in resolving canonical NF-κB activation in macrophages and thus resolving inflammation, by triggering phosphorylation-induced degradation of the NF-κB isoform p65[137]. This observation could imply an atheroprotective function for IKKα as macrophages are atheroprogression-driving cells or rather imply atheroprotection based on the previously revealed anti-atherogenic role of IKKβ/ NF-κB signalling in macrophages[127]. Apart from its function in regulating canonical NF-κB signalling through p65 destabilization, IKKα homodimers are critical for alternative NF-κB

activation[66]. As mentioned in the previous chapter on NF-κB, IKKα mediates alternative pathway signalling through phosphorylation of NF-κB p100, triggering p100 processing and the release and nuclear localization of RelB-p52 dimers[74]. This pathway plays a crucial role in B-cell maturation and could thereby implicate IKKα in atherogenesis through the role of B-cells in atherosclerosis[41].

Furthermore, IKKα has multiple other roles, e.g. IKKα exerts different nuclear functions. Multiple studies have shown that IKKα can be detected in both the cytoplasm and the nucleus, whereas IKKβ is detected predominantly in the cytoplasm[138]. The observation of nuclear/cytoplasm shuttling of IKKα led to the discovery of the first nuclear role of IKKα in phosphorylating histone H3, involved in both NF-κB-dependent as -independent gene expression[139,140]. IKKα has also been involved in negative regulation and termination of gene transcription. For example, diverse pro-inflammatory stimuli trigger IKKα-mediated phosphorylation of the transcriptional repressor PIAS1, which then negatively regulates the expression of a predominantly pro-inflammatory subset of p65- and STAT1-dependent genes[141]. Also, the IKKα-mediated phosphorylation of TAX1BP1 triggers the assembly of the A20 ubiquitin-editing complex, which is an important negative regulator of canonical NF-κB activation[142].

Aside from nuclear regulation of gene transcription, nuclear IKKα has also been associated with functions independent of its kinase activity. For example, in keratinocytes, nuclear IKKα is a critical co-regulator of a Smad4-independent TGFb-Smad2/3 signalling pathway, which induces cell cycle arrest and terminal differentiation[138,143].

In conclusion, the IKKα kinase is involved in diverse functions which could be classified as both pro- as well as anti-inflammatory. Being such a versatile regulator of cell signalling and pro- and anti-inflammatory gene expression, IKKα could play a distinctive role in atherosclerosis.

2. Aim of the study

One of the pressing goals within atherosclerosis research is to find therapeutic strategies to treat plaque development, progression and rupture in order to prevent cardio- and cerebrovascular complications.

Given the versatile functions of IKKα such as e.g. in alternative NF-κB activation[66], termination of the canonical NF-κB activation in macrophages[137] or modulation of gene expression by e.g. phosphorylating histone H3[139], IKKα could potentially be a new therapeutic target for treating atherosclerosis. However, its function in atherogenesis first needs to be studied in detail. Hence, the overall aim of this study was to determine the role of haematopoietic IKKα activation versus the global function of IKKα activation in atherosclerosis. For both approaches an activation-resistant Ikkα ($Ikk\alpha^{AA/AA}$) mouse model, in which the Ikkα kinase activity cannot be activated, was used[144], with a hyperlipidemic Apolipoprotein E-deficient ($Apoe^{-/-}$) background.

(1) In the first part of the study, the role of Ikkα kinase activity in haematopoietic cells was determined, as inflammatory cells are crucial players driving atherosclerosis. Haematopoiesis and atherogenesis were studied after lethal radiation and transplantation of atherosclerosis-prone $Apoe^{-/-}$ mice with bone marrow carrying an activation-resistant $Ikk\alpha^{AA/AA}$ mutant. The mice received a high-fat diet for either 8 or 13 weeks and the haematopoietic profile was investigated with help of flow cytometric analysis to determine the importance of Ikkα in the development and homeostasis of leukocyte populations. The extent of atherosclerotic progression, lesion composition and intracellular lipid accumulation were examined to reveal potential roles of haematopoietic Ikkα kinase activity in atherogenesis and in macrophage lipid uptake, the latter being an important task of macrophages to clean up lipid deposits in the vascular wall. Due to the reported function of Ikkα on canonical NF-κB activation[137], the effect of haematopoietic activation-resistant Ikkα mutation on the activation of the canonical NF-kB isoform p65 was examined in macrophages, as modulation of canonical NF-kB activation could interfere with macrophage function or survival and thus with atherogenesis. In context of the latter, I examined macrophage apoptosis in atherosclerotic lesions from $Ikk\alpha^{AA/AA}Apoe^{-/-}$ mutant *vs* control mice. Furthermore, the effect of Ikkα mutation on inflammatory

gene expression in macrophages was studied, to reveal potential mechanisms how Ikkα could affect inflammatory processes and thus atherogenesis in macrophages.

(2) The second part of the study focussed on the global role of Ikkα kinase activation in atherosclerosis, which was studied by comparing atherosclerosis in *Ikkα^{AA/AA}Apoe^{-/-} vs Ikkα^{+/+}Apoe^{-/-}* mice after 13 weeks of high-fat diet. Similarly as for the first study, the contribution of Ikkα in atherogenesis was studied on the level of plaque size and atherosclerotic lesion composition. Additionally, potential site-specific functions of Ikkα kinase activity were analysed by comparing the effect of Ikkα mutation on atherogenesis in the aortic root, aortic arch and aorta. This is important because previous studies have shown such site-specific effects of other proteins on atherogenesis[145,146]. Furthermore, because of the known role of Ikkα in both NF-κB-dependent as -independent gene expression[139,140], the effect of *Ikkα^{AA}* mutation on downstream signalling, such as NF-κB p65 activity and histone H3 phosphorylation, was studied at different vascular regions, to reveal potential mechanisms on how Ikkα kinase activity could affect atherogenic processes. Also, gene expression studies were performed in *Ikkα^{AA/AA}Apoe^{-/-} vs Ikkα^{+/+}Apoe^{-/-}* mice at different vascular regions, to asses the involvement of Ikkα on site-specific gene regulation. Site-specific expression and activation profiles of Ikkα itself were studied at different vascular regions in *Apoe*-deficient mice to estimate whether flow conditions or different vascular regions would differentially influence Ikkα activity or expression and thereby influence the atherosclerotic outcome. On the same note, a potential role for miRs in controlling and regulating Ikkα expression was investigated, as miRs have been shown to be highly involved in flow-dependent vascular remodeling[58].

The *Ikkα^{AA}* mouse model and all techniques and methods are explained in detail in the following chapter 3.

3.   Materials and Methods

3.1   Materials

3.1.1 General equipment

Table 1: List of general equipment

Equipment	Manufacturer
Autoclave	Systec 2540EL (Systec, Germany)
Balance	Sartorius, Germany
Centrifuges	Eppendorf 5417C (Eppendorf, Germany) Eppendorf 5425 (Eppendorf, Germany)
Flow cytometer	FACSCanto-II (BD Biosciences, USA)
Fluorescence plate reader	Infinite M200 (Tecan, Germany)
Incubator	Hera Cell 240 (Fisher Scientific GmbH, Germany)
Laminar flow hood	Herasafe (Heraeus, Germany)
Microscopes	Leica DM2500 (Leica, Germany) CCD camera
Microtome	Leica RM2245 (Leica, Germany)
Cryotome	Leica CM3050S (Leica, Germany)
pH-meter	InoLab level 1 (WTW, Germany)
PCR thermocyclers	MyCycler (Bio-Rad, Hercules, CA) DNA Engine Opticon (MJResearch, Hercules, CA, USA)
Spectrometer	NanoDrop (Peqlab, Erlangen, Germany)
Homogenizer	TissueLyser LT (Qiagen, Hilden, Germany)
Real-Time PCR Thermocycler	ViiA7 (Applied Biosystems, Life Technologies, Germany)

3.1.2 Mice

Wild-type C57BL/6, *Apolipoprotein E*-deficient (*Apoe$^{-/-}$*) were obtained from the local animal breeding facility. *Apoe$^{-/-}$ mice* are established mouse models to study the development and disease progression of atherosclerosis[147]. To study the effect of Ikkα activation in atherosclerosis, a knock-in mouse model was used expressing an activation-resistant *Ikkα$^{AA/AA}$* mutant, with two serine phospho-acceptor sites in the activation loop replaced by alanines[144]. The *Ikkα$^{AA/AA}$* mutants were then crossed with

atherosclerosis-prone C57BL/6 *Apoe*$^{-/-}$ mice to generate *Ikkα*$^{AA/AA}$*Apoe*$^{-/-}$ mice. The genotyping protocol is described in chapter 3.2.3.2.

3.1.3 General consumables

Table 2: List of consumables

Consumable	Manufacturer
6-well plates (flat bottom) uncoated	Greiner Bio-one, Germany
12-well plates (flat bottom) uncoated	Greiner Bio-one, Germany
24-well plates (flat bottom) uncoated	Greiner Bio-one, Germany
96-well plates (flat bottom)	Becton Dickinson, USA
96-well plates (round bottom)	Nunc, Denmark
Cell strainer (70/100 µm)	BD Biosciences, USA
Culture dishes (15 cm)	Greiner Bio-one, Germany
Culture flasks (T25, T75, T175)	Greiner Bio-one, Germany
FACS-tubes	BD Biosciences, USA
EDTA-coated tubes	Sarstedt, Germany
FACS-tubes	BD Biosciences, USA
Glass microscope slides	Thermo Scientific, Germany
Needles 23/27 G	BD Microlance, USA
PD 10 column	GE Healthcare, Germany
Pipettes (0.1-2 µl; 2-20µl; 10-100µl, 20-200µl, 100-100µl) and Multichannel-Pipette	VWR, USA
Serological pipettes (5 ml, 10 ml, 25 ml)	Corning, USA
Sutures Seraflex, USP 7/0	Naila, Germany
Syringes (1 ml)	Braun, Germany
Syringes (2 ml, 5 ml, 10 ml, 20 ml)	Terumo, Belgium

3.1.4 Miscellaneous reagents, media and buffers

Table 3: List of miscellaneous reagents and suppliers

Reagent	Supplier
Accutase	PAA, Austria
Bovine serum albumin (BSA)	Serva, Germany
Complete mini EDTA-free Protease Inhibitor Cocktail	Roche, Germany
DAPI Vector	Burlingame, USA
1,10-dioctadecyl-3,3,3030-tetramethylindocyanide perchlorate (DiI)	Life Technologies, USA
Eosin G-Solution 0,5%	Roth, Germany
EDTA	Bohringer Mannheim, USA

Materials and Methods

Fetal calf serum (FCS)	PAA, Austria
Gentamycin	Gibco, Germany
Hank´s Buffered Saline Solution (HBSS)	Gibco, Germany
Hematoxylin	Applichem, Germany
Hepes	Gibco, Germany
Human serum	Innovative Research, USA
Isoflurane	Abbott, Germany
Ketamine	CEVA, Germany
LDL	Calbiochem, USA
L-Glutamine	PAA, Austria
Lysis Buffer 10 x	Cell Signaling, USA
Mounting Medium with DAPI	Laboratories Inc., USA
Mouse serum	Sigma-Aldrich, USA
Nile Red	Sigma-Aldrich, USA
Oil-Red-O	Sigma-Aldrich, USA
Paraformaldehyde	Sigma-Aldrich, USA
PBS	PAA, Austria
Penicillin	PAA, Austria
Picric acid	Sigma-Aldrich, USA
Picrofuchsin solution	Merck Milipore, Germany
Rabbit serum	Sigma-Aldrich, USA
Resorcin-Fuchsin solution	Carl Roth, Germany
RNAlater	Ambion Life Technologies, Germany
RPMI 1640	Sigma-Aldrich, USA
Sirius Red	Polysciences, Inc., USA
Tissue Tek® O.C.T compound	Sakura Finetek Europe B.V., Netherland
Vectashield mounting medium w/wo DAPI (4',6-diamidino-2-phenylindol)	Vector Laboratories, Inc., USA
Vitro-Clud	Augenbrinck, Germany
Xylazine	Medistar, Germany

Table 4: Preparation of buffers, solutions and media

Buffer/ Solutions/ Medium	Composition
ASDCL solution	50 ml PBS with 0.4 ml hexazoniumsolution, adjust pH to 6.58 and add 1 ml Naphtol-AS-D Chloroacetate solution
Antibody diluting solution	PBS containing 10% blocking solution
Anesthesia	0.05 ml Xylazine (final dose: 10 mg/kg), 0.1 ml Ketamine (final dose: 100 mg/kg) and 0.85 ml 0.9% sodium chloride
Blocking solution	PBS containing 1% bovine serum albumin (BSA) and 2.5% horse serum

27

Buffer A	10 mM Hepes pH 7.8, 1.5 mM $MgCl_2$, 0.5 mM DTT and freshly added 1× Complete EDTA-free protease inhibitor cocktail
Buffer B	20 mM Hepes pH 7.8, 420 mM NaCl; 1.2 mM $MgCl_2$, 0.2 mM EDTA, 25% glycerol, 0.5 mM DTT and freshly added 1× Complete EDTA-free protease inhibitor cocktail
FACS staining buffer	2% mouse serum, 2% human serum, 2% rabbit serum, 2% BSA in PBS
Hank's complete solution	1 x HBSS containing 0.3 mM EDTA, 0.1% BSA in Millipore water
L929 Culturing Medium	RPMI 1640 with L-Glutamine and 10% FCS, 5 mM Hepes, 1% Penicillin
Macrophage Culturing Medium	RPMI 1640 with L-Glutamine and 10% FCS, 10 mM Hepes, 100 U/mL Gentamycin and 15% LCM (L929-conditioned-medium)
Nile Red Working Solution	Dilute Nile Red stock solution with 75% glycerin to an end concentration of 2.5 µg/ml. Both stock and working solutions should be kept dark and at 4°C. (Concentration Nile Red stock solution 500 µg/ml, dissolved in aceton)
Paraformaldehyde (PFA) fixation solution	4% PFA, 5% sucrose and 0.02 M EDTA in PBS (pH 7.4)
Red blood cell lysis buffer	0.8% NH_4Cl, 10 mM $KHCO_3$ and 0.1 mM EDTA in Millipore water (pH 7.4)
Sirius Red solution	0.1% Sirius Red in picric acid
Sodium citrate cooking buffer	12.6 ml of 0.1 M citric acid, 57.4 ml of 0.1 M sodium-citrate dehydrate and 0.35 ml Tween20 dissolved in 630 ml distilled water
Vitro-Clud mounting medium	Vitro-Clud in xylene
Weigert's A solution	10 g hematoxylin, 1000 ml 96% ethanol
Weigert's B solution	40 ml 29% ferric-chloride-solution, 950ml distilled water, 7.5 ml 37% HCl

3.1.5 Antibodies, cytokines, endotoxins and inhibitors

Table 5: List of cytokines, endotoxins and inhibitors

Cytokine	Manufacturer
Murine Tnf-α	Peprotech, USA
LPS	Sigma Aldrich, USA
Cytochalasin D (CytD)	Abcam, UK

Table 6: List of antibodies

Antibody Target	Specificity	Conjugate	Application	Manufacturer
Cd115	Monocytes, Macrophages	PE	FC	eBioscience, USA
Cd11b	Monocytes, Neutrophils, Macrophages	FITC	FC	BD Biosciences, USA
Cd4	T helper cells	FITC	FC	eBioscience, USA
Cd3	T-cells	APC	FC	BD Biosciences, USA
Cd45	Leukocytes	APC-Cy7	FC	BD Biosciences, USA
Cd8a	Cytotoxic T-cells	PE-Cy7	FC	eBioscience, USA
Gr1	Monocytes, Neutrophils	PerCP	FC	eBioscience, USA
Cd11c	Dendritic cells	Pe-Cy7	FC	eBioscience, USA
Cd19	B-cells	PerCP	FC	BD Biosciences, USA
MHCII	Dendritic cells, plasmacytoid dendritic cells, recheck datasheet, as also on other cell types (eg macrophages)	FITC	FC	BD Biosciences, USA
Cd62L	Naive T-cells, central memory T-cells	FITC	FC	BD Biosciences, USA
Cd44	Effector memory T-cells, central memory T-cells	PerCP	FC	eBioscience, USA
Cd25	Regulatory T-	PE	FC	BD Biosciences,

	cells, B-cells			USA
440c	Plasmacytoid dendritic cells	AF647 (APC)	FC	eBioscience, USA
F4/80	Macrophages	APC	FC	eBioscience, USA
FoxP3	Regulatory T-cells	APC	FC	eBioscience, USA
Mac2	Macrophages	Purified	IFS	Cedarlane, Canada
Sma	Smooth muscle cells	Purified	IFS	Dako, Denmark
Cd3	T-cells	Purified	IFS	AbD Serotec, USA
Goat IgG	Goat IgG	Cy3	IFS	Jackson ImmunoResearch, USA
Rat IgG	Rat IgG	FITC	IFS	Jackson ImmunoResearch, USA
Mouse IgG	Mouse IgG	Cy3	IFS	Jackson ImmunoResearch, USA

3.1.6 Assay kits

Table 7: List of assay kits

Assay	Supplier
Bradford Quick Start Protein Assay	BioRad, Germany
cDNA SuperScript Synthesis Vilo kit	Life Technologies, USA
Cobas Enzymatic Assay cholesterol + triglyceride kit	Roche, Germany
Cytokine Bead Array (CBA) Mouse Inflammation Kit	BD Biosciences, USA
DNase, RNase-free	Qiagen, Germany
In situ Death Detection kit	Roche, Germany
Mcp1 ELISA	R&D Systems, USA
mirVana RNA Isolation kit	Ambion Life Technologies, USA
PathScan Phospho-Histone H3 Sandwich ELISA kit	Cell signaling, USA
PhosphoTracer IKKα (pS176/180) + total IKKα ELISA kit	Abcam, UK
TaqMan MicroRNA Assay	Ambion Life Technologies, USA
TransAM NF-κB p65 ELISA	Active Motif, the Netherlands

3.1.7 Primers

Table 8: List of primers

Primer name	Sequence	Use	Supplier
Ikkα Wildtype	Primer 1*: 5´-GGTTTGTAAAAACATTGGTACCTTTT* and Primer 2: *5´-CAATGTTCCCACAAAAGATGTACAGAGACT*	Genotyping PCR Primers	Sigma Aldrich, USA
Ikkα^{AA/AA} Mutant	Primer 1: 5´-CCTCTCAGTGGCTCACCTTT and Primer 2: 5´-CAATGTTCCCACAAACGCTGTACAGAGCGC	Genotyping PCR Primers	Sigma Aldrich, USA
β-actin	5'-*CAACGAGCGGTTCCGATG* and 5'-*GCCACAGGATTCCATACCCAA*	SYBR Green qPCR	Sigma Aldrich, USA
Ikkα	5'-*CCTCTCAGTGGCTCACCTTT* and 5'-*CAATGTTCCCACAAAAGATGTACAGAGACT*	SYBR Green qPCR	Sigma Aldrich, USA
Ikkα^{AA/AA}	5'-*CCTCTCAGTGGCTCACCTTT* and 5'-*CAATGTTCCCACAAACGCTGTACAGAGCGC*	SYBR Green qPCR	Sigma Aldrich, USA
Il-6	5'-*ATGGATGCTACCAAACTGGAT* and *5´-TGAAGGACTCTGGCTTTGTCT*	SYBR Green qPCR	Sigma Aldrich, USA
Vcam-1	5'-*TGCCGAGCTAAATTACACATTG* and *5´-CCTTGTGGAGGGATGTACAGA*	SYBR Green qPCR	Sigma Aldrich, USA
18S-Rna	5'-*CGGACAGGATTGACAGATTG* and *5´-CAAATCGCTCCACCAACTAA*	SYBR Green qPCR	Sigma Aldrich, USA
Gapdh	*5´-ATTGTCAGCAATGCATCCTG* and *5´-ATGGACTGTGGTCATGAGCC*	SYBR Green qPCR	Sigma Aldrich, USA

The following targets (chuk/ikkα, gapdh, hprt-1, 18S-rna, ccl-19, ccr7, mmp-3-9-13, mir-23a, mir-425, mir-301a/b, let7b, mir-16, mir-152, sno-135 and mir-429) were analysed using Taqman real-time PCR (Life Technologies, USA).

3.1.8 Software

Table 9: List of software

Software	Supplier
Diskus	Hilgers, Germany
FACSDiva	BD Biosciences, USA
FlowJo	Treestar, USA
GraphPad Prism 5	GraphPad Software, USA
Image J	National Institutes of Health, USA

3.2   Methods

3.2.1 Mouse experiments

3.2.1.1   Organ isolation

Eight-weeks old female $Ikk\alpha^{AA/AA}Apoe^{-/-}$ and littermate $Apoe^{-/-}$ mice were fed a high-fat diet containing 21% fat and 0.15% cholesterol (Atromin) for 8 or 13 weeks, respectively, depending on the experimental setup. In some experiments a normal chow diet control group was included. On time of organ isolation, the mice received Ketamin/Xylazin anesthesia and the blood was withdrawn by cardiac puncture, after which the mouse was perfused with 10 ml PBS.

Tissue needed for protein isolation was harvested and stored in ice-cold PBS on ice until further processed (chapter 3.2.4.1). Protein extraction was performed from aortic root, thoracic aorta and aortic arch. If the tissue was needed for RNA isolation, the mouse was perfused with 5 ml RNAlater. Afterwards the tissue was harvested and stored in RNAlater until further processed (chapter 3.2.3.2). RNA was isolated from aortic root, thoracic aorta, aortic arch and carotid arteries.

Tissue needed for cell isolation and subsequent flow cytometric analysis was only perfused with PBS and stored in Hank´s complete (3.2.4.1).

If the tissue was used for atherosclerotic lesion analysis, the mouse was additionally perfused with 10 ml 4% PFA. The extent of atherosclerosis was assessed in aortic root and thoraco-abdominal aorta by staining for lipid deposition with Oil-red-O (3.2.5.2) and in the brachiocephalic artery (BCA) by Elastica-Van-Gieson staining. The relative content of macrophages, neutrophils, Cd3$^+$ T-cells,

SMCs and apoptotic cells was determined by histochemical and immunofluorescent staining (all described in chapter 3.2.5).

The BCA was fixed overnight in 4% PFA at 4°C, dehydrated and then embedded in paraffin. Within a standardized distance (0 to 500 µm) from the bifurcation, serial 5 µm transversal sections from the paraffin-embedded carotid arteries were collected on glass microscopy slides by cutting with a microtome.

The aortic root was fixed overnight in 4% PFA at 4°C, embedded in TissueTek and serial 5 µm transversal sections were made and collected on SuperFrost glass microscopy slides by cutting with a cryotome.

The aorta was fixed overnight in 4% PFA at room temperature. The next day the aorta was opened longitudinally and fixed on a rubber-coated microscopy slide with the endothelium facing upwards.

3.2.1.2   Bone marrow transplantation model

Bone marrow (BM) cells from $Ikk\alpha^{AA/AA}Apoe^{-/-}$ mice and control $Ikk\alpha^{+/+}Apoe^{-/-}$ littermates were isolated from femur and tibia under sterile conditions. The cells were subsequently administered to female C57BL/6 $Apoe^{-/-}$ recipient mice (3×10^6 cells/mouse) by lateral tail vein injection one day after a lethal dose of whole-body irradiation (2×6.5 Gy). After four weeks of recovery, the success of the transplantation was analysed with help of real-time quantitative PCR analysis.

In order to determine the degree of chimerism in the bone marrow-transplanted mice, the mutated $Ikk\alpha^{AA}$ allele was quantified relatively to the wild-type $Ikk\alpha$ allele in genomic DNA isolated from blood cells. Real-time PCR was performed using the Maxima SYBR Green qPCR Mastermix (Fermentas) using specific primer pairs for $Ikk\alpha$, $Ikk\alpha^{AA/AA}$ and β-actin as a reference gene. The method was validated by analyzing a standard curve using genomic DNA from $Ikk\alpha^{AA/AA}Apoe^{-/-}$ and $Ikk\alpha^{+/+}Apoe^{-/-}$ blood cells, mixed at different ratios.

Once the chimerism was confirmed, the mice received a high-fat diet for either 8 or 13 weeks.

3.2.1.3   Partial ligation model

The partial ligation model is a model to create turbulent flow conditions in the carotid artery. Female mice were subjected to partial ligation of the left carotid artery as described earlier[148]. Mice were anesthetized by intraperitoneal injection of ketamine/xylazine (100 mg/kg ketamine and 10 mg/kg xylazine) anesthesia solution. The shaved area of the frontal neck was disinfected and a ventral midline incision was made in the left lateral side of the neck. The left carotid artery was exposed by blunt dissection using a stereo-microscope (Olympus SZX7). The external (ECA), internal (ICA) and the occipital arteries (OA) were completely ligated using sutures allowing blood outflow only via the superior thyroid artery (STA) (Figure 8). The incision was closed with wound clips. The right (RCA) and left carotid artery (LCA) were harvested for RNA isolation after 1, 7 days and 6 weeks respectively, following perfusion with PBS and RNAlater.
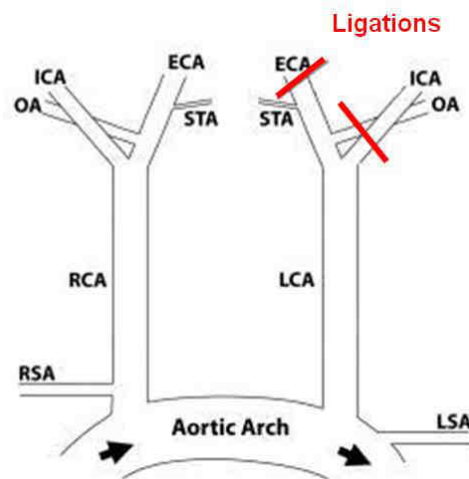
Figure 8: Schematic representation of the partial ligation model. Three branches of the left carotid artery (LCA) get ligated: the external carotid artery (ECA), internal carotid artery (ICA), and occipital artery (OA). The small superior thyroid artery (STA) is left open, so all blood flow from the LCA now runs through the STA under turbulent flow conditions (Figure adapted from Nam, D. et al.[148])

3.2.2 Cell culture

3.2.2.1   Isolation, culturing and stimulation of bone marrow-derived macrophages

The femurs and tibiae from *Ikkα*$^{AA/AA}$*Apoe*$^{-/-}$ and *Apoe*$^{-/-}$ mice were isolated and stored in PBS on ice. Bone marrow was flushed with ice-cold PBS using a 27-G needle under sterile conditions and the bone marrow was resuspended in PBS by repeated

vigorous pipetting. Then the homogenous solution was filtered using a 70 µM cell strainer. The filtered solution was centrifuged, the resulting pellet resuspended in macrophage culture medium and the cells plated on 15 cm untreated culture dishes. Bone marrow-derived macrophages from cryopreserved bone marrow cells were generated as described[149]. Both culturing and stimulation of the macrophages were performed in macrophage cultivation medium, at which the 15% LCM was always added freshly. After 7 days of culturing, differentiated macrophages were used for stimulation experiments and transferred onto untreated 6-well dishes. The cells were left for 24 hours to adhere und were then stimulated with 100 ng/ml LPS, 10 ng/ml mouse Tnf-α or 50 µg/ml mildly oxidized LDL. In all experiments an unstimulated control was included.

3.2.2.2 Generation of L929-conditioned medium (LCM)

Cryopreserved L929 cells were defrosted at 37°C and the cells plated in pre-warmed L929 culture medium in a T-75 flask. Cell were split twice every week with trypsin and subsequently seeded on new T-75 flasks. The cells were expanded for approximately 1 week until enough cells were available to fill 4 T-175. The flasks were filled up with culture medium and the cells left for 11 days at 37°C to incubate. After 11 days the medium was poured off and filtered while the cells were discarded. The filtered L929 conditioned medium (LCM) was aliquoted, flash-frozen and stored at -80°C.

3.2.2.3 Preparation of oxLDL

OxLDL was prepared by oxidation of LDL with a 50 nM copper sulphate solution for 4 hours at 37°C to receive mildly oxidized LDL and overnight for heavily oxidized LDL. The oxidation was stopped by addition of EDTA and afterwards the oxLDL solution was purified over a PD 10 column. The oxLDL solution was kept dark at 4°C and was used for a maximum of 2 weeks.

For lipid uptake experiments heavily oxidized LDL was labelled with Dil. Dil is an orange-red fluorescent lipophilic membrane stain that diffuses laterally to stain the entire cell. The amount of Dil-labeled oxLDL taken up by the macrophages can be measured by flow cytometry. After incubation of 0.5 mg/ml oxLDL with 20 µL of Dil (stock 3 mg/ml in DMSO) overnight at 37°C, the Dil-labelled oxLDL was purified over a PD 10 column and stored at 4°C for a maximum of 2 weeks.

3.2.2.4   Foam cell formation

Foam cells develop from macrophages that take up oxidized lipids such as oxLDL. In order to quantify the uptake of DiI-labelled heavily oxidized LDL by BM-derived macrophages, macrophages were plated on 24-well plates and left to adhere overnight at 37°C. The next day, non-adherent cells were rinsed off with PBS and medium containing 1 µg/ml or 10 µg/ml DiI-oxLDL was added. The actin inhibitor cytochalasin D was used to analyse whether the lipid uptake occurred in an actin-dependent manner. For this set-up, controls were pre-incubated for 1 h with 10 mM cytochalasin D, followed by a stimulation with 10 µg/ml DiI-oxLDL and 10 mM cytochalasin D. The cells were stimulated for 3 or 24 hours, washed with PBS and stained for the macrophage marker F4/80. As control, cells without diI-oxLDL incubation were used to assess background staining resulting from cell autofluorescence of the macrophages. Flow cytometric analysis was performed using a FACSCanto II and the data were analysed using FlowJo software. Data were calculated by subtracting the autofluorescence of the controls from the fluorescence of the diI-oxLDL-treated samples and were expressed as geometric mean fluorescence intensity (gMFI).

To measure the possible cytokine and chemokine secretion from BM-derived macrophages, cells were plated in 6-well plates, left for 24 h to adhere. The next day the macrophages were stimulated with 10 ng/ml murine Tnf-α or 50 µg/ml heavily oxidized LDL. As control, unstimulated cells were included. After 24 h the medium was harvested from the cells, and cytokine and chemokine levels were measured by flow cytometry using a Cytometric Bead Array. In addition, Mcp1 levels were measured using a mouse Mcp1 ELISA.

3.2.3 Molecular methods

3.2.3.1   DNA isolation

Genomic DNA (gDNA) for mouse genotyping was isolated from mouse tail cuts with the Bio Sprinter 96 from Qiagen (Hilden, Germany) according to the manufacturer's protocol.

3.2.3.2   Genotyping for the *Ikkα*^{AA/AA} mutation

DNA was isolated either from blood or mouse tails as described in the previous chapter. Once the DNA concentration was measured and adjusted to 100 ng/µl, a mastermix according to the following composition was made.

Table 10: PCR mastermix for genotyping *Ikkα* mutant (*Ikkα*$^{AA/AA}$) and wildtype allele

Component	Volume	Final Concentration
5x Green Gotaq Flexi buffer	5 µl	1 x
$MgCl_2$	3 µl	3 mM
dNTPs	0.5 µl	0.2 mM
Primer 1	2.5 µl	0.2 µM
Primer 2	2.5 µl	0.2 µM
GoTaq DNA Polymerase	0.13 µl	-
Water	Fill up to 25 µl	-
gDNA	2 µl	-
Total Volume	25 µl	

The primer combinations for detecting the *Ikkα* mutant (*Ikkα*$^{AA/AA)}$ and wildtype allele are given in table 8. Samples as well as controls for Ikkα mutant, wildtype and heterozygote mice were included for testing. The PCR run was designed according to the following conditions described in table 11.

Table 11: PCR run for *Ikkα* genotyping

Step	Temperature	Time
Initial Denaturation	95 °C	10 min
Step 1. Denaturation	95 °C	30 s
Step 2. Annealing	58 °C	30 s
Step 3. Elongation	72 °C	45 s
Final Elongation	72 °C	3 min
Storing	4°C	-
Repeat Step 1-3 in 35 cycles		

The PCR were finally tested on 2% agarose gel at 130 V with 100 bp DNA ladder.

3.2.3.3   RNA Isolation and cDNA synthesis

RNA was isolated from aortic root, arch and thoracic aorta from *Ikkα*$^{AA/AA}$*Apoe*$^{-/-}$ and control mice after 6 weeks of high-fat diet or normal diet. After partial ligation of *Apoe*$^{-/-}$ mice, RNA was isolated from left and right carotid artery. For miR studies

RNA was isolated from aortic root, arch and thoracic aorta from *Apoe*$^{-/-}$ mice after diet conditions, as well as carotid arteries after partial ligation. In all cases the mirVana RNA Isolation kit was used as described by the manufacturer. RNA isolation was followed by digestion of genomic DNA using the RNase-free DNase set according to the manufacturer's protocol.

cDNA for quantitative real-time PCR was reversed transcribed from RNA using the SuperScript cDNA Synthesis Vilo kit. In case of the miR studies the isolated miRs were reverse transcribed into cDNA using the TaqMan miR Reverse Transcription kit. Quantitative real-time PCR for miRs was performed with help of TaqMan miR Assays as described in the manufacturer´s protocol.

3.2.3.4   Quantification of RNA/ DNA

DNA and RNA concentrations and purity were determined by measuring the absorbance at 260 nm (A260) and 280nm (A280) in a spectrophotometer (Nanodrop). Pure DNA or RNA has an A260/A280 ratio of 1.8-2.0 at pH 7.0.

3.2.3.5   Quantitative real-time PCR

Quantitative real-time polymerase chain reaction (qPCR) is a laboratory technique used to amplify, detect and quantify a target DNA molecule. The principle is based on a regular PCR, with the addition that the amplified DNA is detected with help of fluorescent reporters in "real time"[150]. There are basically two main methods for quantitative detection of PCR products. One method is the usage of double-strand binding fluorescent dye as reporter, and the other method is performed with help of fluorescent probe as reporter. In the first method the DNA-binding dye, such as SYBR Green, is unspecific and thereby binds to all double-stranded DNA, causing fluorescence. An increase in DNA product by amplification leads to an increase in fluorescence intensity.

The fluorescent reporter probe only binds to the DNA containing a sequence complementary to the probe sequence. The probe is an oligonucleotide with a fluorescent reporter at one end and a fluorescence quencher at the opposite end of the probe (e.g. Taqman probe). As long as the probe is intact the reporter and quencher stay close to each other, which prevents the emission of any fluorescence. After hybridization of the probe to the complementary DNA sequence the DNA Taq polymerase starts the extension. The 5´endonuclease activity of the DNA Taq

polymerase cleaves the probe during extension, which separates reporter and quencher, thereby releasing the fluorescent reporter and fluorescence can be detected.

An increase of fluorescence over reaction time can be associated with the initial mRNA concentration in both methods. Both methods can be used for relative quantification of gene expression, i.e. relative to the expression of "constantly expressed" housekeeping genes. The quantification is expressed as change in expression compared to a control sample[151].

Quantification and data analysis are done with help of the Ct value. This Ct value is defined as the fractional PCR cycle number at which the reporter fluorescence reaches a threshold fluorescence level, which is (manually) chosen in the exponential region of amplification. With help of a mathematic equation the relative expression level of a target gene can be calculated relative to a sample control. The amount of target gene in the sample is first normalized to a housekeeping gene ($Ct_{target}-Ct_{reference}=\Delta ct$). The next step is to normalize the ΔCt of the sample to the ΔCt of a control sample such as an untreated sample ($\Delta Ct_{sample}- \Delta Ct_{control} = \Delta\Delta Ct$). Finally the relative expression of a target gene is calculated as ($2^{-\Delta\Delta Ct}$)[152].

For this study both the Sybr Green as well as Taqman method were used for quantitative real-time PCR (Primers and Probes listed in chapter 3.1.7.)

At last miR studies were performed for miR-23a, miR-425, miR-301a,b, let7b, miR-16 and miR-152. As reference miRs sno-135 and miR-429 were selected[151]. The miR expression levels were quantified using Taqman miRNA and Taqman universal PCR master mix.

3.2.4 Protein extraction and protein assays

3.2.4.1   Preparation of nuclear extracts and total protein isolation

Nuclear extracts were isolated as previously described[127]. In summary, BM-derived macrophages were washed once with PBS and scraped from the culture dish using PBS with 5 mM EDTA. The cells were centrifuged and the cell pellet was resuspended in 100 µl buffer A and freshly added 1× Complete EDTA-free protease

inhibitor cocktail. After 2 min incubation on ice, 100 µl of buffer A supplemented with 1.28% NP40 was added to the cell suspension and incubated on ice for 10 min. The cells were vortexed for 10 sec and centrifuged for 10 min at 2000 rpm. The supernatant was discarded and the pellet was dissolved in 50 µl buffer B with freshly added Complete EDTA-free protease inhibitor cocktail. The samples were incubated on ice for 30 min with vigorous vortexing every 5 min. Afterwards the samples were centrifuged for 15 min at 4000 rpm. The supernatant, being the nuclear extract, was flash-frozen with liquid nitrogen and the samples were stored at -80°C. The protein concentration was measured using the Quick Start Bradford Protein Assay and then the samples were used for NF-κB p65 DNA-binding ELISA.

Proteins from tissues were isolated at the same day of isolation. After sacrificing the mice and blood withdrawal, the circulatory system was perfused with PBS and the desired tissue was stored in PBS on ice. Then the tissue was added into 1x cell lysis buffer and incubated on ice for 10 min. Afterwards the tissue was homogenized using stainless steel beads in a TissueLyser LT. The tissue was homogenized at 50 Hz for 5 min until all cell clumps were removed. Subsequently the suspension was centrifuged for 10 min at 14,000 x g in a cold microcentrifuge, the supernatant snap-frozen and stored -80°C. Similarly as for the nuclear extracts the protein concentration was determined using the Quick Start Bradford Protein Assay before using the samples for NF-κB p65 ELISA, phospho-histone H3 ELISA, phospho-IKKα and total IKKα ELISA.

3.2.4.2   Flow cytometry

Flow cytometry is used to analyse cells based on their size, granularity and protein expression (by *e.g.* fluorescence-conjugated detection antibodies). In a buffer stream, one cell at a time passes an argon laser, which excites fluorescently labeled cells. Measurements of the size (forward scatter) and granularity (sideward scatter) are independent from the fluorescence signal. Measurement of fluorescence intensity using fluorescence-labelled antibodies was performed to examine and distinguish different cell populations in blood, lymph nodes, spleen, bone marrow and thymus.

In order to examine leukocyte populations in blood samples, the samples first had to undergo red blood cell lysis before staining with specific fluorescence-conjugated antibodies.

Lymph nodes and thymus were grinded and filtered through a 100 µm filter in order to get a homogenous single-cell solution.

Bone marrow from one femur bone was flushed out and the erythrocytes were lysed with erythrocyte lysis buffer in order to prepare the sample for fluorescent staining.

The spleen had to be homogenized similarly as the lymph node and thymus, and subsequently the red blood cells were lysed.

Once a sample was prepared into a homogenous cell solution, the samples were resuspended in FACS staining buffer with specific fluorescence-conjugated antibodies (1:100) and incubated for 30 min on ice, protected from light. Afterwards the cells were washed with Hanks Complete buffer and analysed immediately in a FACS CantoII (BD Biosciences) and evaluated with FlowJo Software (Treestar, Inc, Ashland, OR, USA). As control the fluorescence minus one (FMO) method was used or isotype controls were included. All flow cytometry results were displayed as dot plots showing the logarithmic distribution of the fluorescence intensity or as diagrams demonstrating the change in mean fluorescence intensity (MFI). Cell populations were quantified as percentage of leukocytes or as percentage of the parental subpopulation (e.g. $Cd4^+$ T-cells as percentage of $Cd3^+$ T-cells).

3.2.4.3   Enzyme-linked immunosorbent assay (ELISA)

ELISA (enzyme-linked immunosorbent assay) is an immunological method to detect and quantify the amount of a specific antigen in biological fluids. All ELISAs performed for this study are based on the principle of a sandwich immunoassay. Briefly, a purified capture antibody specific for the antigen of interest is pre-coated onto a microplate. Once samples and standards are added, the antigen of interest, if present, will bind to the capture antibody. After washing to remove unbound proteins, a detection antibody is added, which binds to the captured antigen. So the antigen is bound between the capture and the detection antibody. The detection antibody, or a secondary antibody binding the detection antibody, is either fluorescently labeled or linked to an enzyme that triggers a color change by cleaving a specific substrate. The intensity of the color or fluorescence measured is in proportion to the amount of antigen bound in the initial step. Quantification of the sample values is then performed based on a standard curve.

Nuclear extracts, tissue extracts, mouse sera and cell culture supernatants were analysed for one or more of the following targets: nuclear extracts and tissue protein extracts were analysed for active NF-κB p65 levels with a TransAM NF-κB p65 ELISA. To measure the active NF-κB p65 concentration in the tissue extracts a standard curve was measured using recombinant NF-κB p65 protein. Cell culture supernatants were tested for Mcp-1 with a Mcp-1 ELISA and lastly, tissue protein extracts were analysed for histone 3 phosphorylation levels using a total PathScan Phospho-Histone H3 Sandwich ELISA kit and for total Ikkα and phosphorylated Ikkα levels with the PhosphoTracer IKKα (pS176/180) + total IKKα ELISA kit. For all ELISAs the sample values were corrected for background by incubation with lysis buffer only.

3.2.4.4   Cytokine bead array

Cell culture supernatants and mouse sera were analysed for various cytokines using the BD cytometric bead array "mouse inflammation kit". It simultaneously quantifies 5 different cytokines (Il-6, Il-10, Il-12p, IFN-γ and Tnf) and the chemokine Mcp1 in a single sample. Sample preparation and analysis were performed according to the manufacturer´s protocol.

Briefly, the principle: The bead-based assay contains capture beads which have been conjugated with specific antibodies against the cytokines and chemokine, and which have a specific size for each protein to be quantified. A provided detection reagent, which is a mixture of PE-conjugated antibodies, will bind to bead bound analyte, forming a sandwich complex of capture bead plus analyte plus detection reagent. The intensity of the fluorescent signal of each sandwich complex reveals the concentration of bound analyte. The samples are measured using flow cytometry and the results analysed with help of specific FCAP Array software. The kit provides standards for quantifying cytokine and chemokine concentrations.

The samples were diluted if necessary and both standards and samples were incubated with capture beads and PE detection reagent for 2 h, at room temperature protected from light. The samples and standards were washed, centrifuged and supernatant discarded. The bead pellets were resuspended in wash buffer and the samples and standard were acquired on the flow cytometer. The FCAP Array software helps to create standard curves based on the MFI of the standards for each cytokine/ chemokine in order to quantify sample cytokine/chemokine concentration.

3.2.5 Histochemistry, immunohistochemistry and immunofluorescence

While histochemistry is a branch of histology studying the chemistry of tissues and cells with help of stains, immunohistochemistry (IHC) and immunofluorescence (IF) are techniques used for the detection of antigens on tissues or cells. These antigens can range from amino acids and proteins to infectious agents and specific cellular populations. Instead of using stains for detection, like in histochemistry, IHC and IF use antibodies. IHC/IF are important tools for scientific research and are complementary techniques for the elucidation of differential diagnoses which are not determinable by conventional histochemistry[153].

Within this study the histochemical stainings of Oil-Red O were used for staining lipid depositions in the aortic root and aorta. Chloroesterase staining was used on aortic roots to detect neutrophil content within the atherosclerotic plaques and Sirius red staining to analyse the collagen content. Nile red, as well a histochemical staining, was performed together with fluorescent staining for Mac2, an IF staining for macrophages, to visualize lipid droplets within macrophage foam cells. Last, the histochemical Elastica-van-Gieson staining was performed on BCA to analyse atherosclerotic lesion sizes. Both aortic root and BCA were stained for Mac2 and SMA (staining of SMCs) using IF. Additionally, IF stainings for Cd3$^+$ T-cells and for apoptotic cells (Tunel) were made on aortic root.

In case of the aorta, the whole aorta was stained for Oil-red-O to analyse lipid depositions along the thoraco-abdominal aorta. In case of aortic root 2-3 transversal sections were chosen for staining, in order to establish mean values. Similarly, 10 sections were chosen from BCA (each 40 μm separated) to get mean values of the lesion size and cellular content.

3.2.5.1 Deparaffinization, dehydration and antigen retrieval step

Formalin-fixed, paraffin-embedded tissue sections must be treated to remove the paraffin and unmask the antigen epitopes in preparation for immunohistochemical staining. If these steps are not performed, the antibodies will not have complete access to the tissue and will be unable to bind to the correct epitopes. In case of histochemical stainings the unmasking step is not essential, but still sections need to

be removed from paraffin. Below is a table with the essential steps for paraffin removal.

Table 12: Steps for deparaffinization

Procedure	Time
Xylol	2 x 15 min
100% Isopropanol	2 x 5 min
96% Isopropanol	5 min
70% Isopropanol	5 min
PBS	5 min

In case of paraffin sections which receive histochemical stainings, a subsequent dehydration step is necessary. The table below describes the essential steps.

Table 13: Steps for dehydratation

Procedure	Time
70% Isopropanol	Dip
96% Isopropanol	Dip
100% Isopropanol	Dip
100% Isopropanol	Dip
Xylol	5 min

There are a couple of different antigen retrieval techniques. We used the heat-induced epitope retrieval method by cooking sections in citrate buffer for 20-30 min.

After (immune) histochemical stainings the sections were mounted with Vitroclud mounting medium and sealed with nailpolish, whereas after IF stainings the sections were mounted with Vectashield containing 4',6-diamidino-2-phenylindol (DAPI), which counterstains cell nuclei.

3.2.5.2   Oil-Red-O staining

The extent of atherosclerosis was assessed in aortic roots and on thoraco-abdominal aortas by staining for lipid depositions with 0.5% Oil-red-O. For roots 5 µm transversal sections were used. Aortas were opened longitudinally along the ventral midline, and lesion areas in *en face* preparation were stained. The percentage of lipid deposition was calculated by dividing the stained area by the total surface. The images were made with help of a Leica DM2500 fluorescence microscope and CCD camera and the lesions were quantified with Diskus image analysis.

Table 14: Protocol for Oil-Red-O staining of aortic root and aorta

Procedure	Time
PBS (for roots) Flowing water (for aorta)	5 min dip shortly
60% Isopropanol	10 x dip
0.5% Oil-Red O	15 min
60% Isopropanol	10 x dip
Flowing water	5 min (for root) Shortly (for aorta)
Hemalum	30s (only root)
Flowing water	5 min (only root)
Coverslip with Vectashield mounting medium	For root
Coverslip with glycerin gelantine mounting	For aorta

3.2.5.3 SMA and Mac2 staining

The atherosclerotic plaque in the aortic root and the BCA was analysed for macrophages and SMCs by immunofluorescent co-staining for Mac2 and Sma, respectively, followed by a FITC- or Cy3-conjugated secondary antibody staining. Appropriate IgG antibodies were used as isotype controls. Nuclei were counterstained with DAPI. Images were recorded with a Leica DM2500 fluorescence microscope and CCD camera. The lesion composition was analysed using Diskus Software without prior knowledge of the genotype. A general protocol for iimmunofluorescent staining is given in table 15. In case of Mac2 the primary antibody was rat anti-mouse and the secondary antibody was anti-rat FITC. For SMC staining Sma goat anti-mouse and anti-goat Cy3 was used. Before staining, the BCA was removed from paraffin, and both aortic root and BCA received an antigen retrieval step by cooking the sections in citrate buffer. Both BCA and aortic root were mounted with Vectashield and counter-stained with DAPI after the staining. Quantification of positive cells was made as percentage of all plaque cells and relative to the plaque area.

Table 15: Protocol of immunostaining

Procedure	Time
Cooking in citrate buffer	20 min
PBS (after sections cooled off)	5 min
Blocking solution	30 min
Primary Antibody	Overnight at 4°C
PBS	2 x 5 min
Hemalum	30 s (only root)
Secondary Antibody	1 h, kept cool and dark
PBS	5 min
Vectashield mounting medium with DAPI	-

3.2.5.4   T-cell Cd3$^+$ staining

To analyse the lesion for presence of T-cell lymphocytes, aortic root sections were stained with the primary goat anti-mouse Cd3$^+$ antibody and secondary antibody anti-goat Cy3. The sections were mounted with Vectashield mounting medium with DAPI. Quantification of positive cells was made as percentage of all plaque cells and relative to the plaque area.

3.2.5.5   Tunel/Mac2 Staining

Tunel staining was performed with the in situ death detection kit (TMR red) to visualize apoptotic cells and the double-staining with Mac2 to indicate apoptotic macrophages. The Tunel staining was performed according to manufacturer´s protocol, briefly described in table 16. If a co-staining for Mac2 was made, the sections were first stained for Mac2, followed by Tunel staining.

Table 16: Protocol for In Situ Tunel staining

Procedure	Time
Permeabilize sections in 0.1% Triton X-100 and 0.1% Sodium citrate (2v:1v) on ice	2 min
PBS	5 min
Mix label solution with enzyme solution (take out 100 µl for neg. control from label solution, then mix 50 µl enzyme solution with 450 µl label solution)	-
Label/enzyme solution	15-20 min at room temperature 10 min at 37°C
PBS	2 x 5 min
Vectashield mounting medium with DAPI	-

After the staining the sections were stored protected from light at 4°C. The images were taken at the same day of labeling to prevent loss of staining intensity due to the fluorescence instability. Quantification of apoptotic cells and apoptotic macrophages was made as percentage of plaque cells.

3.2.5.6   Chloroesterase staining

The chloroesterase staining is a histochemical staining to visualize neutrophils. Thereby the naphthol AS-D chloroacetate within the ASDCL solution is enzymatically hydrolyzed by "specific esterase", specific for cells of granulocytic lineage, liberating a free naphthol compound. This then couples with a diazonium compound, forming highly colored deposits at sites of enzyme activity. Aortic roots were stained to analyse the neutrophil content in the atherosclerotic lesions.

Table 17: Protocol for chloroesterase staining

Procedure	Time
PBS	5 min
ASDCL Solution	80 min
Flowing water	-
Hemalum	dip 8 x times
Flowing water	-
Distilled water	5 min
Mounting with Vitroclud	-

3.2.5.7 Elastica-van-Gieson staining

To analyse the atherosclerotic plaque size in the BCA 10 sections per mouse (each 40 µm apart) were stained using the Elastica-van-Gieson (EVG) stain at room temperature. Images were recorded with a Leica DM2500 fluorescence microscope and CCD camera. The lesion area, which is the area between lumen and interna elastica lamina were measured and quantified using Diskus Software.

Table 18: Protocol of EVG staining

Procedure (after deparaffinization)	Time
Distilled water	5 min
Resorcin-Fuchsin solution	15 min (60°C)
Distilled water	Dip
80% ethanol	Dip
Distilled water	-
Weigert's A + B solution	5 min
Distilled water	Dip
0.5% HCl-alcohol	Dip
Distilled water	-
Picrofuchsin	3 min
Distilled water	Dip
Dehydration step, mounting with Vitroclud	

3.2.5.8 Sirius Red staining

To distinguish the collagen content in the aortic root a Sirius Red staining was used. Sirius Red has been shown to be able to detect all types and species of collagen, such as type I to V collagen. Images were recorded with a Leica DM2500 fluorescence microscope and CCD camera. The collagen content was analysed by Image J software.

Table 19: Protocol of Sirius Red staining

Staining Procedure	Time
0.1% Sirius Red staining solution	1h
1% HCl	2 min
Flowing water	Shortly
Coverslip with Vitroclud mounting medium	-

3.2.5.9 Nile Red/ Mac2 staining

Nile Red primarily stains hydrophobic structures and is similar as the Oil-Red- O staining used in lipid staining, with that difference that it is a fluorescent stain[154]. In order to detect foam cells a fluorescent co-staining of Nile Red and Mac2 was performed, and additionally the sections were mounted with DAPI to stain the nuclei. The images were taken with a Leica DM2500 fluorescence microscope and CCD camera, and analysed with Image J.

In order to perform the double-staining the sections first need to be stained for Mac2 (see chapter 3.2.5.3). After the Mac2 staining is complete, 100 µL of Nile Red/Glycerin working solution was added on top of the tissue. After 5 min of incubation in the dark, the sections were washed in PBS and mounted with mounting medium containing DAPI. The images were taken at the day of staining, due to the instability of the Nile Red fluorescence.

3.2.5.10 Lesion classification

After HE staining, atherosclerotic lesions were classified according to their severity. Three categories were distinguished according to their phenotype: (1) early lesions, containing only foam cells, (2) intermediate-type lesions, presenting foam cells, some necrosis and a fibrotic cap formation, (3) advanced lesions, showing extended fibrosis and necrosis and infiltration of the plaque into the media.

3.2.6 Quantification of plasma lipids

Plasma cholesterol and triglyceride levels were quantified using enzymatic assays according to the manufacturer's protocol (Cobas enzymatic assay, Roche). The plasma and standards were diluted with 0.9% NaCl and after adding a chromogenic reagent for 30 minutes at room temperature, the absorbance in plasma was measured at a wavelength of 505 nm by a 96-well plate reader.

3.2.7 Data illustration and statistical analysis

Data are represented as mean ± SEM and analysed by students t-test, 1-way Anova with Newman-Keuls post-test, Tukey´s post-test or Kruskal-Wallis test with Dunn´s post-test. Also the 2-way ANOVA with Bonferroni post-test was used. Differences of

p<0.05 were considered to be statistically significant. All data was processed and displayed with GraphPad Prism 5 software.

4.   Results

The first part will describe experiments performed for the investigation of the haematopoietic role of IKKα in atherosclerosis. For this a bone marrow (BM)-transplantation model was used, in which atherosclerosis-prone *Apoe$^{-/-}$* mice were lethally irradiated to demolish their own bone marrow and transplanted with bone marrow from *Ikkα$^{AA/AA}$Apoe$^{-/-}$* (Ikkα mutant) and *Ikkα$^{+/+}$Apoe$^{-/-}$* (Ikkα wildtype) mice. This model ensured me to only investigate the function of IKKα in haematopoietic or BM-derived cells, in atherosclerosis. After transplantation the mice were fed a high-fat diet for 8 or 13 weeks, and the atherosclerotic lesion size was analysed in aortic root, the BCA and the thoraco-abdominal aorta. Lesion composition and classification were studied in aortic roots. Additionally the haematopoietic profile was examined in blood, bone marrow, spleen, lymph nodes and thymus. A general blood count was made and serum was used for lipid profiling and cytokine measurements. Furthermore, I analysed the function of Ikkα in macrophage activation and foam cell formation in *in vitro* studies.

The second part of this chapter describes experiments carried out to study the global contribution of IKKα in atherosclerosis. Here, *Ikkα$^{AA/AA}$Apoe$^{-/-}$* and *Ikkα$^{+/+}$Apoe$^{-/-}$* mice were set on a high-fat diet for 13 weeks. Similarly as for the first study, the atherosclerotic lesion size was analysed in aortic root, BCA and thoraco-abdominal aorta. Lesion composition was examined both in the aortic root as well as in the BCA. Lipid levels and cytokine levels in serum were quantified and whole blood count was performed. Quantitative real-time PCR studies were done to investigate Ikkα expression profiles:

- under turbulent flow conditions
- in a comparative study of aortic root, arch and thoracic aorta after normal and high-fat diet conditions

Furthermore, expression profiling of inflammatory genes was performed in *Ikkα$^{AA/AA}$Apoe$^{-/-}$* and *Ikkα$^{+/+}$Apoe$^{-/-}$* mice after normal and high-fat diet, comparing aortic root *vs* arch and thoracic aorta. To examine downstream signalling effects of the *Ikkα^{AA}* mutation, histone H3 phosphorylation levels and NF-κB p65 activity were measured in aortic root *vs* arch and thoracic aorta from *Ikkα$^{AA/AA}$Apoe$^{-/-}$* and *Ikkα$^{+/+}$Apoe$^{-/-}$* mice, both after normal as well as high-fat diet. Additionally, distinct miR

expression profiles were studied in order to distinguish whether Ikkα expression could be controlled by miRs. Finally total and active (phosphorylated) Ikkα levels were examined in aortic root *vs* arch and thoracic aorta of *Apoe*$^{-/-}$ mice after normal and high-fat diet.

4.1 Role of haematopoietic Ikkα in atherosclerotic lesion formation and its effects on leukocyte populations and functions related to atherosclerosis

Blood cells are derived from haematopoietic stem cells (HSCs), which reside in the bone marrow. HSCs are self-renewing, which means that when they proliferate some of their daughter cells remain as HSCs, so the pool of stem cells does not become depleted. The other daughter cells of HSCs differentiate into common myeloid (CMP) and common lymphoid progenitor (CLP) cells. While CMPs are progenitor cells for erythrocytes, thrombocytes, monocytes, neutrophils and dendritic cells, CLPs are precursor cells for T- and B-cells (Figure 9). As mentioned in the introduction, leukocytes play a key role in the development and progression of atherosclerosis and therefore I aimed to investigate whether the loss of Ikkα function in haematopoietic cells would influence leukocytosis and atherogenesis.
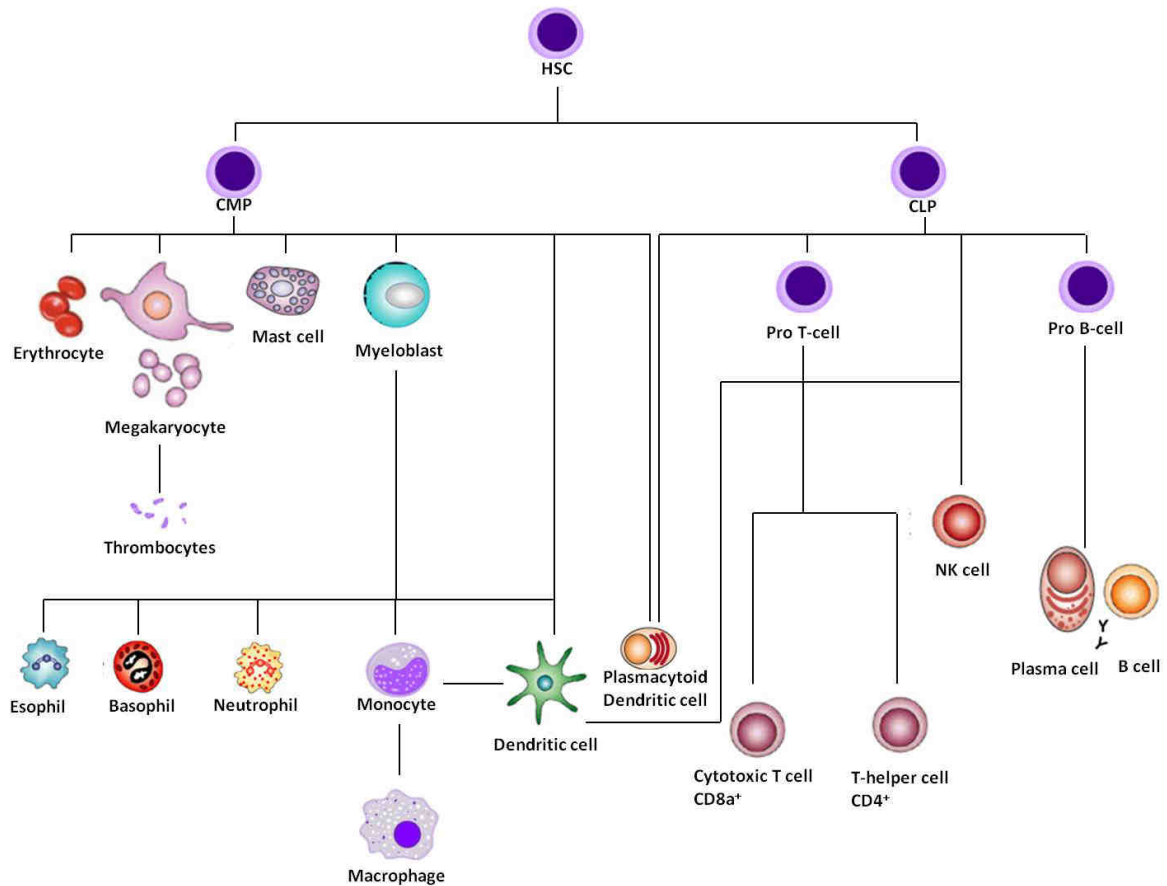
Figure 9: Haematopoiesis. A schematic illustration showing the development of different blood cells from haematopoietic stem cells (HSCs). CMP=common myeloid progenitor cell, CLP=common lymphoid progenitor cell, NK=natural killer cell.

4.1.1 Analysis of transplantation efficiency

To investigate whether engraftment of transplanted $Ikk\alpha^{AA/AA}Apoe^{-/-}$ bone marrow cells was successful, a quantitative real-time PCR was performed to quantify the mutant $Ikk\alpha^{AA}$ allele *vs* the wildtype $Ikk\alpha$ allele in isolated genomic DNA from blood withdrawn from the bone marrow (BM)-transplanted mice, 4 weeks after transplantation. Relative quantification was performed using a standard curve generated from genomic DNA from $Ikk\alpha^{AA/AA}Apoe^{-/-}$ and $Ikk\alpha^{+/+}Apoe^{-/-}$ blood cells, mixed at different ratios.

In a first transplantation study real-time PCR showed that on average 96.1% (±1.2) of leukocytes carried the mutant $Ikk\alpha^{AA/AA}$ allele, confirming a successful transplantation. In a second transplantation study, engraftment was equally efficient, showing the mutant $Ikk\alpha^{AA}$ allele to be present in 94.3% (± 2.7) of blood leukocytes.

4.1.2 Bone marrow-specific loss of Ikkα activity influences leukocyte populations

Apoe^{-/-} mice transplanted with *Ikkα*[AA/AA]*Apoe*^{-/-} vs *Ikkα*^{+/+}*Apoe*^{-/-} BM received a high-fat diet for 13 weeks. After sacrificing the mouse, blood and organs were isolated. Haematopoietic profiling was performed by flow cytometric analysis and different leukocyte subsets were examined with help of fluorescent antibody stainings. B-cells were identified as $Cd45^+Cd19^+$; T-cells as $Cd45^+Cd3^+$; naive T-cells as $Cd44^{low}Cd62L^{high}$ T-cells; effector memory T-cells as $Cd44^{high}Cd62L^{low}$ T-cells; central memory T-cells as $Cd44^{high}Cd62L^{high}$ T-cells; regulatory T-cells (T_{reg} cells) as $Cd4^+Cd25^+Foxp3^+$ T-cells; neutrophils as $Cd45^+Cd115^-Gr1^{high}$; monocytes as $Cd45^+Cd115^+$; conventional DCs (cDCs) as $Cd45^+Cd11c^+MhcII^+$; and pDCs as $Cd45^+Cd11c^+Cd11b^-440c^+$.

As Kaisho et al. reported an essential function of Ikkα in B-cell development[155], B-cell levels were analysed in blood, bone marrow and lymphoid organs. Interestingly, *Ikkα*[AA/AA]*Apoe*^{−/−} bone marrow chimeras showed indeed a significantly reduced $Cd19^+$ B-cell population in peripheral blood. A similar decrease in B-cell number was seen in BM and lymph nodes, whereas no difference was observed in the splenic B-cell population.

Meanwhile, blood and lymph nodes of *Ikkα*[AA/AA]*Apoe*^{−/−} transplanted mice displayed more $Cd3^+$ T-cells among the leukocyte population, whereas $Cd3^+$ T-cell levels in spleen were unaltered. No changes in the relative proportions of cytotoxic $Cd8^+$ T-cells and $Cd4^+$T-helper cells were observed in blood or lymphoid organs (Figure 10).
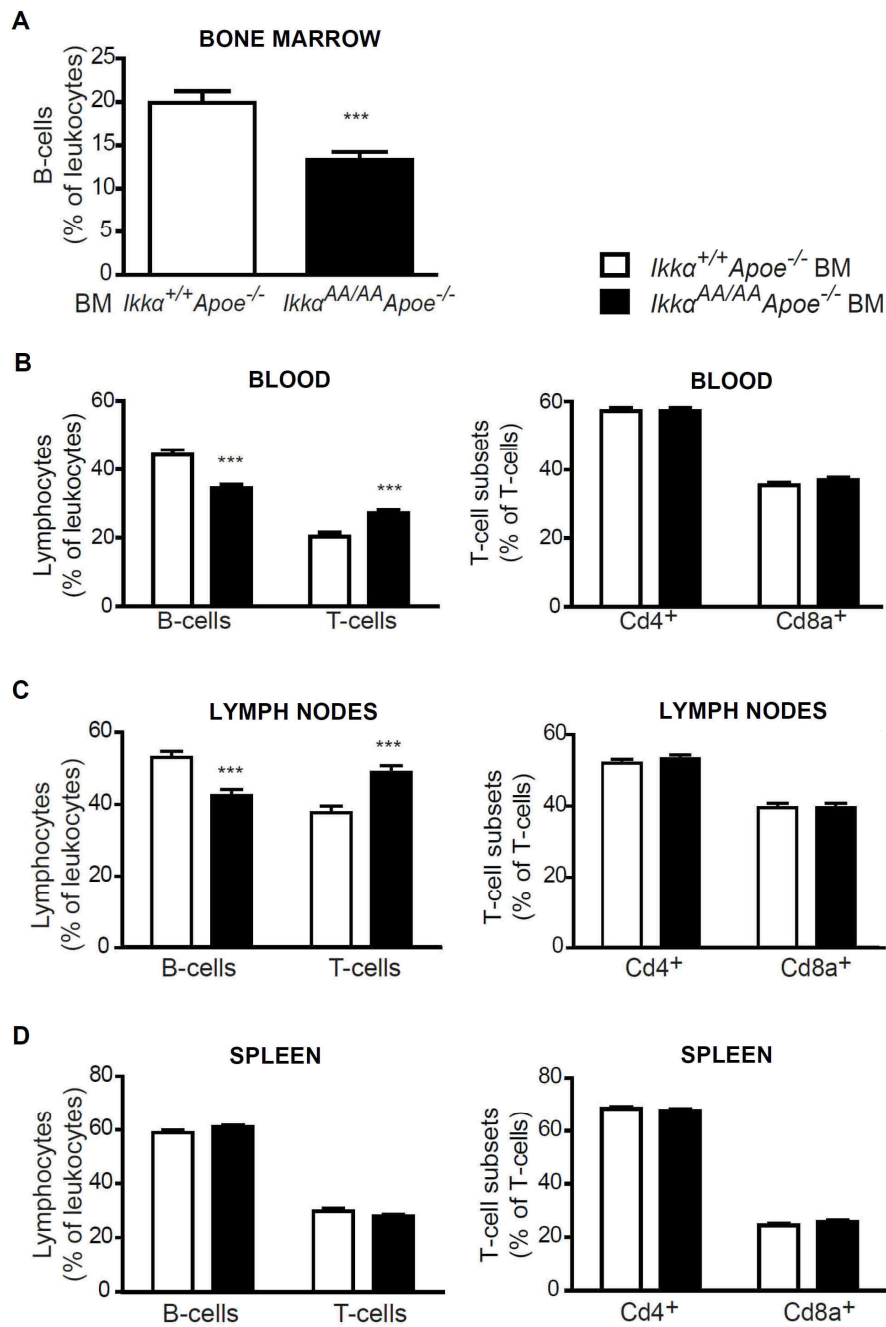
Figure 10: Reduced B-cell and increased T-cell population in *Ikkα$^{AA/AA}$Apoe$^{-/-}$ transplanted mice. FACS analysis of Cd45$^+$ Cd19$^+$ B-cell population in bone marrow **(A)** and of Cd3$^+$ T-cells with Cd8$^+$ and Cd4$^+$ T-cell subsets in blood **(B)**, lymph nodes **(C)** and spleen **(D)** of bone marrow chimeras after 13 weeks of high-fat diet. All graphs represent the mean ± SEM (n=18-19); 2-tailed t-test, ***$p<0.001$.

Also other T-subsets were analysed, such as T$_{regs}$, naive T-cells, effector memory T-cells and central memory T-cells. T$_{reg}$ levels were found to be significantly reduced among the Cd3$^+$ T-cell population in peripheral blood, thymus and secondary lymphoid organs of *Ikkα$^{AA/AA}$Apoe$^{-/-}$ BM-transplanted mice. The T$_{reg}$ frequency was also considerably decreased among Cd45$^+$ leukocytes in blood and

spleen of the *Ikkα*[AA/AA]*Apoe*^{−/−} BM chimeras. However, this was not observed in the lymph nodes (Figure 11).
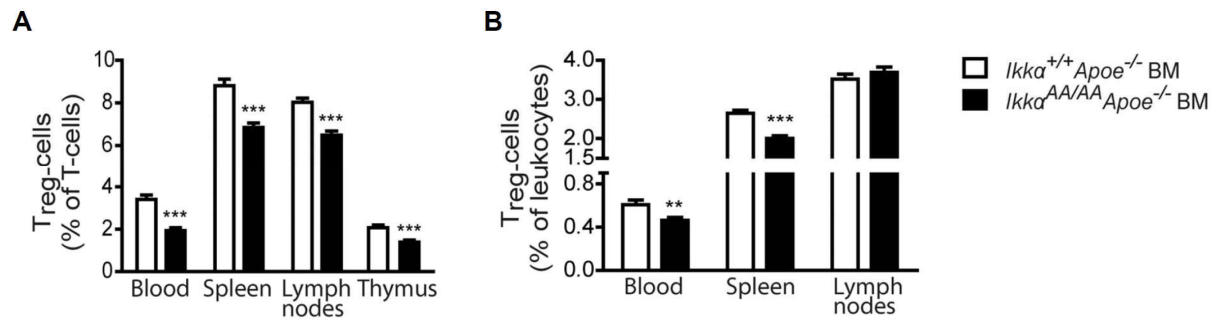
Figure 11: Decrease of T$_{regs}$ in *Ikkα*[AA/AA]*Apoe*^{−/−} BM chimeras. FACS analysis of T$_{regs}$ relatively to Cd45^{+} leukocytes **(B)** and Cd3^{+} T-cells **(A)** in blood, thymus and secondary lymphoid organs of *Apoe*^{−/−} mice transplanted with *Ikkα*[AA/AA]*Apoe*^{−/−} and *Ikkα*^{+/+}*Apoe*^{−/−} BM after 13 weeks of high-fat diet. All graphs represent the mean ± SEM (n=18-19); 2-tailed t-test, **$p<0.01$, ***$p<0.001$.

Additionally, the effector memory T-cell population was significantly diminished in spleen and lymph nodes of *Ikkα*[AA/AA]*Apoe*^{−/−}-transplanted mice, whereas the naive T-cell population displayed a significant increase. Also, the central memory T-cell population was significantly decreased among T-lymphocytes and total leukocytes in spleen. In lymph nodes, central memory T-cells were unaltered among Cd3^{+} T-cells, but displayed increased levels among Cd45^{+} leukocytes (Figure 12).
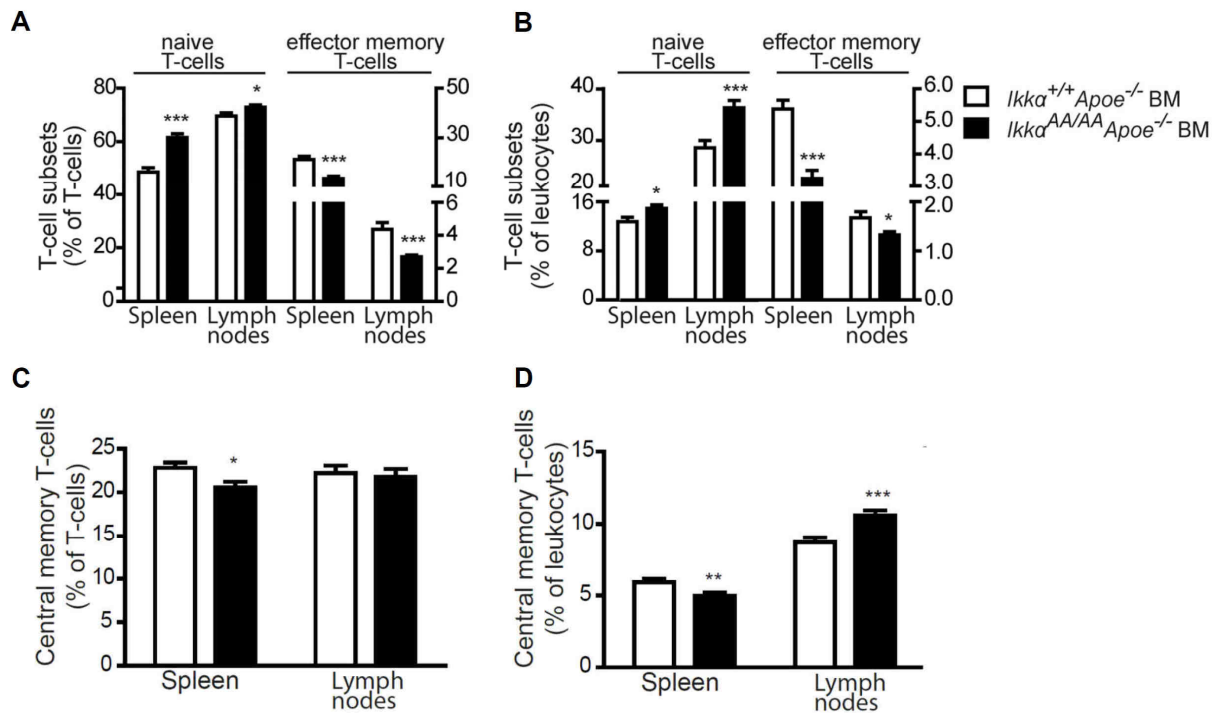
Figure 12: *Ikkα^AA/AA Apoe^-/-* BM chimeras have less effector memory T-cells, but more naive T-cells in spleen and lymph nodes. Splenic central memory T-cells are decreased, whereas lymph nodes display an opposite effect. Shown is flow cytometric analysis of naive, effector memory **(A,B)** and central memory T-cell **(C,D)** subsets in spleen and lymph nodes from *Apoe^-/-* mice transplanted with *Ikkα^AA/AA Apoe^-/-* or *Ikkα^+/+ Apoe^-/-* BM after 13 weeks of high-fat diet. Data are represented as percentage of Cd3^+ T-cells **(A,C)** and as percentage of Cd45^+ leukocytes **(B,D)**. Graphs represent the mean ± SEM (n = 18–19), 2-tailed t-test, *p<0.05, **p<0.01, ***p<0.001.

Flow cytometric analysis of dendritic cells showed comparable frequencies of Cd11c^+MhcII^+ cDCs and Cd11c^+Cd11b^−440c^+ pDCs in spleen. Nonetheless, expression of the activation marker MhcII was significantly reduced on splenic pDCs of *Ikkα^AA/AA Apoe^-/-* BM chimeras (Figure 13). Furthermore, levels of Cd115^−Gr1^+ neutrophils, Cd115^+ monocytes and both Gr1^high and Gr1^low monocyte subsets in peripheral blood were not altered (Table 20).
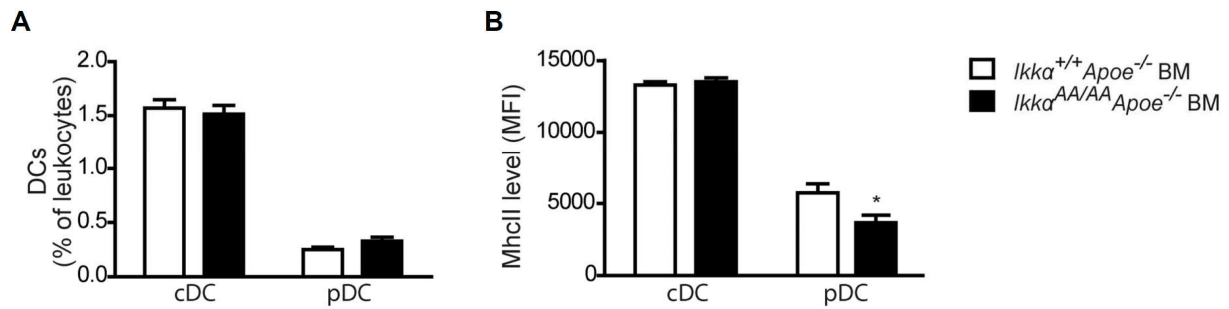
Figure 13: Levels of cDCs and pDCs are unaltered in *Ikkα^AA/AA^Apoe^-/-* BM chimeras. Shown is flow cytometric analysis of splenic cDCs and pDCs and surface expression of MhcII **(B)**. Data are represented as percentage of Cd45^+ leukocytes **(A)**. Graphs represent the mean ± SEM (n = 18–19), 2-tailed t-test, *p<0.05.

Table 20: Monocyte, monocyte subsets and neutrophil population in peripheral blood.

	Ikkα^+/+^Apoe^-/- BM chimeras	*Ikkα^AA/AA^Apoe^-/-* BM chimeras
Monocytes (% of leukocytes)	7.9 ± 0.5	8.7 ± 0.6
Gr1^high^ monocytes (% monocytes	66.0 ± 2.0	68.1 ± 2.7
Gr1^low^ monocytes (% monocytes)	5.2 ± 0.3	5.7 ± 0.3
Gr1^high^ monocytes (% leukocytes)	29.8 ± 2.1	26.9 ± 2.4
Gr1^low^ monocytes (% leukocytes)	2.4 ± 0.3	2.5 ± 0.3
Neutrophils (% of leukocytes)	19.0 ± 1.3	20.4 ± 1.2

These data indicate an important role for Ikkα kinase activity in haematopoiesis, with reduced B-cells and T_regs lymphocytes upon haematopoietic expression of an Ikkα mutant that cannot be activated.

4.1.3 Haematopoietic Ikkα mutation does not alter atherogenesis

Following identification of the importance of Ikkα for lymphocyte populations, the effect of the *Ikkα^AA^* mutation on atherosclerotic lesion formation was studied. After 13 weeks of high-fat diet, lipid levels were measured in serum of *Ikkα^AA/AA^Apoe^−/−* and *Ikkα^+/+^Apoe^−/−* BM chimeras, and the extent of atherosclerosis was analysed in the aorta, the BCA and aortic root. Whereas body weight and serum triglyceride values were similar, cholesterol levels were significantly increased in *Ikkα^AA/AA^Apoe^−/−* vs *Ikkα^+/+^Apoe^−/−* BM-transplanted *Apoe^−/−* mice. This could be attributed to an increase in very low-density lipoprotein (VLDL) and LDL lipoprotein fractions, as shown by a

cholesterol analysis after HPLC-based lipoprotein size separation of pooled serum samples (Figure 14).
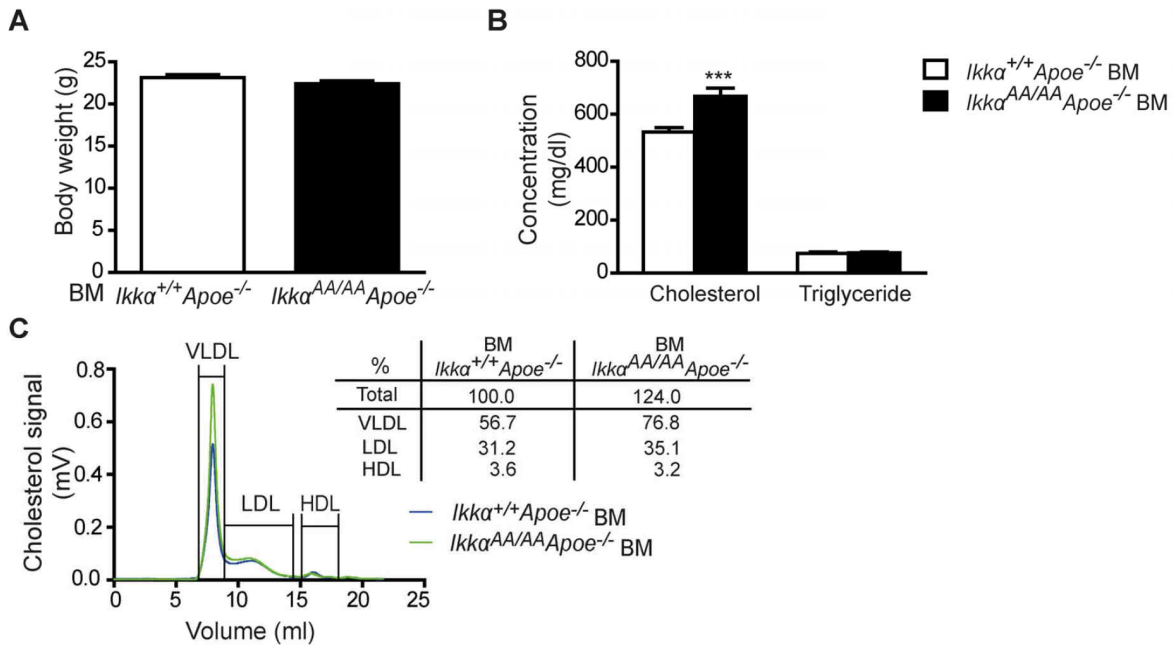
Figure 14: *Ikkα$^{AA/AA}$Apoe$^{-/-}$* **bone marrow chimeras have the same weight as** *Ikkα$^{+/+}$Apoe$^{-/-}$***, but exhibit increased VLDL values and thereby increased cholesterol levels**. After 13 weeks of HFD, body weight **(A)** was recorded and lipid levels **(B)** measured in serum of *Apoe$^{-/-}$* mice transplanted with *Ikkα$^{AA/AA}$Apoe$^{-/-}$* or *Ikkα$^{+/+}$Apoe$^{-/-}$* BM. **(C)** HPLC fractionation of serum showed elevated VLDL levels in *Ikkα$^{AA/AA}$Apoe$^{-/-}$* bone marrow-transplanted mice. (n = 18–27) Graphs represent the mean ± SEM; 2-tailed t-test, ****p<0.001.*

Despite these differences in cholesterol and specifically VLDL levels, atherosclerotic lesion sizes in the aorta, brachiocephalic artery and aortic root were comparable in *Ikkα$^{AA/AA}$Apoe$^{-/-}$* and *Ikkα$^{+/+}$Apoe$^{-/-}$* BM chimeras (Figure 15).
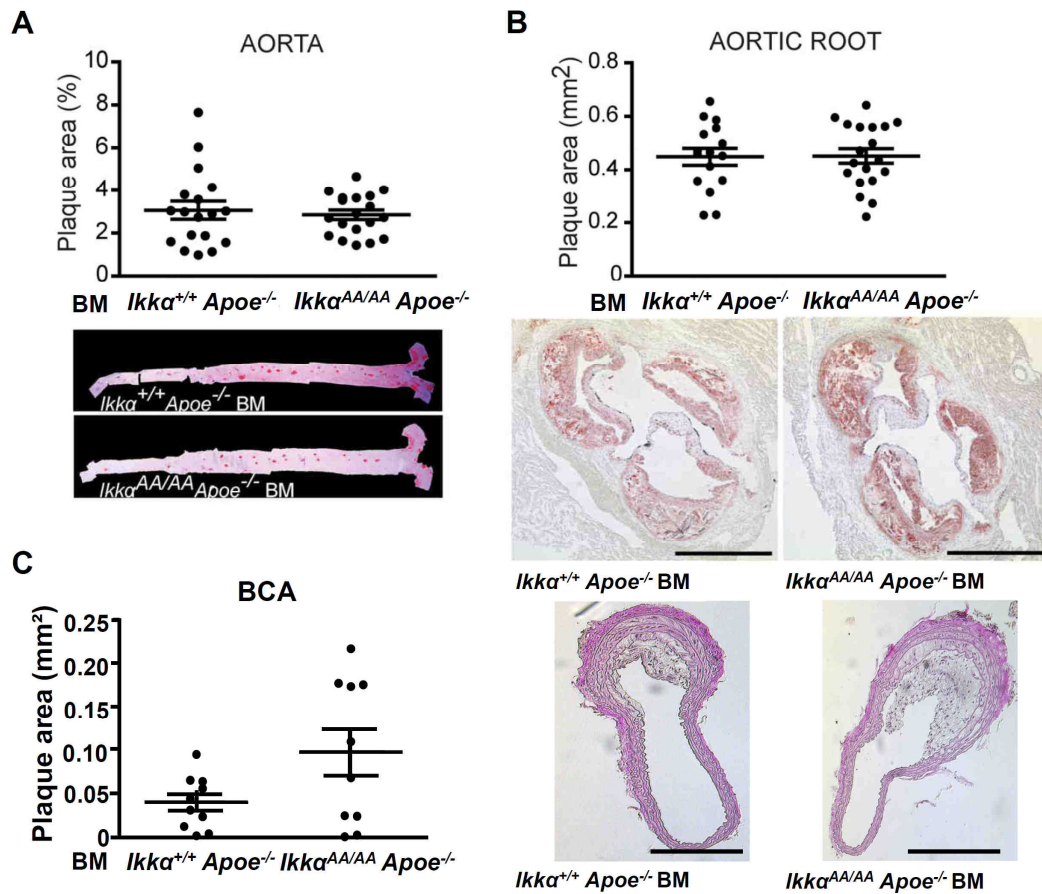
Figure 15: Atherosclerotic lesion analysis in aorta, aortic root and BCA are unaltered in *Ikkα^{AA/AA}Apoe^{–/–}* **BM chimeras**. After 13 weeks of high-fat diet, atherosclerotic plaque sizes were analysed in aorta **(A)**, aortic root **(B)** and BCA **(C)**. Representative pictures of Oil-Red O-stained lipid depositions in aorta and aortic root and of EVG stainings of BCAs are shown. Scale bar aortic root= 500 µm, scale bar BCA= 200 µm. (n = 18–27) Graphs represent the mean ± SEM.

To explore potential qualitative effects on atherosclerosis, atherosclerotic lesions in the aortic root and BCA were classified according to their severity and progression. Lesions were classified into early, intermediate-type and advanced lesions, as previously described[127]. Classification showed that plaques in aortic root were already far progressed, however no differences were found between both groups (Figure 16).

A

BCA

B
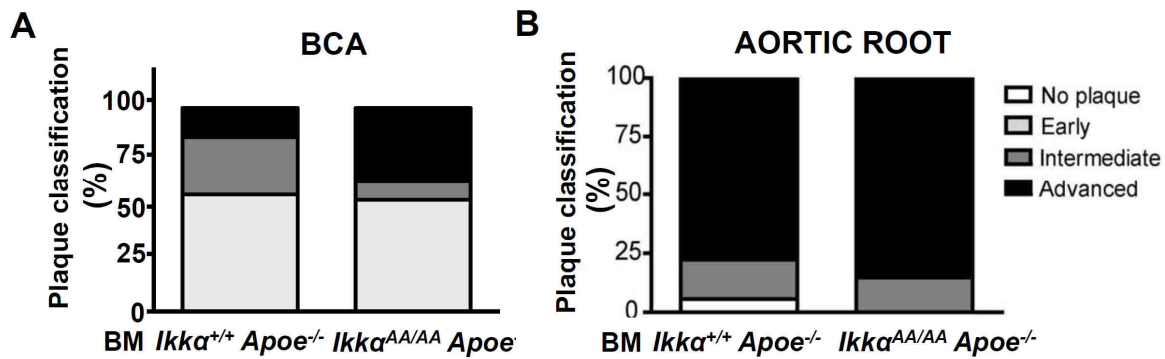
AORTIC ROOT

Figure 16: Atherosclerotic plaque classification show same plaque severity between *Ikkα^{AA/AA}Apoe^{-/-}* and *Ikkα^{+/+}Apoe^{-/-}* BM-transplanted mice in BCA and aortic root. Lesions in BCA **(A)** and aortic root **(B)** were classified according to their phenotype. Data shown is plaque distribution as percentage of total number of lesions analysed. Aortic root (n=22-26), BCA (n=9-5). Graphs represent the mean ± SEM.

In order to assess whether Ikkα would contribute to a different atherosclerotic lesion phenotype, different parameters were analysed in regard to cellular lesion composition, apoptosis (Tunel staining) and lipid uptake by plaque macrophages (lipid depositions with Nile Red staining) in aortic root lesions. Immunofluorescent staining presented equal content of macrophages (Mac2+), SMCs (Sma+) and Cd3+ T-lymphocytes in atherosclerotic plaques (Figure 17).
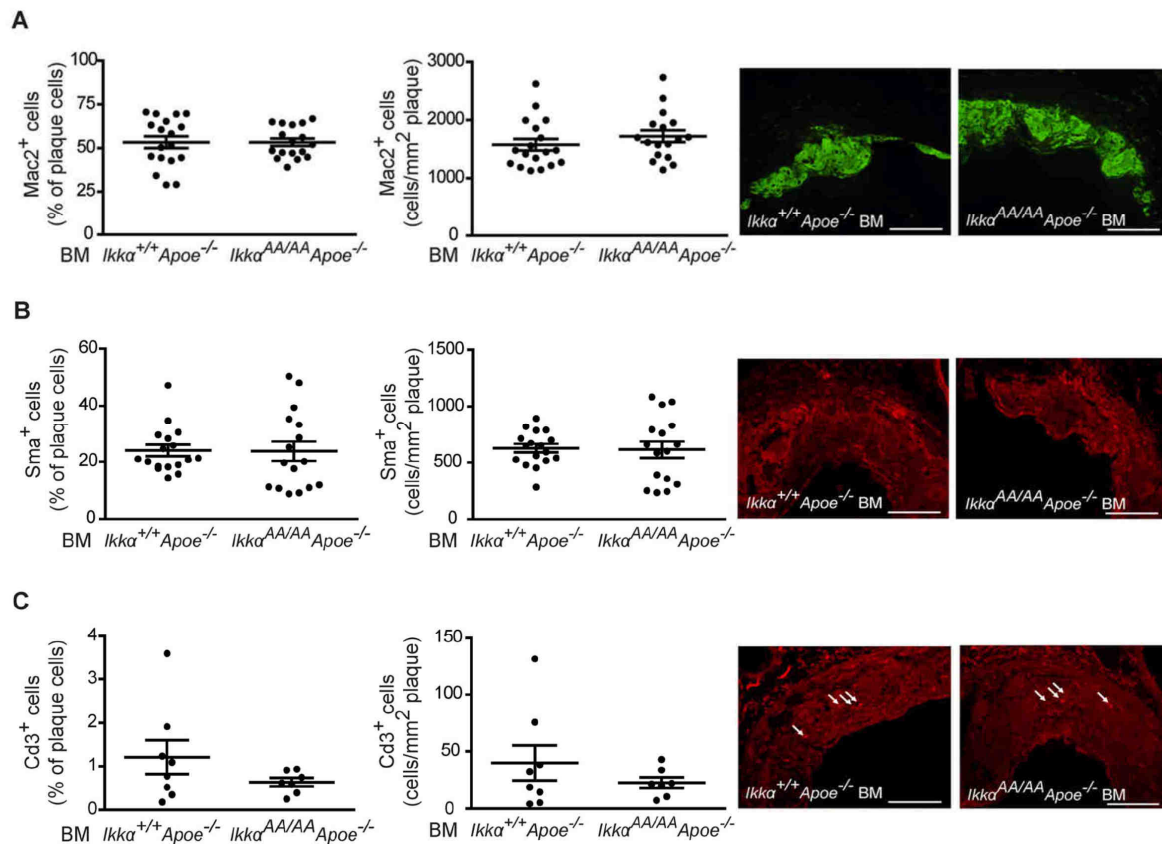
Figure 17: *Ikkα^{AA/AA}* **knock-in in haematopoietic cells does not influence atherosclerotic lesion composition.** Immunofluorescent stainings of aortic roots from *Ikkα^{AA/AA}Apoe^{-/-}* and from *Ikkα^{+/+}Apoe^{-/-}* BM-transplanted mice after high-fat diet for 13 weeks. **(A-C)** Quantification of Mac2^+ macrophages (**A**, n = 17-18), Sma^+ SMCs (**B**, n = 16-17) and Cd3^+ T-cells (**C**, n = 7-8) as percentage of all plaque cells (left) and relative to plaque area (right). Graphs represent mean ± SEM. Representative pictures are shown. Scale bar = 100 µm.

To assess whether *Ikkα^{AA/AA}* BM transplantation would influence neutrophil infiltration and content in atherosclerotic lesions, neutrophils in aortic roots of BM-transplanted mice were stained using histochemical chloroesterase staining. However, despite the present of neutrophils outside the plaque region, no neutrophils could be detected in atherosclerotic lesions of *Ikkα^{AA/AA}Apoe^{-/-}* or *Ikkα^{+/+}Apoe^{-/-}* BM chimeras (Figure 18).
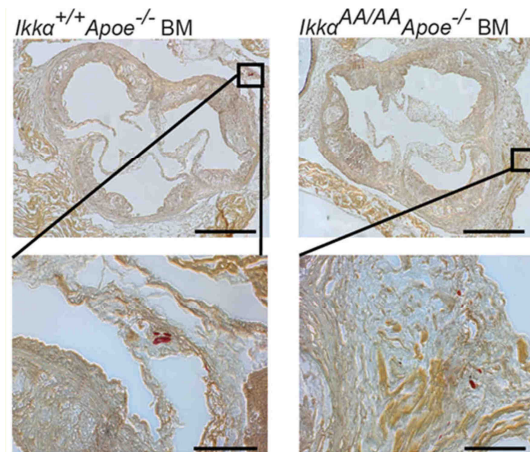
Figure 18: Inactivatable Ikkα kinase knock-in in BM cells does not alter neutrophil infiltration in atherosclerotic lesions. Chloroesterase staining of aortic roots from $Apoe^{-/-}$ mice, transplanted with $Ikka^{+/+ApoE-/-}$ and $Ikka^{AA/AA}Apoe^{-/-}$ BM, after high-fat diet for 13 weeks. Representative pictures show that neither in wildtype nor mutant mice neutrophils could be detected within the atherosclerotic lesions. Graphs represent the mean ± SEM. Scale bar = 500 μm (upper pictures); Scale bar = 200 μm (lower pictures).

Next, necrosis and apoptosis were quantified in aortic root lesions of $Ikka^{AA/AA}Apoe^{-/-}$ and $Ikka^{+/+}Apoe^{-/-}$ BM chimeras after 13 weeks of high-fat diet. Necrotic core was measured after immunofluorescent staining of lesions with DAPI, measuring cell-free areas within the atherosclerotic plaque. In case of apoptosis (visualized with help of a Tunel *in situ* apoptosis detection kit), I analysed not only apoptotic cells but as well apoptotic macrophages, as it has been reported that Ikkα decreases apoptosis of macrophages in inflammatory conditions[137]. As shown in Figure 19, necrotic core sizes were comparable, and no significant differences were found in the content of Tunel$^+$ apoptotic cells and apoptotic macrophages in aortic root lesions of $Ikka^{AA/AA}Apoe^{-/-}$ vs $Ikka^{+/+}Apoe^{-/-}$ BM chimeras.
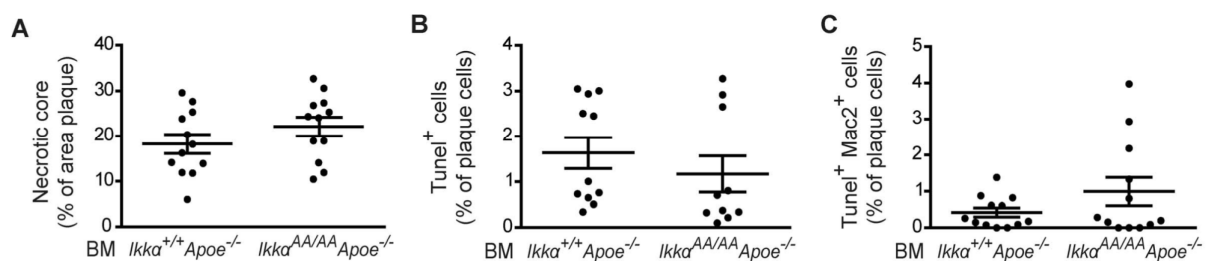
Figure 19: Knock-in of $Ikka^{AA/AA}$ in haematopoietic cells does not influence apoptosis or necrosis in atherosclerotic lesions. Analysis of aortic root lesions of $Apoe^{-/-}$ mice transplanted with $Ikka^{AA/AA}Apoe^{-/-}$ and $Ikka^{+/+}$ $Apoe^{-/-}$ BM after 13 weeks of high-fat diet. **(A)** Quantification of necrotic cores as percentage of plaque area. **(B,C)** Quantification of apoptotic cells (Tunel$^+$, **B**) and apoptotic macrophages (Tunel$^+$Mac2$^+$, **C**) as percentage of all plaque cells. Graphs represent the mean ± SEM (n = 10–12).

Next, I quantified lipid deposits in aortic root lesions of $Ikk\alpha^{AA/AA}Apoe^{-/-}$ and $Ikk\alpha^{+/+}Apoe^{-/-}$ BM chimeras after 13 weeks of high-fat diet using Nile Red staining. Also, Nile Red-positive macrophages after co-staining for Mac2 were quantified. Both the level of lesional lipid deposits as well as the percentage of lipid-laden macrophages were unaltered between $Ikk\alpha^{AA/AA}Apoe^{-/-}$ and $Ikk\alpha^{+/+}Apoe^{-/-}$ BM-transplanted mice (Figure 20).
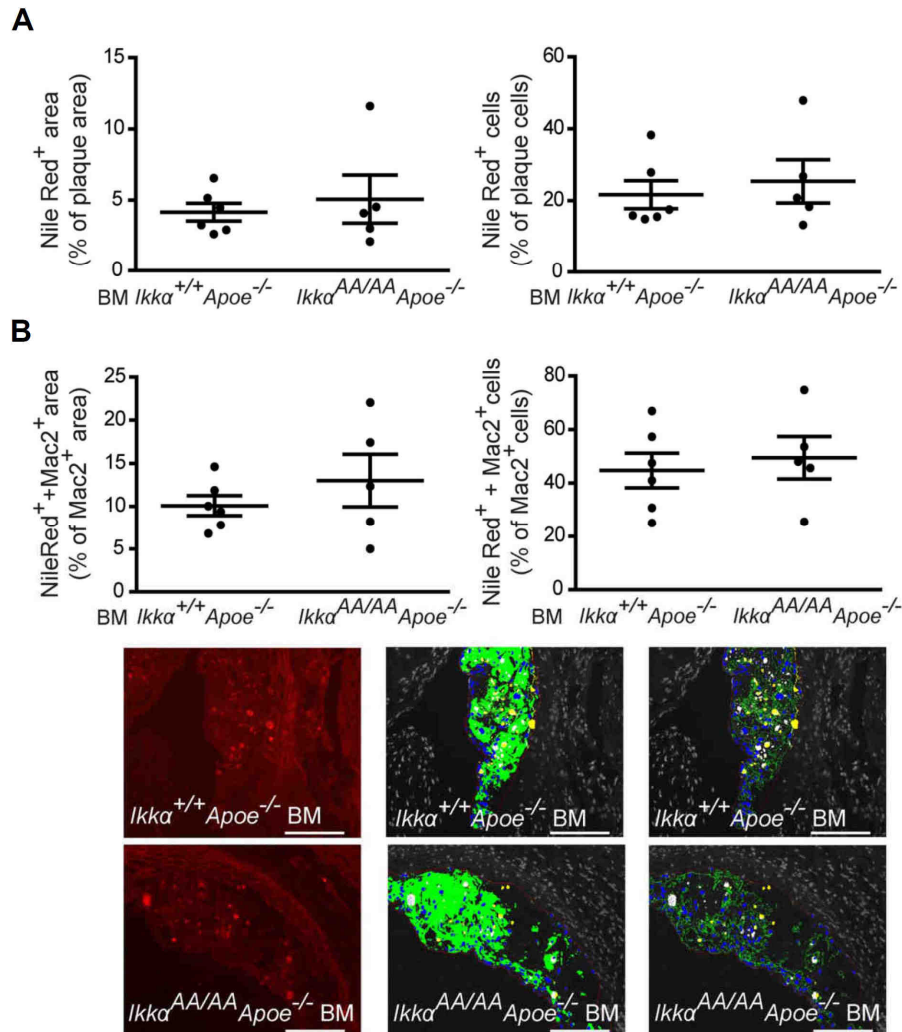
Figure 20: Intracellular lipid depositions and lipid-laden macrophages were not influenced by the activation-resistant Ikkα mutation in haematopoietic cells. Aortic root lesions were stained with Nile Red and co-stained with Mac2 in order to quantify lipid-laden macrophages. **(A)** Nile Red staining was quantified relatively to the plaque area (left graph), and Nile Red+ cells were quantified as percentage of total plaque cells (right graph). **(B)** Lipid uptake by macrophages was quantified as Nile Red$^+$Mac2$^+$ area as % of Mac2$^+$ area (left graph), and as Nile Red$^+$Mac2$^+$ cells as % of Mac2$^+$-cells. Shown are representative pictures from Nile Red stainings (red fluorescence; left image). The middle and right image demonstrate Image J analyses. Displayed are the plaque area (thin red line), macrophage area (green), plaque cell nuclei (blue), Nile Red+ area (yellow) and Mac2+ Nile Red+ area (white, lipid deposits in macrophages). Graphs represent the mean ± SEM (n = 5–6).

Results

Due to highly progressed atherosclerotic lesions within the aortic root (Figure 16), the bone marrow transplantation was repeated and the mice received a high-fat diet for only 8 weeks, in order to investigate whether Ikkα mutation would reveal effects at earlier stages of atherosclerosis.

Similarly as for the previous experiment, the weight was measured before sacrificing the mice. Lipids were assessed in serum and cholesterol fractionation was performed with HPLC.
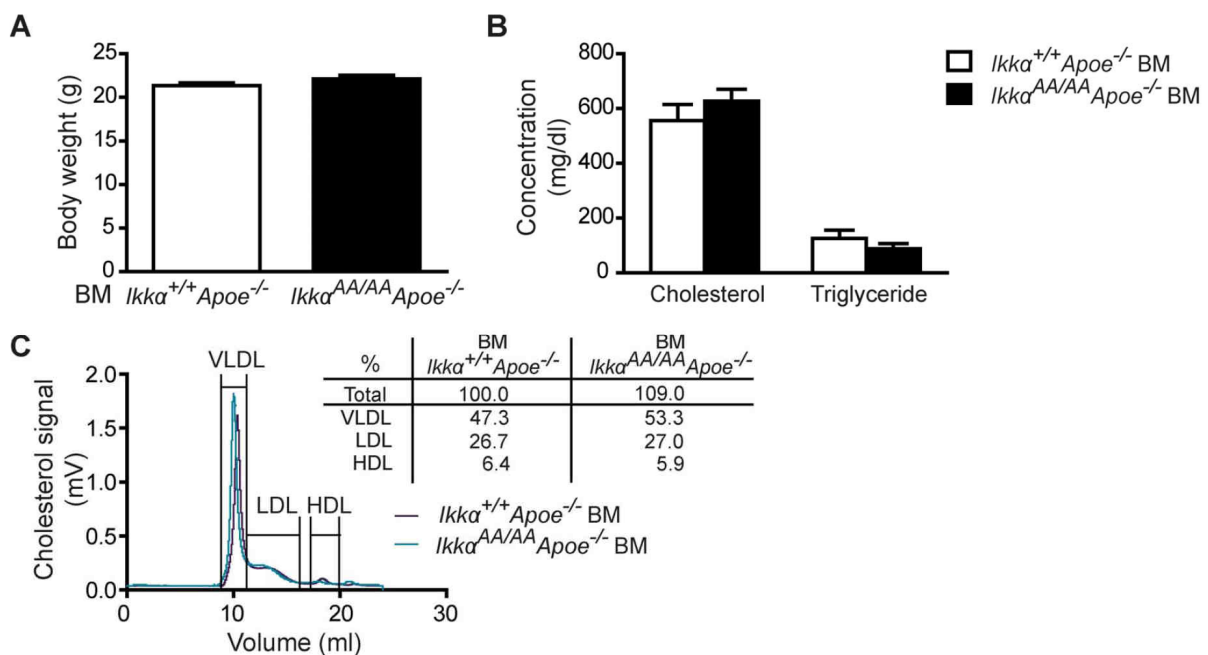
Figure 21: *Ikkα^AA/AA^Apoe^-/-* bone marrow transplantation into *Apoe^-/-* mice does not influence weight or cholesterol levels after 8 weeks of high-fat diet. (A) Body weight and **(B)** lipid analysis in blood serum (n = 7–9) were not changed in Ikkα mutant mice. **(C)** Cholesterol levels after HPLC-based size fractionation of pooled blood serum samples showed comparable levels of VLDL, LDL and HDL in both mice groups. Graphs represent the mean ± SEM.

After this shorter period of high-fat diet, no differences were obtained in body weight or lipid levels in the serum, and also HPLC-based lipoprotein fractionation of pooled serum samples showed similar HDL-, LDL- and VLDL-associated cholesterol peaks (Figure 21). Atherosclerotic lesions were analysed in aorta, aortic root and BCA and lesions classified in aortic root and BCA. Corresponding to the 13 week-high-fat diet study, *Ikkα^AA/AA^Apoe^-/-* and *Ikkα^+/+^Apoe^-/-* BM chimeras presented comparable atherosclerotic lesion sizes in the aorta, aortic root and BCA (Figure 22).
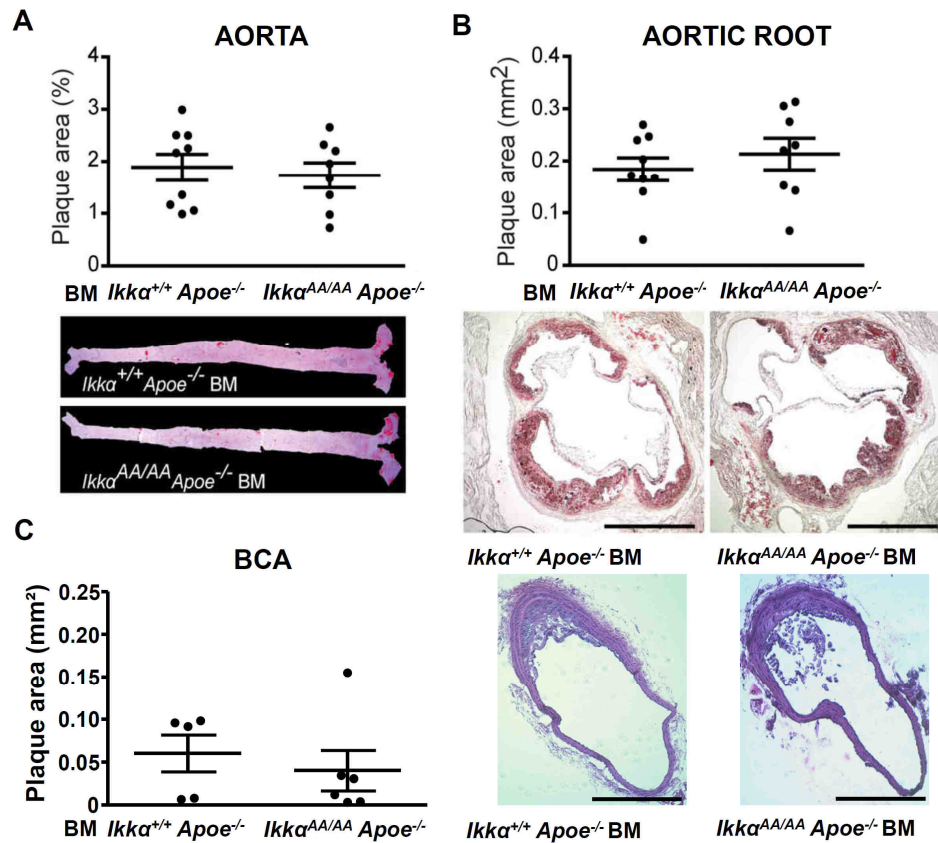
Figure 22: Transplantation of BM carrying an activation-resistant *Ikkα* mutant does not affect early stage atherosclerosis. *Apoe*$^{-/-}$ mice were transplanted with *Ikkα*$^{AA/AA}$*Apoe*$^{-/-}$ or *Ikkα*$^{+/+}$*Apoe*$^{-/-}$ BM and received a high-fat diet for 8 weeks. Atherosclerotic lesion sizes were analysed in the aorta **(A)**, aortic root **(B)** and BCA **(C)**. Representative pictures of Oil-Red-O+ lipid depositions in aorta and aortic root and EVG stainings of BCA are shown. Scale bar = 500 μm (aortic root), scale bar = 200 μm (BCA). Graphs represent the mean ± SEM.

Also, classification of the plaques into early, intermediate or advanced stages revealed comparable lesion stages in *Ikkα*$^{AA/AA}$*Apoe*$^{-/-}$ and *Ikkα*$^{+/+}$*Apoe*$^{-/-}$ BM-transplanted *Apoe*$^{-/-}$ mice, although the lesions were less advanced compared to the 13 week-diet study (Figure 23).
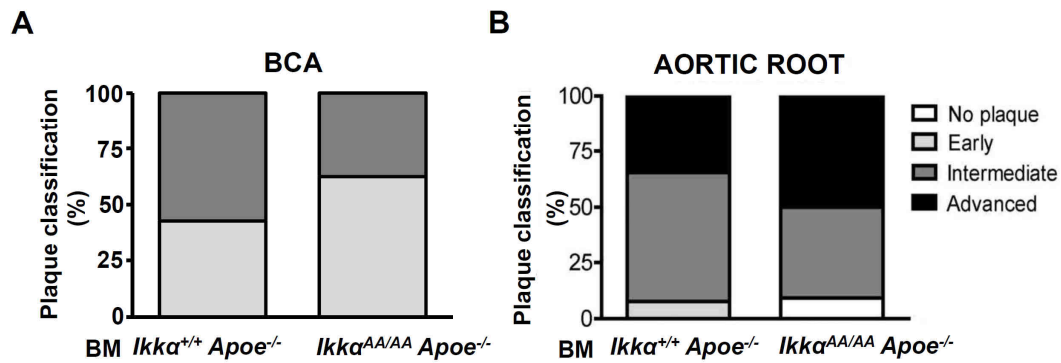
Figure 23: *Ikkα^{AA/AA}* **knock-in in BM cells does not influence lesion classification at early stages of atherogenesis**. Classification of atherosclerotic lesions from *Ikkα^{AA/AA}Apoe^{-/-}* and *Ikkα^{+/+}Apoe^{-/-}* BM chimeras after 8 weeks of high-fat diet. Classification of lesions in aortic root and BCA was performed according to their severity. Shown is the plaque distribution as percentage of the total number of lesions examined. **(B)** Aortic root (n = 22–26), **(A)** BCA (n=9-5); Graphs represent the mean ± SEM; 2-tailed t-test, ***p<0.001.

In summary, these data indicated that transplantation of *Ikkα^{AA/AA}Apoe^{-/-}* -mutant BM does not affect the size, phenotype or cellular content of atherosclerotic lesions in atherosclerosis-prone *Apoe^{-/-}* mice.

4.1.4 BM-specific expression of an activation-resistant *Ikkα* mutant has no effect on inflammatory gene expression or macrophage activation

As described in the introduction, the canonical NF-kB pathway has been shown to play an important role in controlling atheroprogression[65]. In macrophages Ikkα was shown to be able to stop LPS-induced macrophage activation by terminating NF-kB activity through phosphorylation and degradation of the NF-kB isoform p65[137].

Thus, I studied the effect of *Ikkα^{AA/AA}* knock-in on canonical NF-kB activity in macrophages in the context of atherosclerosis. Specifically, the DNA binding capacity of the NF-κB isoform p65 was analysed in nuclear extracts of *Ikkα^{AA/AA}Apoe^{-/-}* vs *Ikkα^{+/+}Apoe^{-/-}* BM-derived macrophages *in vitro*. Macrophages were stimulated with LPS, Tnf-α or mildly oxidized LDL, mimicking inflammatory or pro-atherogenic surroundings. Unexpectedly, *Ikkα^{AA/AA}* knock-in did not enhance or prolong p65 activity in *Apoe*-deficient macrophages upon stimulation. In case of Tnf-α stimulation p65 activation was slowed down in *Ikkα^{AA/AA}Apoe^{-/-}* macrophages. No differences were observed in p65 activity upon LPS or oxLDL stimulation of *Ikkα^{AA/AA}Apoe^{-/-}* vs *Ikkα^{+/+}Apoe^{-/-}* BM-derived macrophages (Figure 24).
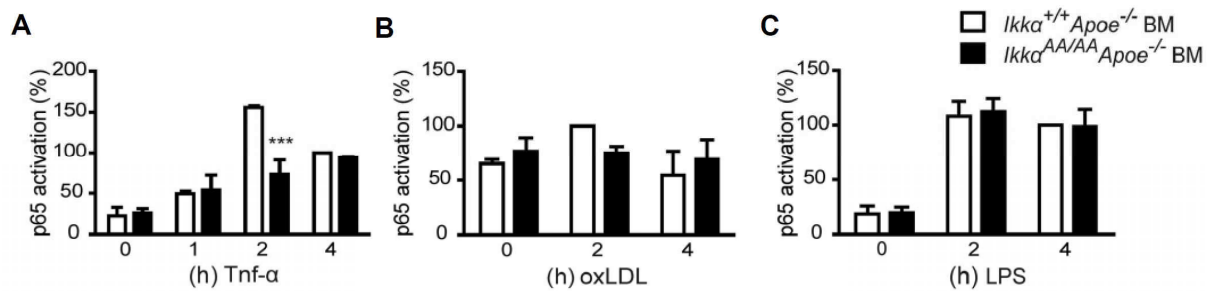
Figure 24: *Ikkα*$^{AA/AA}$ **knock-in does not enhance or prolong NF-kB p65 activity** *in vitro*. Nuclear extracts were isolated from BM-derived macrophages from *Ikkα*$^{AA/AA}$*Apoe*$^{-/-}$ and *Ikkα*$^{+/+}$*Apoe*$^{-/-}$ mice, which were stimulated *in vitro* with **(A)** 10 ng/ml Tnf-α, **(B)** 50 mg/ml of mildly oxidized LDL or **(C)** 100 ng/ml LPS for the indicated time. Activation of p65 was quantified using a TransAm p65 assay. Graphs represent the mean ± range/2 of 2 independent experiments; 2-way Anova with Bonferroni post-test, ***p<0.001.

To determine the potential effect of *Ikkα*$^{AA/AA}$ knock-in on inflammatory protein expression, BM-derived macrophages were stimulated *in vitro* with either Tnfα or heavily oxidized oxLDL for 24 hours and the cytokine and chemokine content in the supernatants were measured with help of a cytometric bead assay (CBA). The concentration of Tnf-α, Il-6 and Mcp1 in supernatants of Tnf-α- or oxLDL-stimulated *Ikkα*$^{AA/AA}$*Apoe*$^{-/-}$ and *Ikkα*$^{+/+}$*Apoe*$^{-/-}$ BM-derived macrophages were not significantly different, although *Ikkα*$^{AA/AA}$ knock-in significantly enhanced the basal secretion of Mcp1, in contrast to Tnf-α or Il-6. Neither Tnf-α nor oxLDL were able to induce secretion of Il-10 or Il-12p70 *in vitro*, although Il-12p70 secretion was found to be significantly higher in oxLDL-stimulated macrophages upon *Ikkα*$^{AA/AA}$ knock-in (Figure 25).
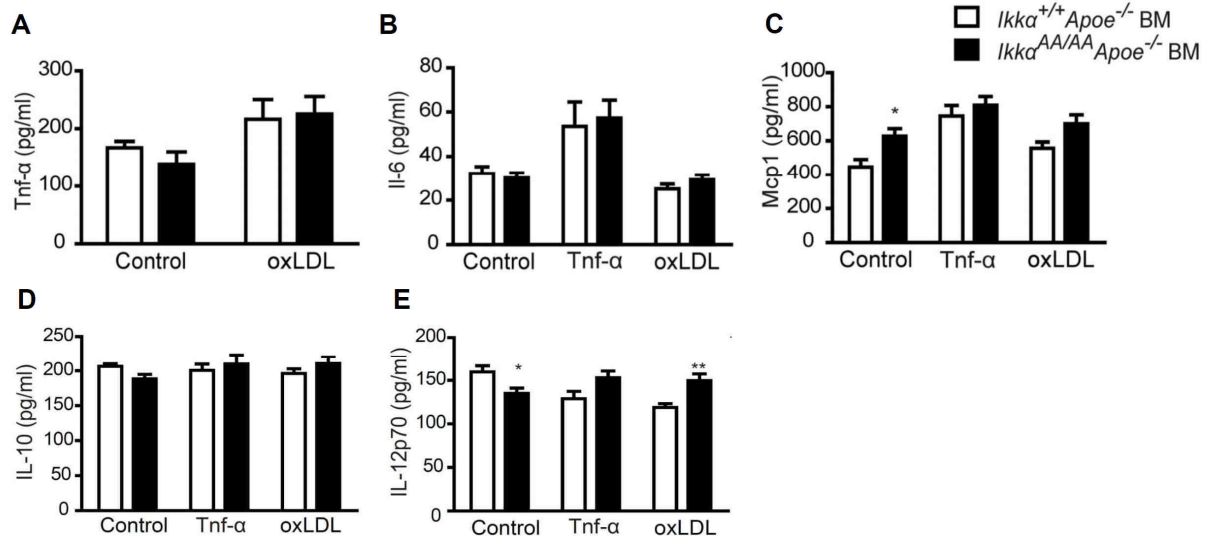
Figure 25: Effect of *Ikkα^{AA/AA}* knock-in on cytokine secretion from BM-derived macrophages. Shown are cytokine concentrations of Tnf-α **(A)**, Il-6 **(B)**, Mcp-1 **(C)**, Il-10 **(D)** and Il-12p70 **(E)** in the supernatants of *Ikkα^{AA/AA}Apoe^{-/-}* or *Ikkα^{+/+}Apoe^{-/-}* BM-derived macrophages, unstimulated (control) or after stimulation for 24 h with 10 ng/ml Tnf-α or 50 µg/ml oxLDL, as indicated. Graphs represent mean ± SEM (n=9 from 3 independent experiments); 2-way Anova with Bonferroni post-test, *$p<0.05$, **$p<0.01$.

In addition, cytokines and chemokines were quantified in serum of *Ikkα^{AA/AA}Apoe^{-/-}* vs *Ikkα^{+/+}Apoe^{-/-}* BM-transplanted mice after 8 weeks of high-fat diet using the CBA assay The concentration of Tnf-α, Il-6 and Mcp1 in serum of *Ikkα^{AA/AA}Apoe^{-/-}* vs *Ikkα^{+/+}Apoe^{-/-}* BM chimeras did not reveal significant differences, whereas the cytokines Ifn-γ, Il-12 and Il-10 remained below the detection limit in both groups (Figure 26).
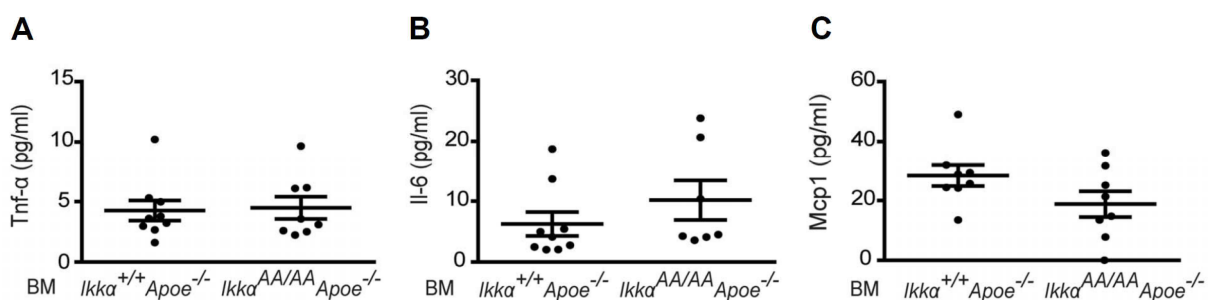

Figure 26: Activation-resistant *Ikkα^{AA/AA}* mutation in haematopoietic cells does not alter cytokine or chemokine concentration *in vivo*. Concentrations of **(A)** Tnf-a, **(B)** Il-6 and **(C)** Mcp1 and in serum of *Apoe^{-/-}* mice transplanted with *Ikkα^{AA/AA}Apoe^{-/-}* or *Ikkα^{+/+}Apoe^{-/-}* BM and receiving a high-fat diet for 8 weeks. Graphs represent the mean ± SEM (n = 7–9).

Given the importance of lipid uptake by macrophages in atherosclerotic lesions, I examined a possible effect of *Ikkα^{AA/AA}* knock-in on macrophage foam cell formation *in vitro*. With 2 different incubation times and oxLDL doses, no significant difference

in oxLDL uptake by *Ikkα^{AA/AA}Apoe^{-/-} vs Ikkα^{+/+}Apoe^{-/-}* BM-derived macrophages was observed. Cytochalasin D severely reduced the oxLDL-associated fluorescence signal, indicating that oxLDL was actively taken up by the cells in an actin-dependent way and not merely binding the cell surface (Figure 27).
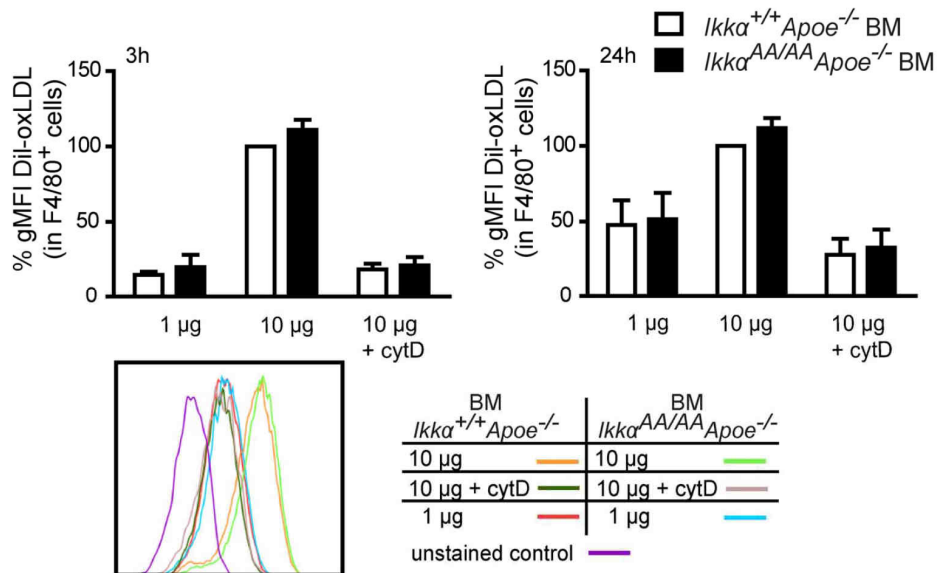
Figure 27: BM-derived macrophages from *Ikkα^{AA/AA}Apoe^{-/-}* mice does not reveal altered lipid uptake. Flow cytometric analysis of Dil-oxLDL uptake by BM-derived macrophages. Cells were incubated without or with Dil-oxLDL (1 mg/ml or 10 mg/ml) for 3 h or 24 h, as indicated. To exclude only cell surface binding of Dil-oxLDL, additional controls were simultaneously treated with cytochalasin D (cytD). Representative flow cytometric histograms are shown. Graphs represent the mean ± SEM (n = 3); 2-way Anova with Bonferroni post-test.

Recapitulating the obtained results, these data show, that knock-in of an activation-resistant *Ikkα^{AA}* mutant in an *Apoe^{-/-}* background does not enhance NF-kB p65 activation or influences the secretion of important inflammatory proteins from Tnf-α- or oxLDL-stimulated macrophages, nor does it significantly affect macrophage foam cell formation.

Taking together the results from this study of haematopoietic Ikkα function, an important and unrecognized role for haematopoietic Ikkα kinase activity in B- and T-cell homeostasis was observed. However, no effect of BM-specific *Ikkα^{AA/AA}* knock-in was revealed on the size or phenotype of atherosclerotic lesions in *Apoe^{-/-}* mice on high-fat diet.

4.2   The global role of Ikkα in the development of atherosclerosis

The dysfunction of resident vascular cells and recruitment of infiltrating leukocyte cells orchestrate a complex interplay of inflammatory processes in the initiation and development of atherosclerosis. In order to determine the global contribution of Ikkα kinase activity to these atherogenic processes, *Ikkα$^{AA/AA}$* knock-in mice were put on high-fat diet for 13 weeks and atherosclerosis was inspected.

4.2.1 Global inactive Ikkα does not alter lipid levels, body weight or serum cytokine levels

Similar to the haematopoietic study, atherosclerosis-prone mice carrying an activation-resistant Ikkα mutant (*Ikkα$^{AA/AA}$Apoe$^{-/-}$*) were put for 6 or 13 weeks on high-fat diet from the age of 8 weeks. Body weights were recorded before sacrifice, lipid levels were measured in serum and serum cytokine/chemokine concentrations were analysed with help of a CBA bead assay. A whole blood cell count was analysed in an automated hematology analyser.

After 13 weeks of high-fat diet, mice had comparable serum total cholesterol, HDL and LDL levels. Also, serum triglyceride values were unaltered. Body weights after 6 weeks and 13 weeks of high-fat diet did not differ between the groups (Figure 28). In addition, quantification of Il-10 and Mcp1 in serum of *Ikkα$^{AA/AA}$Apoe$^{-/-}$ vs Ikkα$^{+/+}$Apoe$^{-/-}$* after 13 weeks of high-fat diet using the cytokine bead assay did not reveal significant differences, whereas the cytokine levels of Ifn-γ, Il-6, Il-12 and Tnf-α were below the detection limit in both groups (Figure 28).
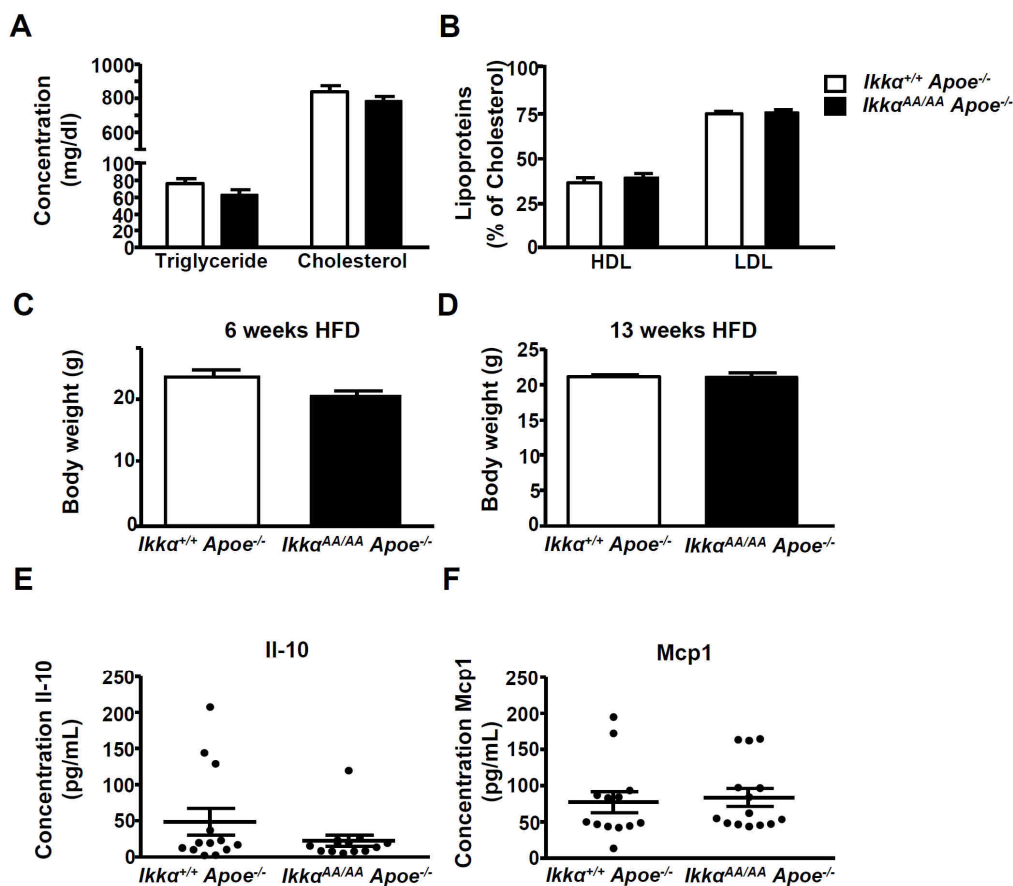
Figure 28: Global knock-in of *Ikkα^{AA/AA}* does not influence body weight, serum lipid levels or cytokine concentrations. *Ikkα^{AA/AA}Apoe^{-/-}* or *Ikkα^{+/+}Apoe^{-/-}* mice received a high-fat diet for 13 weeks before analysis. **(A,B)** Lipid analysis was performed in serum after 13 weeks of high-fat diet (n=17-18) **(C,D)** The body weight was measured after 6 weeks (n = 6) and 13 weeks of high-fat diet (n = 17-18). **(E,F)** Concentrations of Il-10 and Mcp1 in serum of *Ikkα^{AA/AA}Apoe^{-/-}* or *Ikkα^{+/+}Apoe^{-/-}* mice after 13 weeks of high-fat diet (n=13-14). Graphs represent the mean ± SEM.

Whole blood cell count of leukocytes, thrombocytes as well as erythrocytes was not significantly influenced by *Ikkα^{AA/AA}* knock-in.

Table 21: Whole blood cell count from *Ikkα^{AA/AA}Apoe^{-/-}* or *Ikkα^{+/+}Apoe^{-/-}* mice after 6 weeks of high-fat diet.

	Ikkα^{+/+}Apoe^{-/-}	*Ikkα^{AA/AA}Apoe^{-/-}*
Leukocytes (x10^3/µl blood)	6.8 ± 1.1	9.8 ± 1.6 *(P=0.15 ns)*
Erythrocytes (x10^6/µl blood)	8.9 ± 0.3	9.1 ± 0.2
Thrombocytes (x10^3/µl blood)	781.5 ± 158.3	694.3 ± 99.29

4.2.2 Activation-defective Ikkα influences atherosclerotic lesion development site-specifically

Whereas haematopoietic Ikkα did not influence atherosclerosis, the global $Ikka^{AA/AA}$ knock-in revealed interesting effects. After a high-fat diet for 13 weeks, quantification of atherosclerotic lesions in aorta by *en face* staining with Oil-red O revealed increased plaque development in $Ikka^{AA/AA}Apoe^{-/-}$ mice compared to $Apoe^{-/-}$ controls. In order to distinguish potential site-specific effects, lesions in the abdominal and thoracic part of the aorta and the aortic arch were analysed separately. Whereas the lesion area in the abdominal part was unaltered between the groups, the thoracic aorta showed a trend for elevated plaque formation, though not statistically significant. However, the aortic arch exhibited a significant 70% increase in plaque development in the Ikkα-inactive mice compared to the control group (Figure 29).
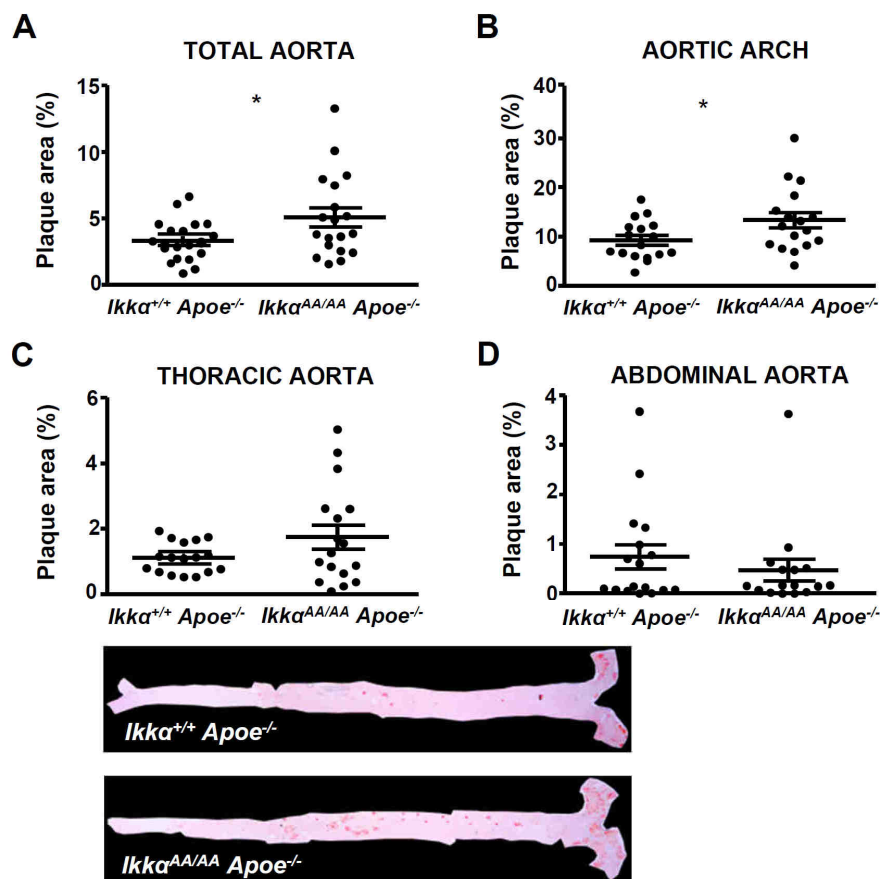
Figure 29: Atherosclerotic plaque sizes are increased in aorta of $Ikka^{AA/AA}Apoe^{-/-}$ compared to $Ikka^{+/+}Apoe^{-/-}$ mice after 13 weeks of high-fat diet. Atherosclerotic lesions were stained in aorta by *en face* Oil-Red O staining. Lesions were quantified in the total aorta **(A)** and separately in aortic arch **(B)**, thoracic aorta **(C)** and abdominal aorta **(D)**. Graphs represent the mean ± SEM; n=17-19, 2-tailed t-test, *p<0.05.

Similarly, the BCA tended to form bigger lesions *in Ikkα*$^{AA/AA}$*Apoe*$^{-/-}$ mice, however without reaching statistical significance (Figure 30).
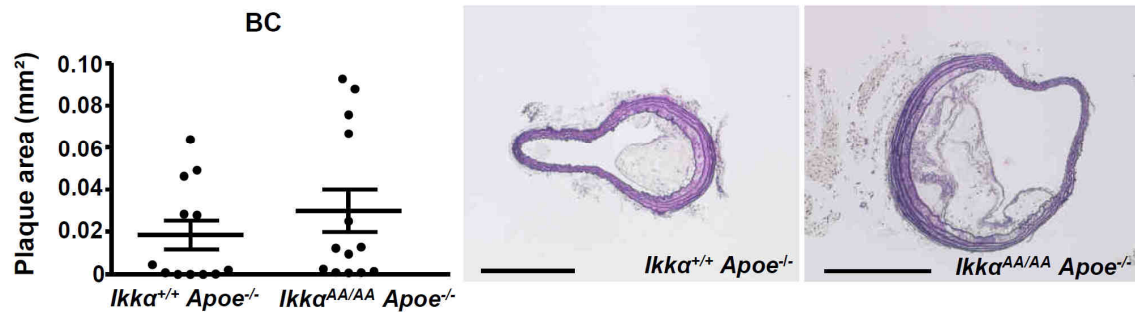
Figure 30: Atherosclerotic plaque sizes show an increased trend in BCA of *Ikkα*$^{AA/AA}$*Apoe*$^{-/-}$ compared to *Ikkα*$^{+/+}$*Apoe*$^{-/-}$ mice after 13 weeks of high-fat diet. Atherosclerotic lesions were stained in BCAs by EVG staining. Graphs represent the mean ± SEM; Scale bar = 200 µm, n=12-13, 2-tailed t-test.

However, *Ikkα*$^{AA/AA}$ knock-in had an adverse effect on atherogenesis in aortic root (Figure 31). The more advanced lesions in aortic root compared to aorta or BCA were significantly decreased in *Ikkα*$^{AA/AA}$*Apoe*$^{-/-}$ mice.
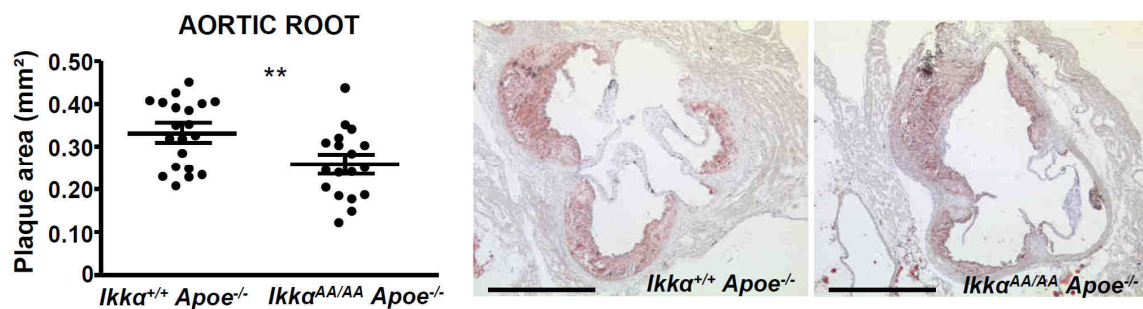
Figure 31: Loss of Ikkα activity decreases atherosclerotic lesion development in aortic roots. Atherosclerotic lesions were stained in aortic root by Oil-Red O staining. Graphs represent the mean ± SEM; Scale bar = 500 µm, n=18-19, 2-tailed t-test, **p<0.01.

These opposite atherosclerotic results in aorta, BCA and aortic root reflect a site-dependent or disease stage-dependent role for Ikkα in atherogenesis.

4.2.3 Defective Ikkα activation does not affect lesion phenotypes

Because the cellular composition of atherosclerotic plaques, along with lesion size, is critically important in atherogenesis, atherosclerotic lesions were characterized in regard to cell composition, apoptosis and matrix components.

The cellular composition of aortic root lesions was comparable, presenting an equal content of macrophages (Mac2$^+$) and SMCs (Sma$^+$) after immunofluorescent stainings. Also for Cd3$^+$ T-lymphocytes, no significant differences were observed, whereas no neutrophils could be detected in the aortic root lesions (Figure 32).
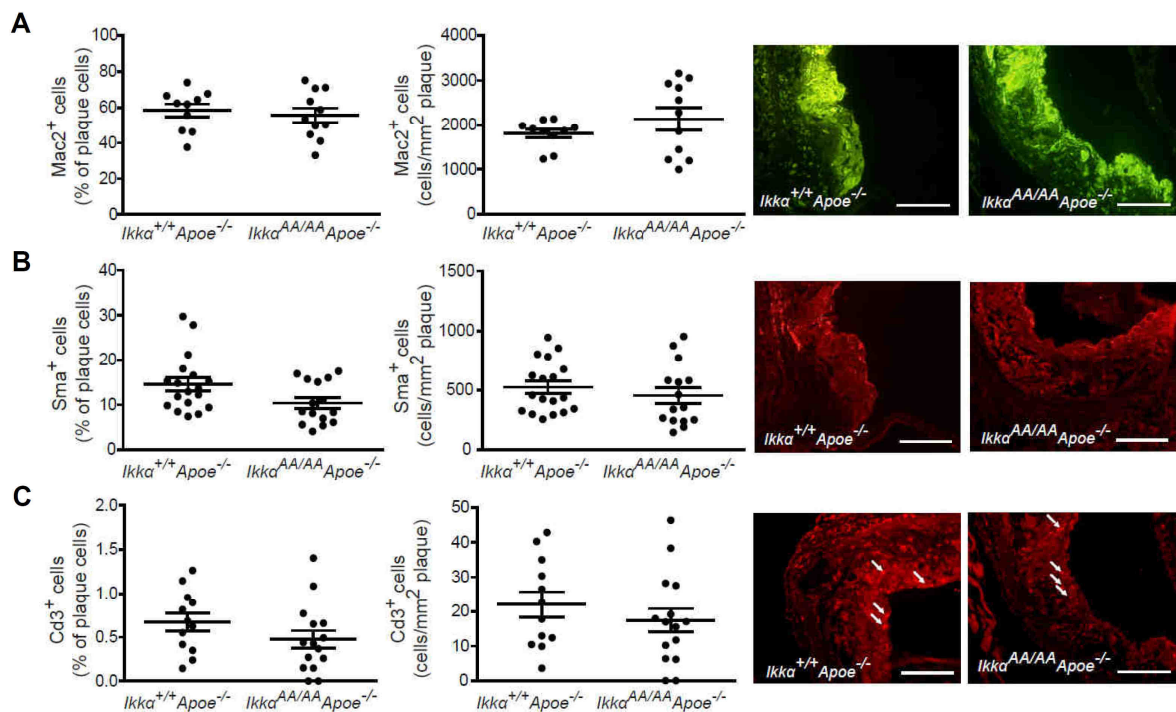
Figure 32: Global *Ikkα$^{AA/AA}$* knock-in does not influence atherosclerotic lesion composition. Immunofluorescent stainings of aortic roots from *Ikkα$^{AA/AA}$Apoe$^{-/-}$* and from *Ikkα$^{+/+}$Apoe$^{-/-}$* mice after high-fat diet for 13 weeks. (**A–C**) Quantification of Mac2$^+$ macrophages (**A,** n = 10–11), Sma$^+$ SMCs (**B,** n = 15–18) and Cd3$^+$ T-cells (**C,** n = 12–15) as percentage of all plaque cells (left) and relative to the plaque area (right). Graphs represent the mean ± SEM. Representative pictures are shown. Scale bar = 100 μm.

Furthermore, no significant differences were found in the content of total Tunel$^+$ apoptotic cells or apoptotic macrophages in aortic root lesions of *Ikkα$^{AA/AA}$Apoe$^{-/-}$* and *Ikkα$^{+/+}$Apoe$^{-/-}$* mice. Also, the collagen deposition within aortic root lesions was similar between the two groups of mice (Figure 33).
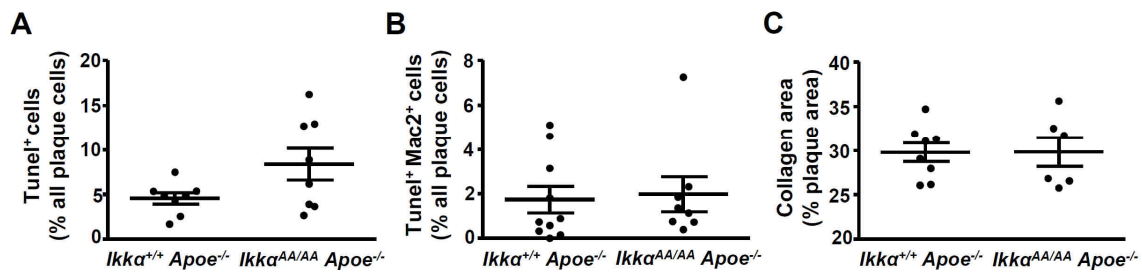
Figure 33: *Ikkα$^{AA/AA}$* **knock-in does not alter apoptosis or the collagen content in atherosclerotic lesions of aortic roots.** Analysis of **(A,B)** apoptosis, apoptotic macrophages and **(C)** collagen content in atherosclerotic plaques of *Ikkα$^{AA/AA}$Apoe$^{-/-}$* and *Ikkα$^{+/+}$Apoe$^{-/-}$* mice in aortic root by Tunel and Sirius Red staining after 13 weeks of high-fat diet. Graphs represent means ± SEM. (n=6-10).

Similarly, content of macrophages (Mac2$^+$) and SMCs (Sma$^+$) in BCA lesions were comparable (Figure 34).
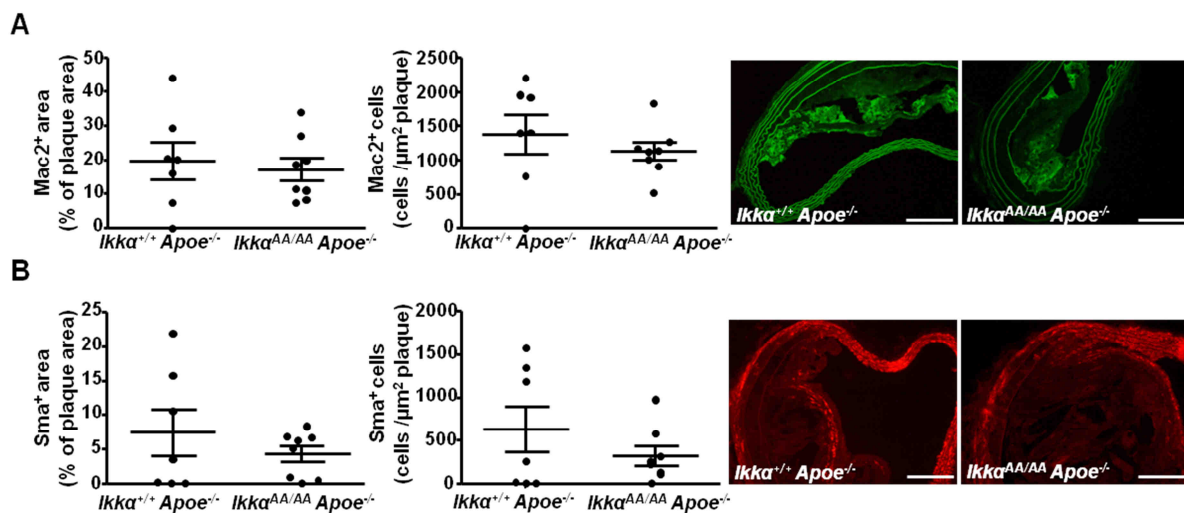
Figure 34: Global *Ikkα$^{AA/AA}$* knock-in does not influence atherosclerotic lesion composition in BCA. Immunofluorescent stainings of BCAs from *Ikkα$^{AA/AA}$Apoe$^{-/-}$* and from *Ikkα$^{+/+}$Apoe$^{-/-}$* mice after high-fat diet for 13 weeks. (**A**) Quantification of Mac2$^+$ macrophages, Sma$^+$ SMCs (**B**) as percentage of all plaque area (left) and cells relative to the plaque area (right). Graphs represent the mean ± SEM. Representative pictures are shown. (n=6-8), Scale bar = 50 µm.

These findings indicate that *Ikkα^{AA}* mutation does not have an effect on lesion composition. Thus, the observed site-specific effects on atherosclerotic lesion size might be induced by differential effects on intracellular signalling and inflammatory gene expression instead, potentially caused by site-specific expression or activation patterns of Ikkα. Hence, I proceeded to analyse potential regional differences of *Ikkα$^{AA/AA}$* knock-in on NF-κB p65 activity and histone H3 phosphorylation, as Ikkα was

previously shown to affect gene expression by negatively regulating canonical NF-κB activation and by controlling phosphorylation of histone H3 (see chapter 4.2.4).

4.2.4 Loss of Ikkα activity does not influence NF-κB activation and reduces histone H3 phosphorylation to an only minor extent specifically in aortic arch

Proteins were extracted from aortic root, arch and thoracic aorta from $Ikka^{AA/AA}Apoe^{-/-}$ vs $Ikka^{+/+}Apoe^{-/-}$ mice after 6 weeks of high-fat diet and the DNA binding capacity of p65 and the levels of phosphorylated histone H3 were studied by ELISA.

Unexpectedly, $Ikka^{AA/AA}$ knock-in did not result in enhanced NF-κB p65 activity in *Apoe*-deficient mice and NF-κB activity levels did not significantly vary between aortic root, arch or thoracic aorta neither in control mice nor in $Ikka^{AA/AA}$ knock-in mice (Figure 35). Comparing histone H3 phosphorylation signals in aortic root, arch and thoracic aorta in $Ikka^{AA/AA}Apoe^{-/-}$ vs $Ikka^{+/+}Apoe^{-/-}$ *mice*, wildtype mice showed a significantly increased level of histone H3 phosphorylation within the aortic arch in comparison to the aorta and a trend for increase compared to root. In contrast, only a trend for increased expression in aortic arch *vs* root and aorta was observed in $Ikka^{AA/AA}$ knock-in mice, without reaching statistical significance (Figure 35). These data indicate that histone H3 phosphorylation is site-specifically controlled between aortic arch *vs* thoracic aorta and root, with a minor role for Ikkα kinase activity in regulating H3 phosphorylation in aortic arch. This might underlie at least to a small extent the observation that $Ikka^{AA/AA}$ knock-in differentially affects atherogenesis in aortic arch (showing significantly increased plaque formation) compared to thoracal aorta (non-significant increase in plaque formation) and aortic root (significant decrease in plaque size).
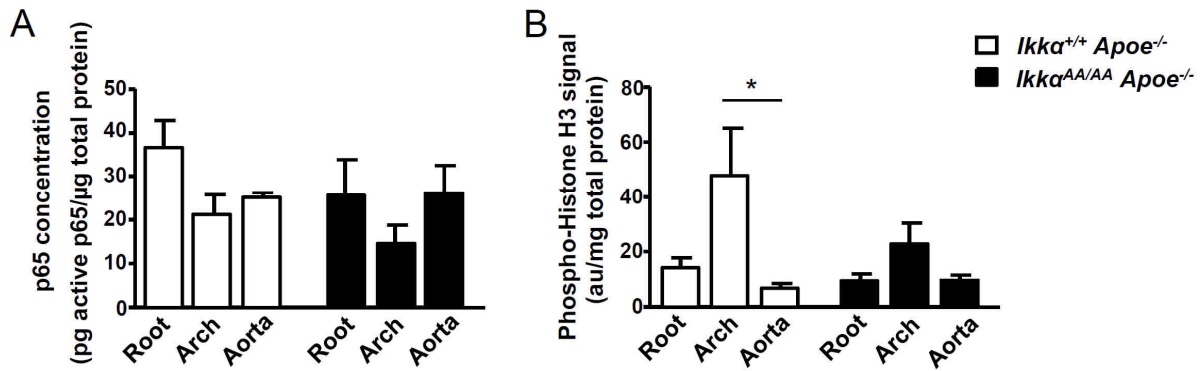
Figure 35: Activation-resistant Ikkα mutation does not alter NF-κB p65 activity, but reduces enhanced histone H3 phosphorylation in aortic arch compared to aorta and aortic root. Proteins were extracted from $Ikka^{AA/AA}Apoe^{-/-}$ vs $Ikka^{+/+}Apoe^{-/-}$ mice after 6 weeks of high-fat diet from aortic root, arch and thoracic aorta. DNA binding capacity of active NF-κB p65 was measured in extracts using a TransAM NF-kB ELISA and binding capacity, revealing p65 activity and concentration, was determined with help of a standard curve **(A)**. Histone H3 phosphorylation was measured by ELISA and signal was normalized to protein extract concentration used for measurement **(B)**. (n=5-6 each). *au = arbitrary units*. Data are expressed as mean ± SEM, 2-way Anova with Bonferroni post-test for comparison of $Ikka^{AA/AA}Apoe^{-/-}$ vs $Ikka^{+/+}Apoe^{-/-}$; 1-way Anova test with Dunnette's post test for comparing organs in between 1 genotype, *$p<0.05$.

4.2.5 Ikkα is differentially expressed and activated at different vascular regions in *Apoe*-deficient mice

To examine whether the regional atherosclerotic differences in the aortic root *vs* arch and aorta would be caused by differential Ikkα expression, $Apoe^{-/-}$ mice were put for 5 and 10 weeks on high-fat diet, or received normal diet as control. Total protein extracts were made from aortic root, arch and thoracic aorta and a specifically designed ELISA was used to detect endogenous levels of total Ikkα and Ikkα when phosphorylated at Ser176/180 (activated form) at the different vascular regions.

Interestingly, protein levels of Ikkα were different between aortic root *vs* arch and aorta. Compared to arch and aorta, the total Ikkα levels were increased in the aortic root both under control conditions as well as after 5 and 10 weeks of high-fat diet. In contrast, the levels of phosphorylated, active Ikkα were significantly reduced in the aortic root compared to the arch/ thoracic aorta. Especially when analyzing the ratio of activated Ikkα to total Ikkα levels, it became obvious that relative phosphorylation of Ikkα was greatly enhanced in arch and thoracic aorta compared to root (Figure 36). As Ikkα phosphorylation at Ser176/S180 is important to activate Ikkα kinase function, these data suggest that regional differences of Ikkα phosphorylation

extent could result in regional-dependent effects of Ikkα kinase functions on atherogenesis.
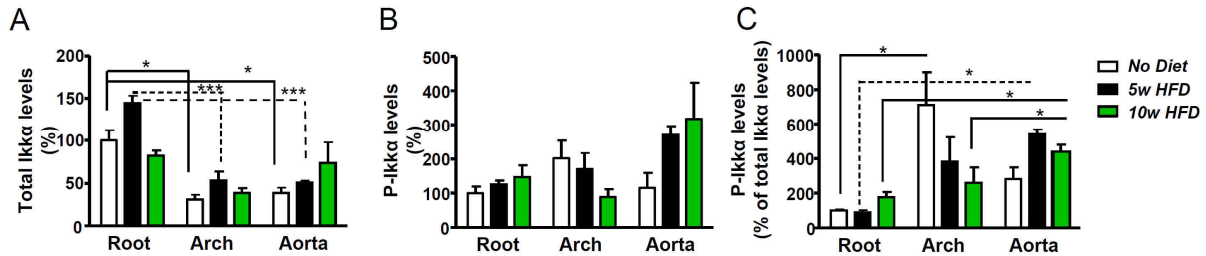
Figure 36: Ikkα is differentially expressed and activated in aortic root compared to arch/thoracic aorta in *Apoe*^{-/-} mice. Total protein extracts were prepared from aortic root, arch and thoracic aorta from *Apoe*^{-/-} mice after normal diet or 5 and 10 weeks of high-fat diet. ELISA quantifying both endogenous total Ikkα protein levels, as well as active, phosphorylated Ikkα (P-Ikkα) was performed, showing higher total Ikkα levels **(A)** in aortic root, whereas arch/thoracic aorta revealed increased levels of P-Ikkα **(B,C)**. 1-way Anova with Tukey´s post-test, all graphs represent the mean ± SEM (n=3, each from pooling 4 mice); *$p<0.05$; **$p<0.01$, ***$p<0.001$.

To investigate whether regional differences in Ikkα protein expression were a direct result from differential gene expression, a qPCR was performed to analyse *Ikkα* expression in aortic root *vs* arch/thoracic aorta in *Apoe*^{-/-} mice after 7 weeks of high-fat diet or normal diet conditions. Surprisingly, qPCR data showed opposite results than protein analysis. Under normal dietary conditions the expression of *Ikkα* was significantly higher in thoracic aorta compared to aortic root. Similarly after 7 weeks of high-fat diet aorta revealed increased mRNA levels of *Ikkα* (Figure 37A).

To exclude that results were influenced due to instable expression of the housekeeping gene *gapdh* in between organs or upon diet conditions (which would make it an inappropriate housekeeping gene), I quantified *gapdh* expression levels relative to input mRNA, and did not observe expression differences, indicating that *gapdh* constitutes a good housekeeping gene (Figure 37B). Furthermore, the same results of *Ikkα* expression were obtained when qPCR data were normalized to a combination of the housekeeping genes *gapdh*, 1*8srna*, *hprt* as described in Vandesompele et al[156] and as shown in Figure 37C.
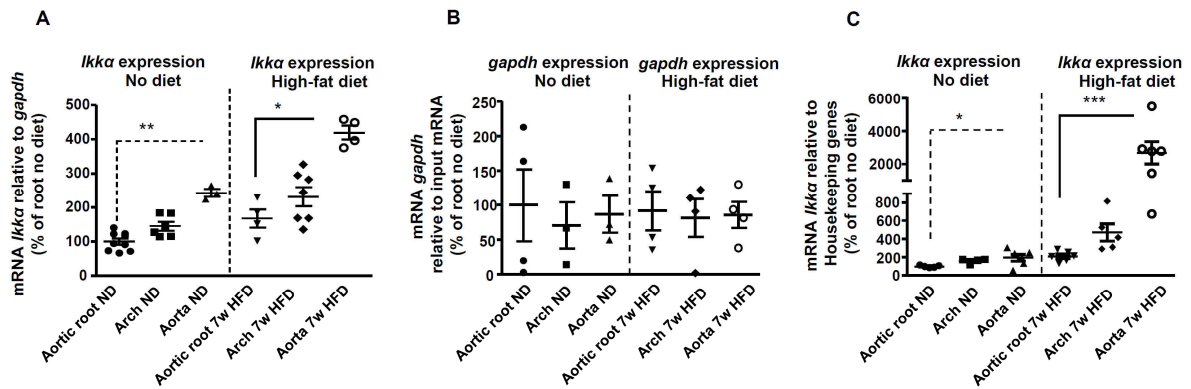
Figure 37: qPCR reveals site-specific differential *Ikkα* expression in aortic root compared to arch/thoracic aorta in *Apoe*^-/- mice under normal diet and 7 weeks of high-fat diet. (A) *Ikkα* mRNA levels measured with help of Taqman qPCR. *Ikkα* mRNA levels were normalized to *gapdh*. n= 3-9 **(B)** *gapdh* expression was measured with help of Taqman qPCR and stability was compared in different tissue and upon diet conditions. mRNA expression shown relative to input RNA used for cDNA synthesis. n= 3-4 **(C)** *Ikkα* mRNA levels measured with help of Taqman qPCR. *Ikkα* mRNA levels were normalized to *gapdh, hprt and 18srna*. n= 5-6. All data shown as percentage of root no diet. ND = normal diet; HFD = high fat diet. Graphs represent mean ± SEM, Kruskal-Wallis test with Dunn´s post-test, *p<0.05, **p<0.01, ***p<0.001.

In conclusion, *Ikkα* mRNA expression was significantly different in aortic root *vs* arch and aorta, although opposite effects were seen compared to Ikkα protein analysis. This suggests that Ikkα protein levels are additionally regulated on post-transcriptional level.

4.2.6 Potential role for miRs in regulating Ikkα mRNA levels

Whereas the thoracic aorta shows a laminar flow pattern, the regions of aortic root and arch are characterized by a disturbed laminar flow. Given the highest expression of *Ikkα* mRNA in aorta (Figure 37), I hypothesized that disturbed laminar flow, which is associated with lower shear stress, might reduce *Ikkα* mRNA levels. Therefore, I generated a region of low shear stress by partial ligation of the carotid artery. *Ikkα* mRNA expression levels were quantified in the carotid artery by qPCR 1 day after ligation, 7 days after ligation and 6 weeks after ligation. As control, non-ligated carotids were used and mRNA levels were normalized to the housekeeping gene *gapdh*. The data exposed a marked upregulation of *Ikkα* expression after partial ligation, which was maximal after 1 day. *Ikkα* expression in the carotid artery was still significantly increased 1 week after ligation and after 6 weeks of ligation, *Ikkα* expression was again partially decreased (Figure 38). Thus, in contrast to my data in

Figure 37, these data would rather suggest that, if flow conditions are indeed regulating *Ikkα* mRNA levels in the partial ligation model, disturbed flow increases instead of reduces *Ikkα* mRNA levels. However, it is also likely that *Ikkα* mRNA levels in the partial ligation model are regulated by acute inflammatory rather than flow conditions, *e.g.* by adhesion of platelets or leukocytes as already visible 1 day after ligation[157].
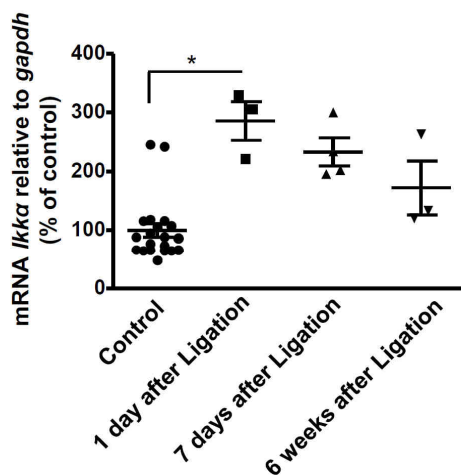
Figure 38: *Ikkα* mRNA expression levels is markedly upregulated under turbulent flow conditions in ligated carotid arteries. *Ikkα* mRNA levels measured with help of Taqman qPCR. RNA isolated from ligated left carotid arteries and non-ligated right carotid arteries (control). *Ikkα* mRNA levels was normalized to *gapdh*. Data shown as percentage of control. (1 day-6 weeks ligation n= 3-4; control n= 20) Graphs represent mean ± SEM, Kruskal Wallis Test with Dunn´s post-test, *p<0.05.

MiRs are important regulators of protein expression, able to induce degradation of target mRNA or repress translation of the mRNA into protein. As expression of miRs has been shown to be altered by haemodynamic forces such as shear stress and thus flow in the vascular system[58], I hypothesized that miR-dependent post-transcriptional repression of *Ikkα* mRNA might contribute to the observed site-specific differences of *Ikkα* mRNA or alternatively, protein expression. Using microRNA.org, 6 miRs (mir-301a/b, mir-16, mir-425, mir-23a and let7b) were chosen that were reported to have *Ikkα* mRNA as target, and their expression profile was analysed in ligated carotid arteries 1 day after ligation, 7 days after ligation and 6 weeks after ligation. Similar as for the housekeeping genes used to normalize *Ikkα* expression, stable expression of the reference miR was analysed (Figure 39). Opposite to the effects observed for *Ikkα* mRNA levels, miR-301a, miR-301b, miR-23a and let7b expression levels were all significantly decreased 1 day after partial ligation (Figure 40). Seven days after ligation also miR-425 showed significantly reduced levels. Expression of these miRs increased again 6 weeks after ligation. Only levels of miR-

16 were not significantly altered by partial ligation of the carotid artery. Compared to the expression profile of *Ikkα* mRNA, these data suggest a potential role for *Ikkα*-targeting miRs in regulating the stability of *Ikkα* mRNA in the partial ligation model.
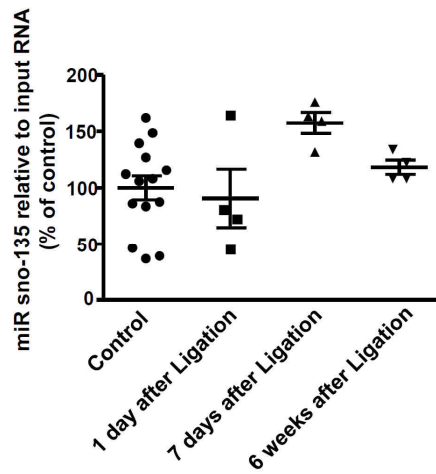
Figure 39: Expression of reference miR sno-135 in ligated carotid arteries. sno-135 miR levels measured with help of Taqman miR assay qPCR. RNA isolated from ligated left carotid arteries and non-ligated right carotid arteries (control). sno-135 miR levels were normalized to input RNA. Data shown as percentage of control. (1 day-6 weeks ligation n= 4; control n= 14). Graphs represent mean ± SEM, Kruskal Wallis Test with Dunn´s post-test.
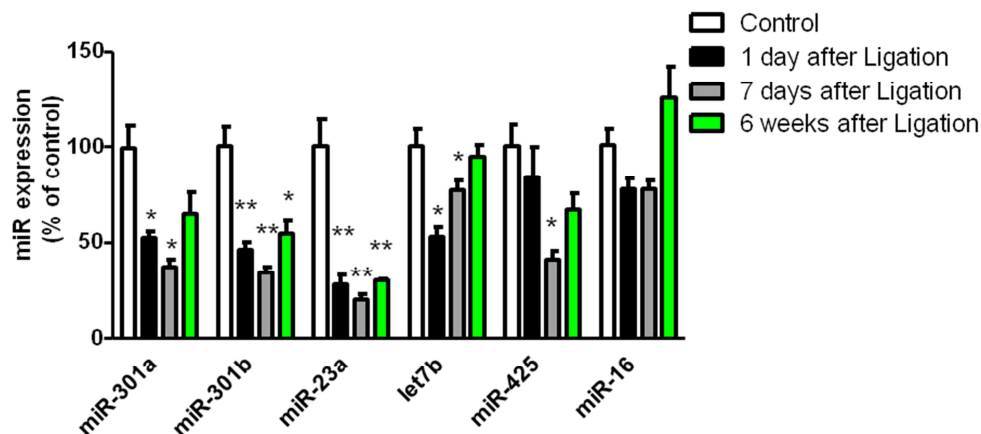
Figure 40: Expression profiles of *Ikkα* targeting miRs in ligated carotid arteries are influenced by turbulent flow conditions. miR were isolated from carotid arteries after partial ligation as indicated and quantified by Taqman miR expression profilin Taqman miR assay qPCR. MiR levels were normalized to a combination of housekeeping miRs sno-135 and miR-429, as described by Vandesompele et al[156]. Data are shown as percentage of non-ligated arteries (control). (1 day-6 weeks ligation n= 4; control n= 14). Graphs represent mean ± SEM, 1-way Anova with Newman-Keuls test, Indicated significance refers to comparison to unligated controls. *p<0.05, **p<0.01.

Similarly, I examined expression profiles of miR-301a/b, miR-23a, let7b, miR-425 and miR-16 in aortic root *vs* thoracic aorta after normal diet and high-fat diet conditions. Both reference miRs sno-135 (Figure 41A) and miR-429 (Figure 41B)

were analysed for stable expression between aortic root and aorta and upon dietary conditions, to ensure that both constitute good reference miRs.
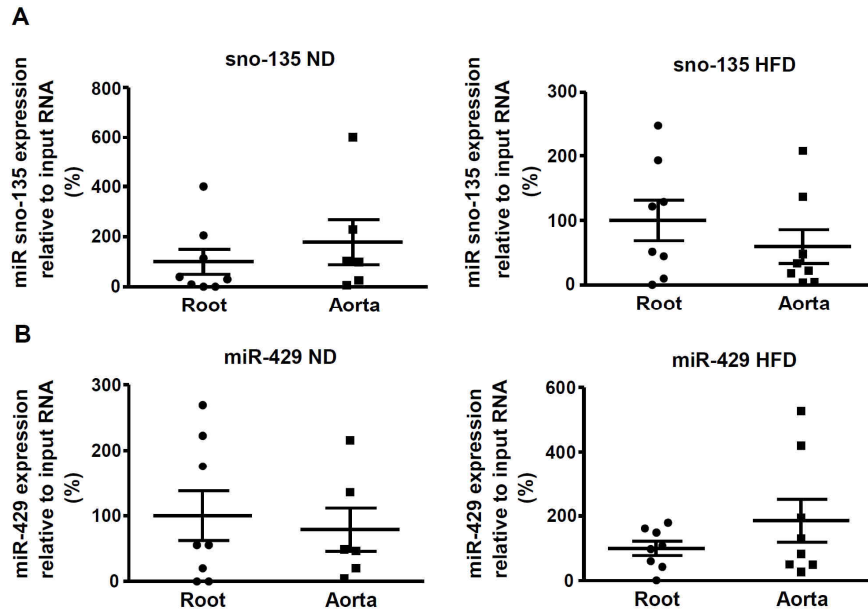
Figure 41: Expression of reference miR sno-135 and miR-429 in aortic root and thoracic aorta. sno-135 **(A)** and miR-429 **(B)** levels were measured with help of Taqman miR assay qPCR. RNA isolated from aortic root and thoracic aorta after no diet and 7w high-fat diet. miR expression levels were normalized to input RNA. Data shown as percentage of root no diet/ root high-fat diet. n=5-8 Graphs represent mean ± SEM.

The expression was quantified in aortic root and aorta, given that the major atherosclerotic effect was observed in these tissues. Except for miR-425 and miR-16, all miRs showed a reduced expression in aorta compared to root (Figure 42). Similarly as in the partial ligation model, this suggests that a lower expression of *Ikkα*-targeting miRs in aorta could contribute to the increased *Ikkα* mRNA level in aorta compared to root by reducing miR-mediated degradation of *Ikkα* mRNA.
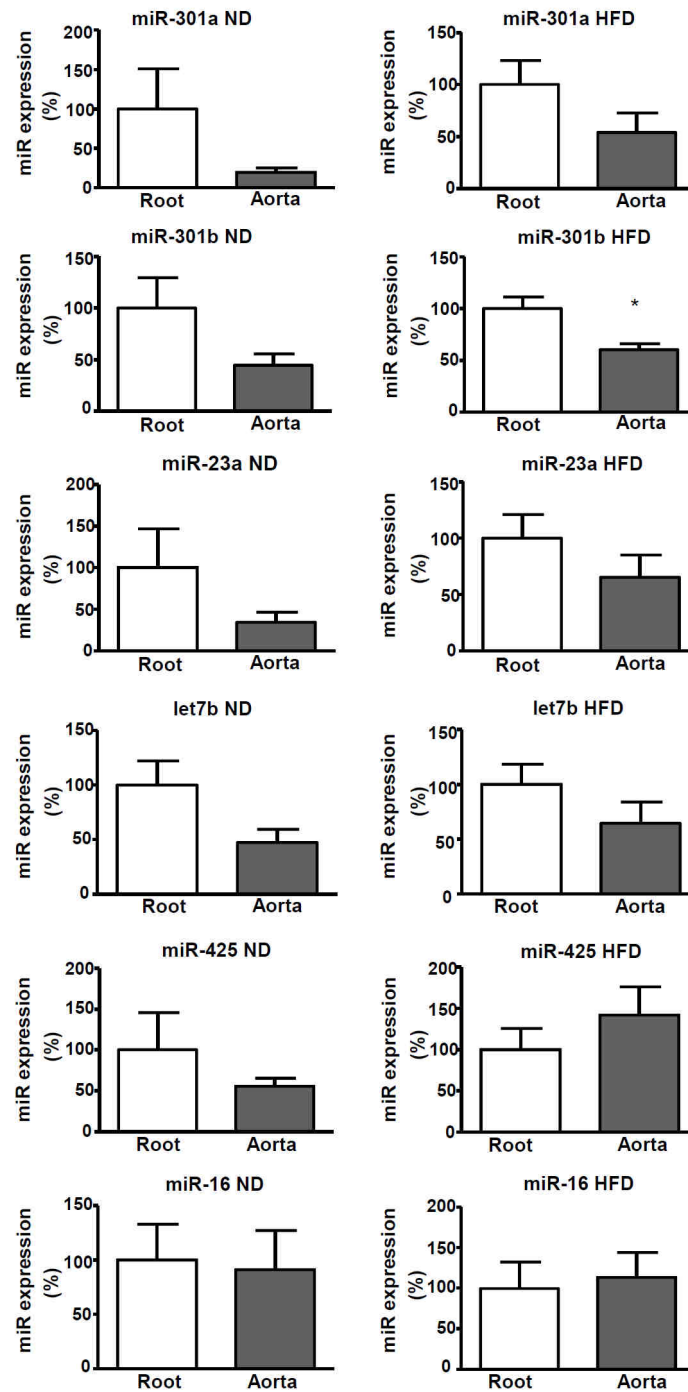
Figure 42: Expression profiles of *Ikkα*-targeting miRs are not significantly altered in aortic root *vs* thoracic aorta, except for miR-301b. miR was isolated from aortic root and thoracic aorta after 7 weeks of normal diet (ND) (left side) or high-fat diet (HFD) (right side) and the expression quantified by **Taqman miR assay qPCR**. MiR levels were normalized to a combination of reference miRs sno-135 and miR-429. Data are shown either as percentage of "Root ND" or as percentage of "Root HFD". (n=4-8) Graphs represent mean ± SEM, 2-tailed t-test, *$p<0.05$.

In summary, these data suggest that *Ikkα* mRNA levels could be controlled by *Ikkα*-targeting miRs, whereas a potential effect of flow conditions on *Ikkα* mRNA levels in aorta *vs* root remains to be further investigated.

4.2.7 Defective Ikkα kinase activation influences gene expression differently in root *vs* aorta and arch

To assess whether defective Ikkα kinase activation would differentially affect gene expression in aortic root *vs* arch or thoracic aorta and could thus contribute to differential effects on atherosclerosis at these regions, I tested the expression profile of various genes, previously linked to atherosclerosis, in aortic root *vs* arch and thoracic aorta in *Ikkα^{AA/AA}Apoe^{-/-} vs Ikkα^{+/+}Apoe^{-/-}* mice after 6 weeks of normal and high-fat diet conditions. Among chemokine *Ccl19* and chemokine receptor *Ccr7*, genes encoding the interleukin *Il-6*, inflammatory marker gene coding for *Tnf-α*, adhesion molecule *Vcam-1* and additionally matrix metalloproteinases *Mmp-3*, *Mmp-9* and *Mmp-13* were analysed.
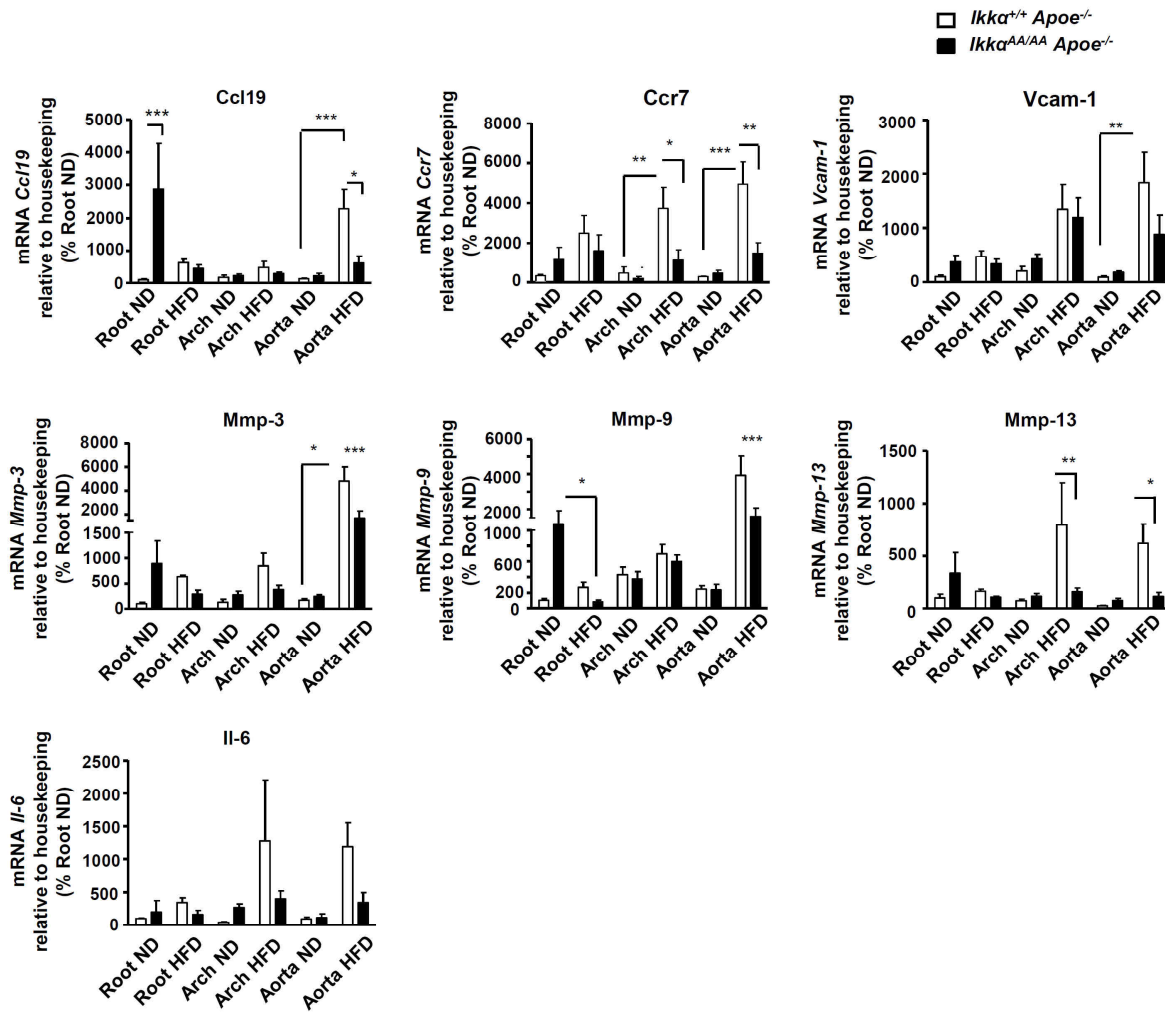
Figure 43: Loss of *Ikkα* activation impacts expression of *Ccl19* and *Ccr7* in aortic arch and thoracic aorta, but not in aortic root. Expression of genes with important roles in atherosclerosis was analysed by qPCR. Study was performed with mRNA isolated from aortic root, arch and thoracic aorta from *Ikkα^AA/AA^Apoe^-/-* and *Ikkα^+/+^Apoe^-/-* mice after 6 weeks of normal (ND) or high-fat dietary (HFD) conditions. Expression of genes was normalized to a combination of the housekeeping genes *gapdh*, *hprt* and *18Srna* as described by Vandesompele et al[156]. Data shown relative to "Root ND *Ikkα^+/+^ Apoe^-/-*"; n=4-6. Graphs represent mean ± SEM, , 2-way Anova with Bonferroni post-test for comparison of *Ikkα^AA/AA^Apoe^-/-* vs *Ikkα^+/+^Apoe^-/-*; 1-way Anova test Kruskal Wallis Test with Dunn´s post-test for comparing organs in between 1 genotype, *$p<0.05$; **$p<0.01$, ***$p<0.001$.

Under normal dietary conditions, the aortic root from *Ikkα^AA/AA^Apoe^-/-* revealed a significantly increased expression of *Ccl19* compared to controls (Figure 43). Expression profiles of *Vcam-1*, *Ccr7*, *Mmp-3*, *Mmp-9* and *Mmp-13* displayed a similar trend, though without reaching statistical significance. In contrast, expression of all these genes was not affected at aortic arch or aorta, with the exception of *Vcam-1*, which also showed a trend for increased expression in aortic arch from *Ikkα^AA/AA^Apoe^-/-* in comparison to controls. Expression of *Il-6* mRNA in aortic root was

not significantly affected by *Ikkα^{AA/AA}* knock-in after normal diet, and was also not significantly altered at aortic arch or aorta.

Upon high-fat diet, *Ikkα^{+/+}Apoe^{-/-}* mice showed an enhanced expression of all targets, which was observed both in aortic root as well as in arch and thoracic aorta. In case of the thoracic aorta from *Ikkα^{+/+}Apoe^{-/-}* mice the expression of *Ccl19*, *Ccr7*, *Vcam-1* and *Mmp-3* increased significantly upon high-fat diet conditions. Remarkably, mRNA levels of *Ccl19* and *Ccr7* were now significantly lower in the aorta of *Ikkα^{AA/AA}Apoe^{-/-}* mice compared to *Apoe^{-/-}* controls. Similarly in the arch, a significant decrease in *Ccr7* expression was observed in *Ikkα^{AA/AA}Apoe^{-/-}* mice, and also *Ccl19* showed a trend for decreased expression in the arch of *Ikkα^{AA/AA}Apoe^{-/-}* mice. In contrast, mRNA levels of *Ccr7* in the root did not vary between *Ikkα^{+/+}Apoe^{-/-}* and *Ikkα^{AA/AA}Apoe^{-/-}* mice after high-fat diet and the effect of increased *Ccl19* expression in *Ikkα^{AA/AA}Apoe^{-/-}* aortic roots under no diet, disappeared under high-fat diet conditions.

Also, expression of *Mmp-3*, *Mmp-9* and *Mmp-13* was significantly lower in *Ikkα^{AA/AA}Apoe^{-/-}* mice compared to controls after high-fat diet in aorta. In the arch similar trends was observed under high-fat diet conditions and significantly decreased expression in *Ikkα^{AA/AA}Apoe^{-/-}* mice was observed for *Mmp-13*. Surprisingly, Tnf-α expression did not significantly differ between *Ikkα^{+/+}Apoe^{-/-}* and *Ikkα^{AA/AA}Apoe^{-/-}* mice or between vascular regions under any dietary condition (data not shown).

Taken together, these data support the hypothesis that effects of *Ikkα^{AA/AA}* knock-in can be site-specific. Under normal diet, the expression of different pro-inflammatory genes was increased by *Ikkα^{AA/AA}* knock-in only in aortic root. However, this was not observed anymore in atherosclerotic conditions. In contrast, under high-fat diet, expression profiles of *Ccr7* and *Ccl19* were significantly reduced by *Ikkα^{AA/AA}* knock-in in arch and thoracic aorta, but not in aortic root. The chemokine *Ccl19* is a target gene of alternative NF-κB activation[158,159], while the *Ccr7* gene expression has been described to be dependent on canonical NF-κB and AP1 activation pathways [160]. With Ikkα performing diverse roles in regulating gene expression, both in NF-κB-dependent as well as -independent manners[115], combined with the differential expression and activation profile of Ikkα in root *vs* aorta and arch (Figure 36), the

data point to increased kinase-dependent functions of Ikkα in arch and aorta compared to aortic root.

5. Discussion

Atherosclerosis is characterized by a chronic inflammation of the vessel wall and many leukocyte subsets play crucial roles in disease initiation and progression, including B- and T-lymphocytes, monocytes and monocyte-derived macrophages, neutrophils and DCs[14,15]. To investigate the function of Ikkα activation in atherosclerosis in detail, its function in haematopoietic cells as well as its overall role during atherosclerosis was studied.

The results showed a versatile function for Ikkα in haematopoietic cells as well as a site-specific role in vascular cells in atherogenesis. Discussed are the results sections separately.

5.1 The haematopoietic role of Ikkα activation in context of atherosclerosis

5.1.1 Bone marrow-specific loss of Ikkα activation affects T-and B-lymphocyte populations

After 13 weeks of high-fat diet the effect of a BM-specific non-activatable *Ikkα^AA/AA* knock-in on haematopoiesis in atherosclerosis was studied. A remarkable reduction of the B-cell population in blood and lymph nodes of atherosclerotic-prone *Ikkα^AA/AA Apoe^-/-* BM chimeras in comparison with *Ikkα^+/+ Apoe^-/-* BM-transplanted *Apoe^-/-* controls was observed. Similar results were obtained in a collaboration with Dr. Toby Lawrence lab, in which a non-atherosclerotic study after transplantation of *Ikkα^AA/AA vs Ikkα^+/+* BM into C57BL/6 recipient mice and *Ikkα^AA/AA* also displayed reduced B-lymphocyte levels in lymph nodes. Already in 2001, Senftleben et al. showed that Ikkα was required for B-cell maturation and Kaisho and colleagues observed also a critical importance of Ikkα in the development of mature B-cells[74,155]. Similarly, reduced B-lymphocyte populations were seen in *Baff^-/-* mice, which together with the results of Ikkα studies indicate a crucial role for the non-canonical Baff-Baffr-Nik-Ikkα pathway in B-cell maturation and survival[161]. In this study, the Cd19^+B-cell population was not only reduced in secondary lymphoid organs and blood, but B-cells were also significantly decreased in BM of *Ikkα^AA/AA Apoe^-/-* -transplanted *Apoe^-/-* mice after 13 weeks of high-fat diet, suggesting an involvement of Ikkα activity in BM

89

B-cell development. This observation corresponds to recent findings of Balkhi and colleagues, who identified that Ikkα-mediated signalling regulates early B lymphopoiesis during haematopoiesis[162]. They observed a decreased Cd19$^+$, B220$^+$ and Cd19$^+$B220$^+$ B-cell population in the BM of kinase-dead Ikkα (*Ikkα$^{KA/KA}$*) knock-in mice and *Ikkα$^{KA/KA}$* BM chimeras, and also revealed less B220$^+$Cd19$^+$ B-cells in the BM of irradiated *Rag$^{-/-}$* mice reconstituted with *Ikkα$^{-/-}$* fetal liver cells. Thus, the data obtained in my study support this recently identified role for Ikkα kinase activity in early B-cell development in the BM, which was revealed to involve both the canonical as well as the non-canonical NF-kB pathway[162].

Furthermore, *Ikkα$^{AA/AA}$Apoe$^{-/-}$* BM transplanted mice displayed an increase in the Cd62L^{high}Cd44^{low} naive T-cell population in secondary lymphoid organs, whereas Cd62L^{low}Cd44^{high} effector memory T-cells were decreased. Naïve T-cells can differentiate into different subtypes of Th1, Th2, Th17 and T$_{reg}$ cells, which have been involved in both pro- as well as anti-atherogenic processes[163], whereas effector memory T-cells have been associated with increased atherosclerosis both in human as well as in animal models[164]. My findings correspond with a previous observation of Mancino and colleagues, who revealed that Ikkα kinase activity is required in DCs for priming antigen-specific T cells[165]. Mice deficient for Nik (kinase activating Ikkα in the non-canonical NF-κB signalling pathway) and *Nik$^{-/-}$* BM chimeras also demonstrate similar effects on the ratio of naive *vs* effector memory T-cells, which was linked to a cell-intrinsic role of Nik in the generation or maintenance of effector memory T-cells[166,167]. *Nik$^{aly/aly}$* mice, which carry a point mutation in the *Nik* gene causing Nik to be unable to bind Ikkα and showing decreased NF-κB activation[168,169], showed Nik to play a pivotal role in DCs and suggested that thymic DCs require Nik to shape the formation of Cd4$^+$ T effector lineages during early development[125]. Also, splenic *Nik$^{aly/aly}$* DCs expressed a considerably lower level of MhcII compared to *Nik$^{aly/+}$* DCs[170], suggesting an inability of *Nik$^{aly/aly}$* DCs to deliver T-cell co-stimulatory signals and contribute to the development of effector T-cells[171]. In agreement with this, also my *Ikkα$^{AA/AA}$Apoe$^{-/-}$* BM transplanted mice displayed a significantly reduced MhcII expression on splenic pDCs. The combination of observations by Mancino et al. and my new findings, suggest that the impact of Ikkα activity on cell-intrinsic *vs* DC-mediated effects on the increased ratio of naive *vs* effector memory T-cells remains to be studied in further detail.

Additionally to the reduced effector memory T-cell levels, $Ikka^{AA/AA}Apoe^{-/-}$ BM chimeras displayed remarkably reduced T_{reg} populations. T_{regs} develop in the thymus and in peripheral sites from naive Cd4$^+$ T-cells, and have been indicated to exert atheroprotective functions[34]. When Kaijura et al examined *Nik*-mutant mice for factors controlling the physical contact between thymocytes and the thymic stroma essential for T-cell maturation, they observed a disorganized thymic structure with abnormal expression of Rel proteins in the stroma. This was associated with a defective establishment of self-tolerance and reduced T_{reg} numbers[172]. Recently, a study of single $Nik^{-/-}$ *vs* mixed $Nik^{-/-}/Nik^{+/+}$ BM chimeras indicated an additional cell-intrinsic role for Nik in the maintenance of peripheral T_{reg} T-cells[167]. Furthermore, Nik and Ikkα were previously shown to be required in human DCs to trigger the development of T_{reg} cells from naive Cd4$^+$ T-cells *in vitro*[173]. One study revealed, that pDC-triggered T_{reg} development from naive T-cells was associated with the induction of indoleamine 2,3-dioxygenase (IDO) in pDCs and required NIK-mediated non-canonical NF-kB activation[174,175] . With Ikkα being a crucial player in non-canonical NF-kB activation, this study directly demonstrates a role for haematopoietic Ikkα kinase activation in the generation of T_{reg} cells *in vivo*. Yet, the relative importance of T_{reg}-intrinsic *vs* DC-mediated mechanisms remains to be investigated, both in the periphery as thymus, given that peripheral DCs can migrate into the thymus to actively contribute to thymic T_{reg} generation[176].

Taken together, flow cytometric analysis of $Ikka^{AA/AA}$ knock-in mice after 13 weeks of high-fat diet shows a critical role for Ikkα in B-cell development, in naive and effector memory T-cell ratios and in generation of T_{regs}.

5.1.2 Atherosclerotic lesions are unaltered in $Ikka^{AA/AA}Apoe^{-/-}$ bone marrow chimeras

Surprisingly, although Ikkα showed a great impact on haematopoietic lymphocytes and VLDL levels were altered in $Ikka^{AA/AA}Apoe^{-/-}$ BM transplanted mice, $Ikka^{AA/AA}$ knock-in showed no effect on the size, phenotype or cell composition of atherosclerotic lesions in the aortic root or aorta. The increased levels of VLDL in $Ikka^{AA/AA}Apoe^{-/-}$ BM chimeras can be associated with the reduced T_{reg} population, as

depletion of T$_{reg}$ T-cells was recently discovered to enhance VLDL levels through reduced VLDL clearance[177].

Given the reduced B-cell population in *Ikkα*$^{AA/AA}$*Apoe*$^{-/-}$ BM-transplanted mice, an atheroprogressive effect was expected due to the findings of Major and colleagues, who showed increased atherosclerosis in B-lymphocyte deficient mice[178]. Also several other studies have suggested an atheroprotective function for B-cells[43,41]. However, B-cells have been involved in various stages of atherosclerosis[40] and different B-cell subsets can have opposing pro-atherogenic and atheroprotective roles in atherosclerosis[179]. Whereas B2 B-cells exacerbate atherosclerosis, B1 B-cells have been indicated to be rather atheroprotective by the secretion of natural IgM, which increases IgM deposits and reduces necrotic cores in atherosclerotic lesions[41,180]. In this context, mice deficient in *Baff*[161], a stimulus for the non-canonical NF-κB activation, or its receptor *Baffr*[181], exhibited a lack of B2 B-cells, whereas the B1 B-cell population was preserved. Accordingly to these observations, *Baffr*$^{-/-}$*Apoe*$^{-/-}$ or *Baffr*$^{-/-}$ BM-transplanted *Ldlr*$^{-/-}$ mice showed decreased atherosclerotic lesion sizes[182]. Depletion of only B2 B-cells in *Baffr*$^{-/-}$*Apoe*$^{-/-}$ mice attenuated atherosclerosis and the administration of a blocking Baffr mAb in hyperlipidemic *Apoe*$^{-/-}$ mice reduced the progression of atherosclerosis by the depletion of mature B2 cells[183,184]. Although my study did not examine B-cell subsets, Senftleben et al. observed a reduction in the mature IgM^{low}IgD^{high} B-cell population in *Ikkα*$^{AA/AA}$ mice and *Ikkα*$^{AA/AA}$ BM transplanted mice, with IgD being a surface marker of follicular B2 B-cells[74,41,185]. Accordingly, one could assume that the reduced B-cell population in my *Ikkα*$^{AA/AA}$*Apoe*$^{-/-}$ BM chimeras may provide atheroprotective effects through a potential decrease in B2 B-cells.

Although blood and lymph nodes of *Ikkα*$^{AA/AA}$*Apoe*$^{-/-}$ transplanted mice displayed increased Cd3$^+$ T-cell levels in blood, the Cd3$^+$ T-cell content in atherosclerotic lesions of aortic root did not differ between the two mouse groups. This could be caused by different ratios of naive T-cells *vs* effector memory T-cells and T$_{reg}$ cells, creating an equalizing effect on the lesion content. Previously, effector memory T-cells have been shown to be present in atherosclerotic lesions and to positively influence the extent of atherosclerosis in hyperlipidemic mice[164]. Naive T-cells on the contrary were associated with an atheroprotective function in atherosclerotic lesions in the aortic sinus[164]. Also, regulatory T-cells have been

attributed with atheroprotective properties[34] and many studies have shown that decreased T_{reg} numbers are associated with increased disease activity[186]. The pro-atherogenic effects of decreased T_{reg} numbers in *Ikkα*$^{AA/AA}$*Apoe*$^{-/-}$ BM chimeras may be compensated by atheroprotective effects of increased naive *vs* effector memory T-cells. Similar observations were made by Lutgens and colleagues upon deficiency of Cd40-Traf2/3/5 signalling in *Apoe*$^{-/-}$ mice, which did not affect atherosclerosis despite an increase in both atheroprogressive effector memory T-cells and atheroprotective T_{reg} cells[187].

To summarize, the missing effect on atherosclerotic plaque development, phenotype and composition in *Ikkα*$^{AA/AA}$*Apoe*$^{-/-}$ *vs Ikkα*$^{+/+}$ *Apoe*$^{-/-}$ BM chimeras could be based on simultaneous changes in lymphocyte subsets with both atheroprogressive and -protective effects, which cancel each other out leading to no visible effect on atherosclerosis.

5.1.3 Haematopoietic knock-in of the *Ikkα*$^{AA/AA}$ mutant does not affect systemic inflammatory gene expression in *Apoe*-deficient mice

Macrophages play a crucial role in the progression of atherosclerosis[56], and Ikkα has been attributed an anti-inflammatory function in macrophages by the resolution of canonical NF-κB activation and thereby termination of pro-inflammatory gene expression[137]. Also other subsequent studies have reported, that Ikkα negatively regulates canonical NF-κB activation in both *Ikkα*$^{-/-}$ mouse macrophages[188] and zebrafish with a targeted mutation in the mammalian IKKα orthologue[189].

Therefore, I examined the influence of *Ikkα*$^{AA/AA}$*Apoe*$^{-/-}$ knock-in on macrophage lipid uptake, on lesional apoptosis and necrotic core size, NF-kB p65 activity and cytokine/ chemokine expression. As macrophages play an important role in the uptake of modified lipids in atherosclerotic lesions[15,190], the intracellular lipid accumulation in macrophages was studied both *in vitro* and *in vivo*. However, no significant differences were observed *in vitro* after stimulation with Dil-labeled oxLDL or in atherosclerotic lesions of *Ikkα*$^{AA/AA}$*Apoe*$^{-/-}$ *vs Ikkα*$^{+/+}$*Apoe*$^{-/-}$ BM chimeras. A similar effect was reported for *Ldlr*$^{-/-}$ mice with a myeloid-specific deletion of Ikkβ[127].

Despite the expected important impact of Ikkα on macrophages, the macrophage content in atherosclerotic lesions of BM chimeras was also comparable.

Furthermore, Lawrence et al showed that macrophages carrying the *Ikkα^AA/AA* knock-in mutation were more resistant to pathogen-induced apoptosis[137]. Apoptosis is an important process in atherogenesis, and its effect is dual. At early stages it can exert atheroprotective properties, as apoptotic death of SMCs and inflammatory cells may delay the atherosclerotic process. However, in later disease phases it is associated with plaque necrosis and atheroprogression, and at the end can lead to plaque rupture and thrombosis[191,192]. Given the reported resistance of *Ikkα^AA/AA* macrophages to apoptosis, cellular and macrophage apoptosis in *Ikkα^AA/AA Apoe^-/-* and *Ikkα^+/+ Apoe^-/-* BM chimeras was analysed in atherosclerotic lesions. In addition, also necrotic core sizes were examined. However, no significant differences were observed in cellular or macrophage apoptosis, and also necrotic core sizes were comparable.

Next, the activity of p65 in *Ikkα^AA/AA Apoe^-/-* vs *Ikka^+/+ Apoe^-/-* BM-derived macrophages upon LPS stimulation was assessed. In previous studies *Ikkα^AA/AA* macrophages displayed prolonged NF-κB activation upon stimulation with LPS. Yet, this study did not show any differential NF-kB activity between knock-in mutant and wildtype macrophages after LPS stimulation, and upon atherogenic (i.e. Tnf-α, oxLDL) exposure, even decreased p65 activation was observed in *Ikkα^AA/AA Apoe^-/-* macrophages. These differential observations between my study and the effects of *Ikkα^AA/AA* on NF-kB activation described by Lawrence and colleagues[137] are surprising. Potentially these differential effects can be attributed to the *Apoe*-deficient background used in this study. ApoE combines with lipid in the body to form molecules called lipoproteins. Lipoproteins are responsible for packaging cholesterol and other fats and carrying them through the bloodstream. *Apoe^-/-* mice are commonly used atherosclerosis-prone mice, which upon high-fat diet develop atherosclerotic lesions morphologically similar to those found in humans[193]. Despite the widespread use of the *Apoe^-/-* transgenic mouse model, it also carries several disadvantages. ApoE has been recognized to affect macrophage biology, immune function and adipose tissue biology[194]. In macrophages ApoE was revealed to be an important immunomodulator promoting the anti-inflammatory M2 phenotype[195]. Also, it is know that NF-κB signalling is very complex and diverse, which is thought to be

important for facilitating the differential and highly selective regulation of NF-κB target genes. The regulation of NF-κB activation behaves in a cell type-specific manner, also in the context of Ikkα-mediated NF-κB regulation[196]. Whereas LPS stimulation of *Ikkα^{AA/AA}* BM-derived macrophages showed enhanced NF-κB activity in the study of Lawrence and colleagues[137], canonical NF-κB signalling was not affected in BM-derived *Ikkα^{AA/AA}* DCs[165] and *Ikkα^{AA/AA}* B-cells even displayed a small reduction in basal and LPS-induced NF-kB activation[74]. Furthermore, NF-kB regulatory mechanisms are not only cell type-specific but also stimulus-dependent and various intrinsic and extrinsic mechanisms allow NF-κB to regulate genes in a different way different cell types and in response to different stimuli[196], as demonstrated in a study in which *Ikkα^{AA/AA}* knock-in did not affect Tnf-α-mediated NF-κB activation in fibroblasts or mammary epithelial cells[144]. Hence, the dissimilar effects of impaired Ikkα activity on LPS-/Tnf-α-/oxLDL-induced NF-kB p65 activity in macrophages in my study compared to previous reports[137] could be due to differential macrophage phenotypes induced by *Apoe*-deficiency or could be based even on different culturing conditions.

Despite the known diverse roles of Ikkα kinase in modulating gene expression in an NF-κB-dependent or -independent manner, my investigation did not discover any differences between the levels of inflammatory cytokines and chemokines. The supernatants of Tnf-α- or oxLDL-stimulated *Ikkα^{AA/AA}Apoe^{-/-}* vs *Ikkα^{+/+}Apoe^{-/-}* BM-derived macrophages did not show any differences in cytokine levels, with the exception of Il-12 which showed a significant increase in oxLDL-stimulated macrophages upon *Ikkα^{AA/AA}* knock-in. Also in serum of atherosclerotic *Ikkα^{AA/AA}Apoe^{-/-}* vs *Ikkα^{+/+}Apoe^{-/-}* mice no significant differences in cytokine and chemokine levels were measured. Thus, the reported functions of Ikkα in regulation of gene expression do not seem strong enough in the context of atherogenesis to produce a major effect on systemic protein expression upon *Ikkα^{AA/AA}* knock-in.

5.1.4 Conclusions and perspectives of BM-specific inactivation of Ikkα kinase during atherogenesis

This study demonstrated a significant effect of knocking-in an activation-resistant Ikkα mutant on many leukocyte subsets, yet an overall zero effect on atherosclerosis and canonical NF-κB activation in macrophages. Taken together the data suggest

that the zero effect on atherosclerosis is at least partially the result of counterbalanced effects on different B- and T-leukocyte subsets. Also, the effects of *Apoe*^{-/-} background on different biological processes in macrophages could overrule a potential impact of *Ikkα*[AA/AA] knock-in on macrophage biology in the context of atherosclerosis.

Future studies are needed to investigate the role of the Ikkα kinase in atherosclerosis in different leukocyte subsets individually, for example it would be interesting to perform a detailed characterization on the effect of a DC- or T$_{reg}$-specific *Ikkα*[AA/AA] mutation on atherogenesis. A recent report identified both IKKα and IKKβ to be important in neutrophil chemotaxis to HMGB1, a nuclear protein released by necrotic cells, but the functions of the IKKα kinase activity in neutrophil responses and molecular signalling in the context of inflammation and atherosclerosis have not yet been investigated[197].

In human atherosclerotic lesions the NF-κB isoforms p65, c-Rel and p50 have been observed[85], but the effect of the IKKα kinase on NF-kB stability in macrophages has so far only been studied for the isoforms p65 and c-Rel. It has been suggested that p50-p50 homodimers represent the main NF-κB activity during inflammation resolution, which could correspond to the findings of Kanters et al, who observed haematopoietic *p50* deficiency to result in a higher inflammatory phenotype of atherosclerotic lesions in *Ldlr*^{-/-} mice[104]. A study focusing on the canonical and non-canonical NF-κB isoform activity in different stages of atherosclerosis and the potential effect of *Ikkα*[A/A] mutation on activity of all isoforms is required.

5.2   The global role of Ikkα activation in atherosclerosis

5.2.1 Global Ikkα inactivity causes oppositional atherosclerotic effects at different vascular locations

Atherosclerosis is a chronic inflammatory disease in which lipids and inflammatory cells accumulate inside the inner wall of arteries, causing the build-up of plaques. Over time, the plaque progresses and narrows the artery[18]. Atherosclerotic lesions develop predominantly at sites that are exposed to disturbed blood flow e.g. bifurcations or bends[6]. These areas are characterized by low/oscillatory shear stress on the vessel wall and these haemodynamic forces alter endothelial cell physiology

Discussion

by enhancing inflammatory activation[198]. On the other hand, regions of the arterial tree that are exposed to uniform, unidirectional blood flow and experience high shear stress are protected from inflammation and lesion development. It has been shown that vascular ECs sense shear stress with help of mechanoreceptors, which transduce shear stress signals into biochemical signals resulting in the modulation of pro-inflammatory signalling pathways[47]. Several signalling pathways, especially NF-κB-mediated signalling[93,84], play crucial roles in these shear stress-induced pathophysiological processes and recently, miRNAs have emerged as important regulators of EC function by fine-tuning gene expression[57].

My study of BM-restricted $Ikk\alpha^{AA/AA}$ knock-in showed that only haematopoietic inactivation of Ikkα was not strong enough to influence atherogenesis. However, the study of global Ikkα inactivity demonstrated a striking effect of Ikkα inactivity on atherosclerotic lesion area in the aortic root, yet with an opposite effect at the aortic arch and thoracic aorta. $Ikk\alpha^{AA/AA}$ mutation decreased lesion area in aortic root by 22%, whereas in $Ikk\alpha^{AA/AA}Apoe^{-/-}$ mice the lesions were increased by 65% in the total aorta and by 70% in the aortic arch. This dissimilar effect on lesion size was not associated with a differential effect on lesion composition, as $Ikk\alpha^{AA/AA}$ knock-in did not alter the cellular composition of atherosclerotic lesions in the aortic root or in the BCA. Previous studies similarly observed intriguing, site-specific atherosclerotic effects when inspecting distinctive vascular regions such as the aortic sinus *vs* thoraco-abdominal aorta. In one study, Teupser et al discovered a major reduction of atherosclerosis in fractalkine-deficient mice in the BCA, but not in the aortic root[146]. Another study showed Pecam-1 to be pro-atherosclerotic in the inner curvature of the aortic arch, whereas it exerted atheroprotective effects in the aortic root, branching arteries and descending aorta[145]. Witting et al observed an increase in lesion area in aortic root of male $Apoe^{-/-}$ mice after Western-type diet with 1% probucol for 24 weeks, but a decrease at the aortic arch, descending aorta, and proximal abdominal aorta[199]. Ebselen, a glutathione peroxidase-1 (GPx1) mimic, reduced atherosclerotic lesions in the aorta of diabetic $Apoe^{-/-}$ mice, but not within the aortic sinus[200]. The concept that local haemodynamic factors account for differences in atherosclerotic lesion formation at different vascular sites has become almost universally accepted by researchers in the field[201]. There is evidence that disturbed flow patterns influence the expression of a large number of genes in ECs, which in turn would mean that

97

depending on the flow conditions and particular vascular location, the gene expression profile of vascular ECs could either promote or attenuate the development of atherosclerosis at these sites[202].

My study is the first one to demonstrate a site-specific effect of *Ikkα*[AA/AA] mutation on atherosclerosis, which could be triggered by a differential extent of Ikkα activation at different vascular locations under atherosclerotic conditions (as explained in more detail in the next chapter). However, the underlying processes triggering the observed effects on atherosclerosis remain currently unclear. I could not observe effects of *Ikkα*[AA/AA] knock-in on the plaque phenotype or its cellular composition.

In conclusion, my data suggested strongly a site-specific role for Ikkα kinase activation in atherogenesis in aortic root *vs* aortic arch and thoracic aorta, independent from effects on lesional cellular composition. As the first part of my study did not reveal an effect of haemotopoeietic knock-in of *Ikkα*[AA/AA] on atherosclerosis, the observed effects are expected to be associated with effects on vascular cells, being ECs or SMCs.

5.2.2 Site-specific effect of Ikkα on atherosclerosis based upon differential Ikkα expression and activation profiles

Changes in gene expression at sites of oscillatory/turbulent flow with low shear stress are at least partly mediated by NF-κB and have been associated with reduced levels of IκBα in a flow-dependent fashion, which in turn is related to enhanced IKK activation[203]. These *in vitro* findings have also been mirrored in *in vivo* models demonstrating high activation of NF-κB in the lesser curvature of mouse aorta, which has a disrupted flow pattern and is susceptible to atherosclerosis[84]. Both IKKα and IKKβ have been presented to be up-regulated under low shear stress conditions, but a significant proportion of low shear-induced-kinase activity activating NF-κB is contributed by IKKβ[130]. Also, histone H3 phosphorylation has been associated to be induced by high shear stress[204] and given the importance of IKKα in histone H3 phosphorylation[139], a gene-modulating role for IKKα regulated by shear stress could be assumed.

Discussion

Therefore, I examined whether the opposite regional effects of $Ikk\alpha^{AA/AA}$ knock-in on atherosclerosis could be caused either by differential, site-specific effects on canonical NF-κB p65 activity or oppositional effects on histone H3 phosphorylation. However, NF-κB p65 DNA binding-activity did not show any variation between the $Ikk\alpha^{AA/AA}Apoe^{-/-}$ mice and the control group in any of the vascular sites examined. Despite the reported findings of shear stress and flow condition-induced NF-κB activation[205], the NF- κB p65 activity profile was similar between root, arch and thoracic aorta. A possible cause for a missing effect of defective Ikkα activation could be compensating effects of Ikkβ in NF-κB activation[136]. Furthermore, examination of histone H3 phosphorylation within the aortic root, arch and thoracic aorta revealed that wildtype mice exhibited increased histone H3 phosphorylation levels within the aortic arch compared to aorta and aortic root. This was not observed in $Ikk\alpha^{AA/AA}$ knock-in mice, in which histone H3 phosphorylation levels in aortic arch were decreased compared to wildtype controls. In contrast to aortic arch, histone H3 phosphorylation levels in aortic root and aorta of $Ikk\alpha^{AA/AA}$ knock-in mice were unaltered compared to wildtype controls. These data indicated that histone H3 phosphorylation is site-specifically regulated by Ikkα, with a role for Ikkα in histone H3 phosphorylation only in aortic arch. These findings could partially contribute to the differential effect of $Ikk\alpha^{AA/AA}$ knock-in on atherosclerosis in aortic root *vs* arch. However, they do not explain why a similar effect was observed on atherosclerosis in thoracic aorta and arch, as histone H3 phosphorylation was differentially affected by $Ikk\alpha^{AA/AA}$ knock-in at these vascular sites.

Additionally, Ikkα protein expression and activation were analysed in the aortic root *vs* arch and thoracic aorta, to examine whether a differential, site-specific expression or activation profile of Ikkα could underlie site-specific effects of $Ikk\alpha^{AA/AA}$ knock-in on atherosclerosis. Comparing aortic root *vs* arch and thoracic aorta, site-specific differences in total Ikkα protein levels were revealed as well as site-specific differences in the activation of Ikkα. Whereas the aortic root showed increased amounts of total endogenous Ikkα, significantly higher Ikkα phosphorylation levels were detected in the arch and thoracic aorta. Together, these data suggest that differential expression and/or activation of Ikkα could exert regional-dependent functions. To examine whether differential protein expression was a result from differential mRNA production, the expression profiles of *Ikkα* mRNA were evaluated

with help of real-time qPCR after high-fat diet and normal diet in aortic root as well as arch and thoracic aorta. Surprisingly, qPCR data revealed opposite results compared to the protein data, showing significantly enhanced *Ikkα* mRNA expression in arch and thoracic aorta compared to aortic root. This suggests that Ikkα protein levels are further regulated on post-transcriptional level. Although the qPCR method is one of the most commonly used techniques for detection of gene expression due to its sensitivity, specificity and ease of use, many regulatory processes occur only after mRNA expression such as post-transcriptional and post-translational regulation, as well as regulation of protein stability[206]. These processes need to be considered when looking into protein concentrations and might explain the different effects observed in Ikkα levels when comparing mRNA *vs* protein data.

5.2.3 Potential role for miRs in regulating Ikkα mRNA levels

My study examining whether *Ikkα* mRNA expression could be triggered by flow conditions did not reveal a conclusive result. The highest expression of *Ikkα* mRNA in aorta would suggest that laminar flow (and thus higher shear stress) would increase *Ikkα* mRNA levels compared to aortic arch and root, which would be more subjective to turbulent and oscillatory, pulsatile flow conditions and thus lower shear stress[207]. In contrast, data from the partial ligation model would rather suggest that, if flow conditions are indeed regulating *Ikkα* mRNA levels in this model, disturbed laminar flow increases instead of reduces *Ikkα* mRNA levels. However, it is also likely that *Ikkα* mRNA levels in the partial ligation model are regulated by acute inflammatory rather than flow conditions, *e.g.* by adhesion of platelets or leukocytes as already visible 1 day after ligation[157]. On the other hand, it is also possible that *Ikkα* mRNA expression in aortic root, arch and aorta is regulated differently due to phenotypic diversity in vascular ECs and SMCs[208]. Thus, more studies are required whether and how differential flow would affect *Ikkα* mRNA levels.

MiRs have been reported to be important regulators of post-transcriptional repression. They are able to induce degradation of their target mRNA or repress translation of the mRNA into protein, and could thus be a reason for the regional differences in Ikkα expression profiles, either on mRNA or protein level[58]. As flow conditions, shear stress and the susceptibility of atherosclerosis have been

Discussion

associated with the expression of miRs, expression profiles were studied for 6 Ikkα-targeting miRs. Corresponding with the upregulation of *Ikkα* mRNA under turbulent flow conditions in the partial ligation model, miR-301a, miR-301b, miR-23a and let7b expression levels were all greatly decreased 1 day after partial ligation of the carotid artery. Similarly, when comparing miR expression profiles in aortic root, arch and thoracic aorta, all miRs except for miR-425 and miR-16 showed a reduced expression in aorta compared to root, corresponding with the highest *Ikkα* expression in aorta. Thus, both in the partial ligation model as well as in the atherosclerosis model, my data indicate that a lower expression of *Ikkα*-targeting miRs is associated with an increased *Ikkα* mRNA level, suggesting a role for these miRs in miR-mediated degradation of *Ikkα* mRNA. However, a more detailed study would be necessary to confirm a direct role of these miRs in regulating *Ikkα* in these mouse models and whether this is controlled in a flow-specific manner.

Although most of these miRs have not been previously reported to be regulated by turbulent flow conditions, most of them have been priorly implicated in cardiovascular diseases and shown to be expressed in endothelial cells. miR-301a/b and let7b were shown to be suppressed in endothelial cell-specific *Dicer* knock-out mice and let-7b has been reported to be expressed in different EC types and thereby to be involved in EC phenotypic differences[209]. The cluster miR-23-27-24 was demonstrated to be increased by shear stress, yet only miR-23b was described to have an atheroprotective role[59]. miR-301a was shown to elevate NF-κB activation[210] and miR-16 was reported to modulate non-canonical NF-κB activation by regulating Ikkα expression during macrophage differentiation[211]. Thus, these findings support the *in vivo* relevance of studying effects of miRs on gene expression in the context of pathological processes, such as atherosclerosis.

In conclusion, these data show that the aortic root exhibits different Ikkα protein levels as well as a different extent of Ikkα phosphorylation/activation compared to aortic arch and thoracic aorta. This differential activation pattern could imply different functions of Ikkα in aortic root compared to aortic arch/thoracic aorta. As the aortic root showed higher levels of total Ikkα, increased kinase-independent functions could be suspected to be more relevant at this vasculature site. In contrast, the high levels of active Ikkα at aortic arch and thoracic aorta rather point to increased kinase-dependent functions, such as histone H3 phosphorylation or non-canonical NF-κB

activation. However as *Ikkα*^AA/AA^ knock-in has also a significant effect on atherosclerotic lesion development within the aortic root, Ikkα clearly also exerts important kinase-dependent functions within the aortic root. These Ikkα kinase-dependent functions however seem to be site-specific, given that the atherosclerotic outcome of *Ikkα*^AA/AA^ knock-in in aortic root compared to arch and thoracic aorta is oppositional. The different Ikkα expression profiles could trigger differential interactions of Ikkα with other proteins, causing differential atherosclerotic effects. Or Ikkα target proteins, which become modulated by Ikkα, could be differentially expressed in aortic root *vs* arch and aorta and could thus lead to opposing effects of *Ikkα*^AA/AA^ knock-in on atherosclerosis. To summarize, the site-specific differences in Ikkα expression and activation profiles may underlie the differential effects of *Ikkα*^AA/AA^ knock-in on atherosclerosis in aortic root *vs* aortic arch and aorta.
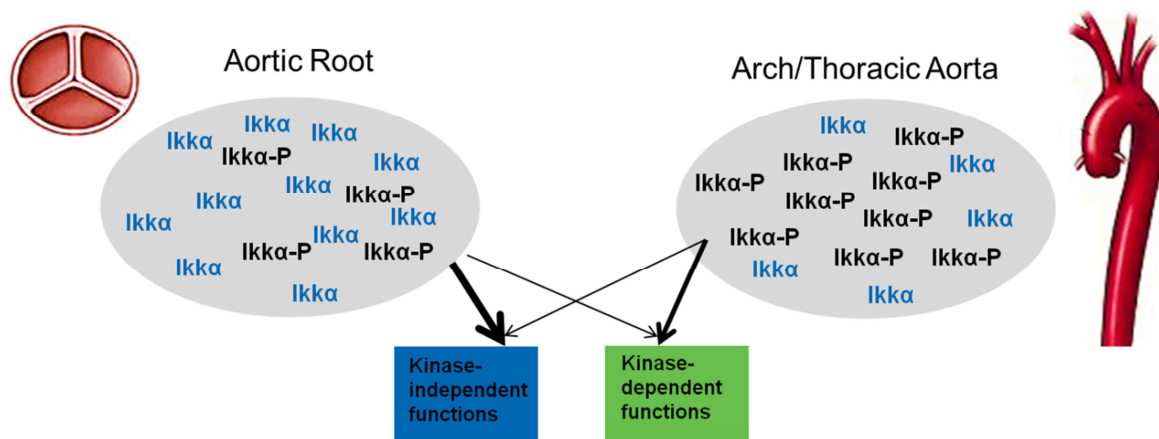
Figure 44: Schematic drawing of suggested regional site-specific Ikkα functions. The aortic arch and thoracic aorta displayed higher levels of phosphorylated (active) Ikkα, whereas within the aortic root elevated total Ikkα levels were found. This leads to the suggestion that even under regular conditions Ikkα may exert different functions depending on the vascular region, e.g. in the arch and aorta Ikkα could regulate gene expression through kinase-dependent functions, whereas in the aortic root Ikkα could exert more kinase-independent functions or different kinase-dependent functions than in arch and aorta.

5.2.4 Site-specific roles of Ikkα regulate gene expression differently and may thereby cause regional differences in athero-susceptibility

Studies in endothelial cells have shown remarkable expression differences of a variety of genes upon different flow patterns[6,212]. Ikkα has been reported to have diverse roles in regulating gene expression, both in NF-κB-dependent as well as -independent manners[115]. Ikkα has been found to shuttle between the cytoplasm and the nucleus and the nuclear-specific roles of Ikkα have brought increasing complexity to its biological function, including to its kinase activity[138]. However, so far no study has associated Ikkα with flow-dependent or site-specific gene regulation. Thus, a gene expression study was performed with the hypothesis that differences in atherosclerosis susceptibility were based on differences in Ikkα functions at the different vascular regions. Various different genes, previously linked to atherosclerosis, were tested for their expression profile in aortic root *vs* arch and thoracic aorta in *Ikkα^AA/AA^Apoe^-/-^ vs Ikkα^+/+^Apoe^-/-* mice after 6 weeks of normal or high-fat diet conditions, among them chemokine *Ccl19* and chemokine receptor *Ccr7*, interleukin *Il-6*, adhesion protein *Vcam-1* and additionally matrix metalloproteinases *Mmp-3*, *Mmp-9* and *Mmp-13*. Especially the differential expression profile of *Ccr7* and *Ccl19* in aortic root compared to arch and aorta in *Ikkα^+/+^Apoe^-/-* mice *vs Ikkα^AA/AA^Apoe^-/-* mice reflected the hypothesis that due to site-specific Ikkα kinase functions, specific genes are differentially regulated leading to different atherosclerosis susceptibility. The chemokine receptor Ccr7 and its ligands Ccl19 and Ccl21 play a crucial role in the homing of lymphocytes and dendritic cells to secondary lymphoid tissues. The Ccr7 ligand Ccl19 has been shown to be regulated by alternative NF-κB activation[213,159] , whereas *Ccr7* gene expression has been suggested to be dependent on NF-κB and AP1 activation pathways[160]. Both Ccr7 as well as its ligands Ccl19 and Ccl21 play a role in atherosclerosis, yet, their impact on atherogenesis has been controversially discussed[214]. Some studies have suggested a rather pro-atherogenic effect for Ccl19 and Ccr7. For example Damas et al found increased levels of Ccl19 and Ccl21 within atherosclerotic lesions of *Apoe^-/-^* mice and in human atherosclerotic carotid plaques compared to healthy vessels, and in plasma of patients with coronary artery disease compared to healthy controls[215]. Halvorsen et al observed that Ccl19 is able to induce proliferation and MMP-1 expression in vascular SMCs, which could contribute to a pro-atherogenic potential[216]. Also, a

recent study described a pro-atherosclerotic function for the Ccl19/Ccr7 axis by promoting human monocyte adhesion and migration[217]. On the other hand, some studies suggested a protective effect. In a mouse study of atherosclerosis regression, *Ccr7* expression levels increased in regressing lesions, potentially suggesting an anti-atherogenic effect of Ccr7[218]. A study from Wan et al also showed protective functions, as they found that genetic *Ccr7*-deficiency exacerbated atherogenesis in *Apoe*$^{-/-}$ mice by increased T-lymphocyte accumulation in the vessel wall[219]. Combining my plaque data with the gene expression profile of *Ccr7* and *Ccl19* in aortic arch and thoracic aorta, my study suggests that Ccr7 and Ccl19 may exert an anti-atherogenic function and that differential expression of *Ccr7* and *Ccl19* at different vascular sites could contribute to the observed differential effects of *Ikkα*$^{AA/AA}$ knock-in on atherosclerosis.

Matrix metalloproteinases contribute to the destruction of extracellular matrix at shoulder regions of plaques and have been shown to be linked to plaque destabilization[97,98]. Given that the *Mmp-3*, *Mmp-9* and *Mmp-13* expression in the aorta of *Ikkα*$^{+/+}$*Apoe*$^{-/-}$ mice was remarkably higher compared to *Ikkα* mutant mice after high-fat diet, my data would implicate a plaque de-stabilizing function for Ikkα through regulation of *Mmp* expression. However, this did not reflect on the atherosclerotic lesions in aorta, where increased atherosclerosis was observed upon *Ikkα*$^{AA/AA}$ knock-in.

Taken together, the data support the hypothesis of a region-specific function for Ikkα kinase activity. Given the assumption drawn from the Ikkα ELISA that within arch and thoracic aorta more activated Ikkα-P is present than in aortic root, in combination with the significantly decreased *Ccr7* and *Ccl19* expression only in arch and aorta upon *Ikkα*$^{AA/AA}$ knock-in, these observations point to increased kinase-dependent Ikkα functions in arch and aorta compared to aortic root and a differential Ikkα-mediated regulation of *Ccr7* and *Ccl19* expression at these vascular regions. A future study examining the atheroprotective effect of *Ikkα*$^{AA/AA}$ knock-in mutation in aortic root needs to performed, as both phenotypic lesion characterization as well as gene expression studies in roots of *Ikkα*$^{AA/AA}$ knock-in mice did not reveal an indication of underlying mechanisms protecting against atherosclerosis.

5.2.5 Conclusions and perspectives on site-specific roles of Ikkα in atherosclerosis

In conclusion, this study illustrates for the first time the functional diversity of Ikkα in atherosclerosis. Whereas within the aortic root Ikkα seems to have a pro-atherogenic function, in the aortic arch and thoracic aorta Ikkα has a protective function instead. The opposite atherosclerotic susceptibility is caused by differential kinase-dependent Ikkα functions. Whether these site-specific differences in Ikkα functions are caused in response to flow conditions should be studied further. Site-specific differences in atherosclerosis can be influenced by multiple factors[202]. Genetic background has been implicated to lead to variations in arterial atherosclerosis by regulating genes that are of variable importance at different anatomic sites, thereby causing site-specific atherosclerotic effects[220]. Also, in the mouse model atherosclerosis develops at first at the aortic root[221], and although Ikkα could have similar functions during the initiation of atherosclerosis, the progressed plaques in the aortic root after 13 weeks of high-fat diet might cause a shift in the kinase function at later stages of disease. Furthermore, a detailed characterization of the differences in EC phenotypic in aortic root compared to arch and thoracic aorta and its effect on the regulation and function of the Ikkα kinase could be highly interesting. The vascular origin of ECs strongly affects their cell-cell junctions, orientation to flow, vesicle formation as well as microvilli count and studies have revealed macrovascular ECs from the aorta to behave differently than microvascular ECs isolated from liver sinusoids[222,223]. Finally, an extensive study on the detailed involvement of Ikkα in resident vascular cells and its functions related to atherosclerosis would be helpful to explain the observed effects on atherosclerosis.

Taken together, my study showed that Ikkα has diverse functions, which can exert both pro- as well as anti-atherogenic effects depending on the vascular region. This suggests that Ikkα would not be an ideal target for systemic drug application. Still, understanding the role of Ikkα kinase activity in atherosclerosis is important, as drugs targeting specifically Ikkα have been suggested to be useful in preventing B-cell-mediated autoimmune diseases[108], however so far only drugs targeting Ikkβ are available. Furthermore, this study clearly underlines the importance to study effects of gene manipulations or drug treatments on atherosclerosis at different anatomic sites, which is currently not always standardly performed in atherosclerosis studies.

6. Summary

Most fatal cardio- and cerebrovascular incidents are caused by atherosclerosis, a chronic inflammatory disease of the vessel wall in which the transcription factor NF-κB has been shown to be involved. Two main pathways activate NF-κB: whereas inflammatory signals induce "canonical" NF-κB activation through the IKKβ/IKKγ kinase complex, "alternative" NF-κB activation, triggered by e.g. RANKL, CD40L and LT-β depends on the IKKα kinase. In addition, IKKα was reported to terminate the canonical NF-κB activation in macrophages, thereby contributing to the resolution of inflammation. Furthermore, IKKα exerts multiple NF-κB-independent functions, e.g. modulating gene expression by phosphorylating histone H3. Despite these known functions of IKKα, the contribution of IKKα to atherogenesis remained unexplored. Thus, the aim of this study was to identify the role of haematopoietic IKKα activation versus the global function of IKKα activation in atherosclerosis. For both approaches an activation-resistant Ikkα (*Ikkα^AA/AA*) mouse model was used, with a hyperlipidemic Apolipoprotein E-deficient (*Apoe^-/-*) background.

To study the bone marrow-specific function of Ikkα kinase activity, *Ikkα^AA/AA^Apoe^-/-* or *Apoe^-/-* bone marrow was transplanted in lethally-irradiated *Apoe^-/-* mice, followed by high-fat diet for 8 or 13 weeks. Haematopoietic profiling revealed a significant decrease in B-cells, regulatory T-cells and effector memory T-cells in *Ikkα^AA/AA^Apoe^-/-* bone marrow chimeras, whereas the naive T-cell population was increased. However, an overall zero effect on atherosclerosis, canonical NF-κB activation in macrophages and gene expression was observed. Taken together, the data indicate that diverse functions of Ikkα in haematopoietic cells may counterbalance each other or may not be strong enough to influence atherogenesis, and reveal that targeting haematopoietic Ikkα kinase activity alone does not represent a suitable therapeutic approach.

Furthermore, the global role of Ikkα in atherosclerosis was studied in *Ikkα^AA/AA^Apoe^-/-* mice after 13 weeks of high-fat diet. *Ikkα^AA/AA^Apoe^-/-* mice showed significantly increased plaque formation in the aorta compared to wildtype controls, but surprisingly the lesions in aortic root were significantly reduced compared to the control group. These site-specific effects could not be attributed to differences in leukocyte infiltration as lesion phenotypes were comparable between the groups. Also, NF-κB p65 activation showed similar levels between *Ikkα^AA/AA^Apoe^-/-* and

Summary

Ikkα$^{+/+}$*Apoe*$^{-/-}$ mice. However, *Ikkα*$^{AA/AA}$ knock-in reduced histone H3 phosphorylation in aortic arch. Furthermore, the aortic root showed increased amounts of total endogenous Ikkα compared to aortic arch and aorta, whereas levels of activated, phosphorylated Ikkα were significantly higher in arch and thoracic aorta. Also, gene expression studies in *Ikkα*$^{AA/AA}$*Apoe*$^{-/-}$ *vs Ikkα*$^{+/+}$*Apoe*$^{-/-}$ mice revealed site-specific gene expression variations when comparing aortic root to arch and aorta, with *Ccr7* and *Ccl19* to be significantly reduced in *Ikkα*$^{AA/AA}$*Apoe*$^{-/-}$ mice only in arch and aorta but not in aortic root. The combination of the Ikkα activation profile and the gene studies point to regional differences of Ikkα kinase function, which might cause the site-specific atherosclerotic effects, although the exact mechanisms remain to be further examined.

Thus, my data illustrate the functional diversity of the Ikkα kinase and indicate that an exploration of site-specific effects of Ikkα-targeting drugs and of drugs in general on atherosclerosis is required before potential therapeutic application can be considered.

7. Zusammenfassung

Die meisten kardio- und zerebrovaskulären Ereignisse werden durch Atherosklerose verursacht, einer chronisch-entzündlichen Erkrankung der Gefäßwand, in dem der Transkriptionsfaktor NF-κB involviert ist. NF-κB kann über zwei Signaltransduktionswege aktiviert werden: Während pro-inflammatorische Signale die "kanonischen" NF-κB-Aktivierung induzieren, in welcher die Aktivierung abhängig ist vom IKKβ/IKKγ Kinase-Komplex, ist die "alternative" NF-κB-Aktivierung, induziert durch z.B. RANKL , CD40L und LT-β, abhängig von der IKKα Kinase. Darüber hinaus wurde gezeigt, dass IKKα in der Lage ist die kanonische NF-κB-Aktivierung in Makrophagen zu beenden und somit zur Auflösung der Entzündungsreaktion beiträgt. Zudem übt IKKα auch mehrere NF-κB-unabhängige Funktionen aus, wie z.B. die Modulation der Genexpression durch Histon H3 Phosphorylierung. Trotz dieser bereits bekannten Funktionen von IKKα, war der Beitrag von IKKα in der Atherogenese bisher noch unbekannt. Daher war das Ziel dieser Studie, die Rolle der hämatopoetischen IKKα Aktivierung gegenüber der globalen Funktion der IKKα Aktivierung in Atherosklerose zu identifizieren. Für beide Studien wurde ein aktivierungsresistentes Ikkα (*Ikkα$^{AA/AA}$*) Mausmodell verwendet, mit einem hyperlididämischen Apolipoprotein E-defizienten (*Apoe$^{-/-}$*) Hintergrund. Um die knochenmark-spezifische Funktion der Ikkα Kinase-Aktivität zu untersuchen, wurden *Apoe$^{-/-}$* Mäuse zunächst lethal bestrahlt und dann entweder mit Knochenmark von *Ikkα$^{AA/AA}$Apoe$^{-/-}$* oder *Apoe$^{-/-}$* Mäusen transplantiert, gefolgt von einer fettreichen Diät für 8 oder 13 Wochen. Das hämatopoetische Profil zeigte eine signifikante Abnahme der B-Zellen, der regulatorischen T-Zellen und der Effektor-Memory-T-Zellen in den *Ikkα$^{AA/AA}$Apoe$^{-/-}$* Knochenmark-Chimären, während die naive T-Zellpopulation erhöht war. Allerdings konnte keine Auswirkung von *Ikkα$^{AA/AA}$* auf die Atherosklerose, auf die kanonische NF-κB-Aktivierung in Makrophagen oder auf Genexpression festgestellt werden. Zusammengefasst zeigten die Daten, dass die vielfältigen Funktionen von Ikkα in hämatopoetischen Zellen sich entweder gegenseitig ausgleichen oder nicht stark genug sind um die Atherogenese beeinzuflussen, und zeigen weiterhin, dass die Hemmung der hämatopoetische IKKα Kinase-Aktivität als Drugtarget kein geeigneter Therapieansatz darstellt. Darüber hinaus wurde die globale Rolle von Ikkα in der Atherosklerose untersucht in *Ikkα$^{AA/AA}$Apoe$^{-/-}$* und *Ikkα$^{+/+}$Apoe$^{-/-}$* Mäusen nach 13 Wochen fettreicher Diät.

Zusammenfassung

Ikkα^{AA/AA}Apoe^{-/-} Mäuse zeigten eine signifikant erhöhte Plaquebildung in der Aorta im Vergleich zu den Wildtyp-Kontrollen, aber überraschenderweise waren die Läsionen in der Aortenwurzel signifikant reduziert im Vergleich zur Kontrollgruppe, obwohl die Läsionen weiter fortgeschritten waren als in der Aorta. Diese orts-spezifischen Effekte konnten nicht auf Unterschiede in der Leukozyteninfiltration beruhen, da die Läsionsphänotypen zwischen den Gruppen vergleichbar waren. Weiterhin zeigte NF-κB p65 Aktivierung ähnliche Niveaus zwischen *Ikkα^{AA/AA}Apoe^{-/-}* und *Ikkα^{+/+}Apoe^{-/-}* Mäusen. Allerdings bewirkte der *Ikkα^{AA/AA}* Knock-in eine Reduzierung der Histon H3-Phosphorylierung im Aortenbogen. Außerdem zeigte die Aortenwurzel eine erhöhte Mengen an gesamt endogenen Ikkα im Vergleich zum Aortenbogen und der Aorta, während die Mengen an aktivierten, phosphorylierten Ikkα deutlich höher waren im Aortenbogen und in der thorakalen Aorta. Auch Genexpressionsstudien in *Ikkα^{AA/AA}Apoe^{-/-} vs Ikkα^{+/+}Apoe^{-/-}* Mäusen zeigten orts-spezifische Schwankungen in der Genexpression im Vergleich von der Aortenwurzel zur Aorta, wobei die Expression von *Ccr7* und *Ccl19* in *Ikkα^{AA/AA}Apoe^{-/-}* im Aortenbogen und Aorta deutlich reduziert waren, jedoch nicht in der Aortenwurzel. Die Kombination des Ikkα Aktivierungsprofils und die Ergebnisse der Genstudien weisen auf regionale Unterschiede der Ikkα Kinase-Funktion hin, die wiederum standortspezifische atherosklerotische Auswirkungen haben könnten, obwohl die genauen Mechanismen weiterhin untersucht werden müssen.

Meine Daten veranschaulichen die Funktionsvielfalt der Ikkα Kinase und zeigen, dass eine Studie der standortspezifischen Auswirkungen von Medikamenten zur Hemmung von Ikkα und standortsspezifische Auswirkungen allgemeiner Medikamente zur Behandlung der Atherosklerose erforderlich sind, bevor mögliche therapeutische Anwendungen in Betracht gezogen werden können.

8.   References

1.   WHO. Global status report on noncommunicable diseases 2010: World Health Organization; 2011.

2.   Mathers CD, Loncar D. Projections of global mortality and burden of disease from 2002 to 2030. PLoS Med. 2006;3:e442.

3.   Gaziano T, Reddy KS, Paccaud F, Horton S, Chaturvedi V. Cardiovascular Disease. 2006.

4.   Greenberg H. Global cardiovascular disease and the academic public health curriculum. Prog Cardiovasc Dis;56:322-325.

5.   Go AS. Heart Disease and Stroke Statistics-2013 Update: A Report From the American Heart Association (vol 127, pg e6, 2013). Circulation. 2013;127:E841-E841.

6.   Chiu JJ, Chien S. Effects of disturbed flow on vascular endothelium: pathophysiological basis and clinical perspectives. Physiol Rev. 2011;91:327-387.

7.   George S.J. JJ ed Atherosclerosis: Wiley-Blackwell; 2010.

8.   Lusis AJ. Atherosclerosis. Nature. 2000;407:233-241.

9.   Davignon J, Ganz P. Role of endothelial dysfunction in atherosclerosis. Circulation. 2004;109:III27-32.

10.   Hopkins PN. Molecular biology of atherosclerosis. Physiol Rev. 2013;93:1317-1542.

11.   Chatzizisis YS, Jonas M, Coskun AU, Beigel R, Stone BV, Maynard C, Gerrity RG, Daley W, Rogers C, Edelman ER, Feldman CL, Stone PH. Prediction of the localization of high-risk coronary atherosclerotic plaques on the basis of low endothelial shear stress: an intravascular ultrasound and histopathology natural history study. Circulation. 2008;117:993-1002.

12.   Chatzizisis YS, Coskun AU, Jonas M, Edelman ER, Feldman CL, Stone PH. Role of endothelial shear stress in the natural history of coronary atherosclerosis and vascular remodeling: molecular, cellular, and vascular behavior. J Am Coll Cardiol. 2007;49:2379-2393.

13.   Tousoulis D, Kampoli AM, Tentolouris C, Papageorgiou N, Stefanadis C. The role of nitric oxide on endothelial function. Curr Vasc Pharmacol. 2012;10:4-18.

14.   Weber C, Noels H. Atherosclerosis: current pathogenesis and therapeutic options. Nat Med. 2011;17:1410-1422.

15.   Packard RR, Lichtman AH, Libby P. Innate and adaptive immunity in atherosclerosis. Semin Immunopathol. 2009;31:5-22.

16.   Chatzizisis YS, Baker AB, Sukhova GK, Koskinas KC, Papafaklis MI, Beigel R, Jonas M, Coskun AU, Stone BV, Maynard C, Shi GP, Libby P, Feldman CL, Edelman ER, Stone PH. Augmented expression and activity of extracellular matrix-degrading enzymes in regions of low endothelial shear stress colocalize with coronary atheromata with thin fibrous caps in pigs. Circulation;123:621-630.

17.   Libby P. Inflammation in atherosclerosis. Nature. 2002;420:868-874.

18.   Libby P, Ridker PM, Hansson GK. Progress and challenges in translating the biology of atherosclerosis. Nature. 2011;473:317-325.

19.   Weber C, Zernecke A, Libby P. The multifaceted contributions of leukocyte subsets to atherosclerosis: lessons from mouse models. Nat Rev Immunol. 2008;8:802-815.

References

20.   Stoger JL, Gijbels MJ, van der Velden S, Manca M, van der Loos CM, Biessen EA, Daemen MJ, Lutgens E, de Winther MP. Distribution of macrophage polarization markers in human atherosclerosis. Atherosclerosis. 2012;225:461-468.

21.   Butcher MJ, Galkina EV. Phenotypic and functional heterogeneity of macrophages and dendritic cell subsets in the healthy and atherosclerosis-prone aorta. Front Physiol. 2012;3:44.

22.   Savage ND, de Boer T, Walburg KV, Joosten SA, van Meijgaarden K, Geluk A, Ottenhoff TH. Human anti-inflammatory macrophages induce Foxp3+ GITR+ CD25+ regulatory T cells, which suppress via membrane-bound TGFbeta-1. J Immunol. 2008;181:2220-2226.

23.   De Paoli F, Staels B, Chinetti-Gbaguidi G. Macrophage phenotypes and their modulation in atherosclerosis. Circ J. 2013;78:1775-1781.

24.   Mantovani A, Biswas SK, Galdiero MR, Sica A, Locati M. Macrophage plasticity and polarization in tissue repair and remodelling. J Pathol. 2013;229:176-185.

25.   Drechsler M, Megens RT, van Zandvoort M, Weber C, Soehnlein O. Hyperlipidemia-triggered neutrophilia promotes early atherosclerosis. Circulation. 2010;122:1837-1845.

26.   Soehnlein O. Multiple roles for neutrophils in atherosclerosis. Circ Res. 2012;110:875-888.

27.   Megens RT, Vijayan S, Lievens D, Doring Y, van Zandvoort MA, Grommes J, Weber C, Soehnlein O. Presence of luminal neutrophil extracellular traps in atherosclerosis. Thromb Haemost. 2012;107:597-598.

28.   Fuchs TA, Brill A, Duerschmied D, Schatzberg D, Monestier M, Myers DD, Jr., Wrobleski SK, Wakefield TW, Hartwig JH, Wagner DD. Extracellular DNA traps promote thrombosis. Proc Natl Acad Sci U S A. 2010;107:15880-15885.

29.   Noels H, Weber C. Catching up with important players in atherosclerosis: type I interferons and neutrophils. Curr Opin Lipidol. 2011;22:144-145.

30.   Tedgui A, Mallat Z. Cytokines in atherosclerosis: pathogenic and regulatory pathways. Physiol Rev. 2006;86:515-581.

31.   Gao Q, Jiang Y, Ma T, Zhu F, Gao F, Zhang P, Guo C, Wang Q, Wang X, Ma C, Zhang Y, Chen W, Zhang L. A critical function of Th17 proinflammatory cells in the development of atherosclerotic plaque in mice. J Immunol. 2010;185:5820-5827.

32.   King VL, Szilvassy SJ, Daugherty A. Interleukin-4 deficiency decreases atherosclerotic lesion formation in a site-specific manner in female LDL receptor-/- mice. Arterioscler Thromb Vasc Biol. 2002;22:456-461.

33.   Huber SA, Sakkinen P, David C, Newell MK, Tracy RP. T helper-cell phenotype regulates atherosclerosis in mice under conditions of mild hypercholesterolemia. Circulation. 2001;103:2610-2616.

34.   Ait-Oufella H, Salomon BL, Potteaux S, Robertson AK, Gourdy P, Zoll J, Merval R, Esposito B, Cohen JL, Fisson S, Flavell RA, Hansson GK, Klatzmann D, Tedgui A, Mallat Z. Natural regulatory T cells control the development of atherosclerosis in mice. Nat Med. 2006;12:178-180.

35.   Jongstra-Bilen J, Haidari M, Zhu SN, Chen M, Guha D, Cybulsky MI. Low-grade chronic inflammation in regions of the normal mouse arterial intima predisposed to atherosclerosis. J Exp Med. 2006;203:2073-2083.

36.   Liu P, Yu YR, Spencer JA, Johnson AE, Vallanat CT, Fong AM, Patterson C, Patel DD. CX3CR1 deficiency impairs dendritic cell accumulation in arterial intima and reduces atherosclerotic burden. Arterioscler Thromb Vasc Biol. 2008;28:243-250.

37.   Doring Y, Manthey HD, Drechsler M, Lievens D, Megens RT, Soehnlein O, Busch M, Manca M, Koenen RR, Pelisek J, Daemen MJ, Lutgens E, Zenke M, Binder CJ, Weber C, Zernecke A. Auto-antigenic protein-DNA complexes stimulate plasmacytoid dendritic cells to promote atherosclerosis. Circulation. 2012;125:1673-1683.

38.   Niessner A, Weyand CM. Dendritic cells in atherosclerotic disease. Clin Immunol. 2010;134:25-32.

39.   Daissormont IT, Christ A, Temmerman L, Sampedro Millares S, Seijkens T, Manca M, Rousch M, Poggi M, Boon L, van der Loos C, Daemen M, Lutgens E, Halvorsen B, Aukrust P, Janssen E, Biessen EA. Plasmacytoid dendritic cells protect against atherosclerosis by tuning T-cell proliferation and activity. Circ Res. 2011;109:1387-1395.

40.   Zhou X, Hansson GK. Detection of B cells and proinflammatory cytokines in atherosclerotic plaques of hypercholesterolaemic apolipoprotein E knockout mice. Scand J Immunol. 1999;50:25-30.

41.   Perry HM, Bender TP, McNamara CA. B cell subsets in atherosclerosis. Front Immunol. 2012;3:373.

42.   Galkina E, Ley K. Immune and inflammatory mechanisms of atherosclerosis (*). Annu Rev Immunol. 2009;27:165-197.

43.   Hansson GK, Hermansson A. The immune system in atherosclerosis. Nat Immunol. 2011;12:204-212.

44.   Deanfield JE, Halcox JP, Rabelink TJ. Endothelial function and dysfunction: testing and clinical relevance. Circulation. 2007;115:1285-1295.

45.   Koskinas KC, Chatzizisis YS, Baker AB, Edelman ER, Stone PH, Feldman CL. The role of low endothelial shear stress in the conversion of atherosclerotic lesions from stable to unstable plaque. Curr Opin Cardiol. 2009;24:580-590.

46.   Wentzel JJ, Chatzizisis YS, Gijsen FJ, Giannoglou GD, Feldman CL, Stone PH. Endothelial shear stress in the evolution of coronary atherosclerotic plaque and vascular remodelling: current understanding and remaining questions. Cardiovasc Res. 2012;96:234-243.

47.   White CR, Frangos JA. The shear stress of it all: the cell membrane and mechanochemical transduction. Philos Trans R Soc Lond B Biol Sci. 2007;362:1459-1467.

48.   Johnson BD, Mather KJ, Wallace JP. Mechanotransduction of shear in the endothelium: basic studies and clinical implications. Vasc Med. 2011;16:365-377.

49.   Hsieh HJ, Liu CA, Huang B, Tseng AH, Wang DL. Shear-induced endothelial mechanotransduction: the interplay between reactive oxygen species (ROS) and nitric oxide (NO) and the pathophysiological implications. J Biomed Sci. 2014;21:3.

50.   Davies PF, Civelek M, Fang Y, Fleming I. The atherosusceptible endothelium: endothelial phenotypes in complex haemodynamic shear stress regions in vivo. Cardiovasc Res. 2013;99:315-327.

51.   Marin T, Gongol B, Chen Z, Woo B, Subramaniam S, Chien S, Shyy JY. Mechanosensitive microRNAs-role in endothelial responses to shear stress and redox state. Free Radic Biol Med. 2013;64:61-68.

52.   Gargalionis AN, Basdra EK. Insights in microRNAs biology. Curr Top Med Chem. 2013;13:1493-1502.

53.   Pager CT, Wehner KA, Fuchs G, Sarnow P. MicroRNA-mediated gene silencing. Prog Mol Biol Transl Sci. 2009;90:187-210.

54.   Yamakuchi M. MicroRNAs in Vascular Biology. Int J Vasc Med. 2012;2012:794898.

References

55.   Bronze-da-Rocha E. MicroRNAs expression profiles in cardiovascular diseases. Biomed Res Int. 2014;2014:985408.

56.   Weber C, Schober A, Zernecke A. MicroRNAs in arterial remodelling, inflammation and atherosclerosis. Curr Drug Targets. 2010;11:950-956.

57.   Sun X, Belkin N, Feinberg MW. Endothelial microRNAs and atherosclerosis. Curr Atheroscler Rep. 2013;15:372.

58.   Neth P, Nazari-Jahantigh M, Schober A, Weber C. MicroRNAs in flow-dependent vascular remodelling. Cardiovasc Res. 2013;99:294-303.

59.   Boon RA, Hergenreider E, Dimmeler S. Atheroprotective mechanisms of shear stress-regulated microRNAs. Thromb Haemost. 2012;108:616-620.

60.   Staszel T, Zapala B, Polus A, Sadakierska-Chudy A, Kiec-Wilk B, Stepien E, Wybranska I, Chojnacka M, Dembinska-Kiec A. Role of microRNAs in endothelial cell pathophysiology. Pol Arch Med Wewn. 2011;121:361-366.

61.   Hergenreider E, Heydt S, Treguer K, Boettger T, Horrevoets AJ, Zeiher AM, Scheffer MP, Frangakis AS, Yin X, Mayr M, Braun T, Urbich C, Boon RA, Dimmeler S. Atheroprotective communication between endothelial cells and smooth muscle cells through miRNAs. Nat Cell Biol. 2012;14:249-256.

62.   Wei Y, Schober A, Weber C. Pathogenic arterial remodeling: the good and bad of microRNAs. Am J Physiol Heart Circ Physiol. 2013;304:H1050-1059.

63.   Nazari-Jahantigh M, Wei Y, Schober A. The role of microRNAs in arterial remodelling. Thromb Haemost. 2012;107:611-618.

64.   Sen R, Baltimore D. Multiple nuclear factors interact with the immunoglobulin enhancer sequences. Cell. 1986;46:705-716.

65.   de Winther MP, Kanters E, Kraal G, Hofker MH. Nuclear factor kappaB signaling in atherogenesis. Arterioscler Thromb Vasc Biol. 2005;25:904-914.

66.   Oeckinghaus A, Hayden MS, Ghosh S. Crosstalk in NF-kappaB signaling pathways. Nat Immunol. 2011;12:695-708.

67.   Pahl HL. Activators and target genes of Rel/NF-kappaB transcription factors. Oncogene. 1999;18:6853-6866.

68.   Bonizzi G, Karin M. The two NF-kappaB activation pathways and their role in innate and adaptive immunity. Trends Immunol. 2004;25:280-288.

69.   Ofengeim D, Yuan J. Regulation of RIP1 kinase signalling at the crossroads of inflammation and cell death. Nat Rev Mol Cell Biol. 2013;14:727-736.

70.   Karin M, Ben-Neriah Y. Phosphorylation meets ubiquitination: the control of NF-[kappa]B activity. Annu Rev Immunol. 2000;18:621-663.

71.   Hayden MS, Ghosh S. Signaling to NF-kappaB. Genes Dev. 2004;18:2195-2224.

72.   Oeckinghaus A, Ghosh S. The NF-kappaB family of transcription factors and its regulation. Cold Spring Harb Perspect Biol. 2009;1:a000034.

73.   Xiao G, Rabson AB, Young W, Qing G, Qu Z. Alternative pathways of NF-kappaB activation: a double-edged sword in health and disease. Cytokine Growth Factor Rev. 2006;17:281-293.

74.   Senftleben U, Cao Y, Xiao G, Greten FR, Krahn G, Bonizzi G, Chen Y, Hu Y, Fong A, Sun SC, Karin M. Activation by IKKalpha of a second, evolutionary conserved, NF-kappa B signaling pathway. Science. 2001;293:1495-1499.

75.   Liao G, Zhang M, Harhaj EW, Sun SC. Regulation of the NF-kappaB-inducing kinase by tumor necrosis factor receptor-associated factor 3-induced degradation. J Biol Chem. 2004;279:26243-26250.

113

76.	He JQ, Saha SK, Kang JR, Zarnegar B, Cheng G. Specificity of TRAF3 in its negative regulation of the noncanonical NF-kappa B pathway. J Biol Chem. 2007;282:3688-3694.

77.	Razani B, Reichardt AD, Cheng G. Non-canonical NF-kappaB signaling activation and regulation: principles and perspectives. Immunol Rev. 2011;244:44-54.

78.	Sun SC. The noncanonical NF-kappaB pathway. Immunol Rev. 2012;246:125-140.

79.	Hu H, Brittain GC, Chang JH, Puebla-Osorio N, Jin J, Zal A, Xiao Y, Cheng X, Chang M, Fu YX, Zal T, Zhu C, Sun SC. OTUD7B controls non-canonical NF-kappaB activation through deubiquitination of TRAF3. Nature. 2013;494:371-374.

80.	Van der Heiden K, Cuhlmann S, Luong le A, Zakkar M, Evans PC. Role of nuclear factor kappaB in cardiovascular health and disease. Clin Sci (Lond). 2010;118:593-605.

81.	Dabek J, Kulach A, Gasior Z. Nuclear factor kappa-light-chain-enhancer of activated B cells (NF-kappaB): a new potential therapeutic target in atherosclerosis? Pharmacol Rep. 2010;62:778-783.

82.	Brand K, Page S, Rogler G, Bartsch A, Brandl R, Knuechel R, Page M, Kaltschmidt C, Baeuerle PA, Neumeier D. Activated transcription factor nuclear factor-kappa B is present in the atherosclerotic lesion. J Clin Invest. 1996;97:1715-1722.

83.	Zhang W, Xing SS, Sun XL, Xing QC. Overexpression of activated nuclear factor-kappa B in aorta of patients with coronary atherosclerosis. Clin Cardiol. 2009;32:E42-47.

84.	Hajra L, Evans AI, Chen M, Hyduk SJ, Collins T, Cybulsky MI. The NF-kappa B signal transduction pathway in aortic endothelial cells is primed for activation in regions predisposed to atherosclerotic lesion formation. Proc Natl Acad Sci U S A. 2000;97:9052-9057.

85.	Monaco C, Andreakos E, Kiriakidis S, Mauri C, Bicknell C, Foxwell B, Cheshire N, Paleolog E, Feldmann M. Canonical pathway of nuclear factor kappa B activation selectively regulates proinflammatory and prothrombotic responses in human atherosclerosis. Proc Natl Acad Sci U S A. 2004;101:5634-5639.

86.	Spiecker M, Peng HB, Liao JK. Inhibition of endothelial vascular cell adhesion molecule-1 expression by nitric oxide involves the induction and nuclear translocation of IkappaBalpha. J Biol Chem. 1997;272:30969-30974.

87.	Davel AP, Wenceslau CF, Akamine EH, Xavier FE, Couto GK, Oliveira HT, Rossoni LV. Endothelial dysfunction in cardiovascular and endocrine-metabolic diseases: an update. Braz J Med Biol Res. 2011;44:920-932.

88.	Cunningham KS, Gotlieb AI. The role of shear stress in the pathogenesis of atherosclerosis. Lab Invest. 2005;85:9-23.

89.	Nakashima Y, Raines EW, Plump AS, Breslow JL, Ross R. Upregulation of VCAM-1 and ICAM-1 at atherosclerosis-prone sites on the endothelium in the ApoE-deficient mouse. Arterioscler Thromb Vasc Biol. 1998;18:842-851.

90.	Mohan S, Mohan N, Sprague EA. Differential activation of NF-kappa B in human aortic endothelial cells conditioned to specific flow environments. Am J Physiol. 1997;273:C572-578.

91.	Atkins GB, Simon DI. Interplay between NF-kappaB and Kruppel-like factors in vascular inflammation and atherosclerosis: location, location, location. J Am Heart Assoc. 2013;2:e000290.

92.	Chiu JJ, Usami S, Chien S. Vascular endothelial responses to altered shear stress: pathologic implications for atherosclerosis. Ann Med. 2009;41:19-28.

References

93. Collins T, Cybulsky MI. NF-kappaB: pivotal mediator or innocent bystander in atherogenesis? J Clin Invest. 2001;107:255-264.

94. Bourcier T, Sukhova G, Libby P. The nuclear factor kappa-B signaling pathway participates in dysregulation of vascular smooth muscle cells in vitro and in human atherosclerosis. J Biol Chem. 1997;272:15817-15824.

95. Ritchie ME. Nuclear factor-kappaB is selectively and markedly activated in humans with unstable angina pectoris. Circulation. 1998;98:1707-1713.

96. Ren S, Fan X, Peng L, Pan L, Yu C, Tong J, Zhang W, Liu P. Expression of NF-kappaB, CD68 and CD105 in carotid atherosclerotic plaque. J Thorac Dis. 2013;5:771-776.

97. Newby AC. Metalloproteinase expression in monocytes and macrophages and its relationship to atherosclerotic plaque instability. Arterioscler Thromb Vasc Biol. 2008;28:2108-2114.

98. Bond M, Chase AJ, Baker AH, Newby AC. Inhibition of transcription factor NF-kappaB reduces matrix metalloproteinase-1, -3 and -9 production by vascular smooth muscle cells. Cardiovasc Res. 2001;50:556-565.

99. Madonna R, De Caterina R. Relevance of new drug discovery to reduce NF-kappaB activation in cardiovascular disease. Vascul Pharmacol. 2012;57:41-47.

100. Chiba T, Kondo Y, Shinozaki S, Kaneko E, Ishigami A, Maruyama N, Umezawa K, Shimokado K. A selective NFkappaB inhibitor, DHMEQ, reduced atherosclerosis in ApoE-deficient mice. J Atheroscler Thromb. 2006;13:308-313.

101. Yoshida T, Yamashita M, Horimai C, Hayashi M. Smooth muscle-selective inhibition of nuclear factor-kappaB attenuates smooth muscle phenotypic switching and neointima formation following vascular injury. J Am Heart Assoc. 2013;2:e000230.

102. Djuric Z, Kashif M, Fleming T, Muhammad S, Piel D, von Bauer R, Bea F, Herzig S, Zeier M, Pizzi M, Isermann B, Hecker M, Schwaninger M, Bierhaus A, Nawroth PP. Targeting activation of specific NF-kappaB subunits prevents stress-dependent atherothrombotic gene expression. Mol Med. 2012;18:1375-1386.

103. Goossens P, Vergouwe MN, Gijbels MJ, Curfs DM, van Woezik JH, Hoeksema MA, Xanthoulea S, Leenen PJ, Rupec RA, Hofker MH, de Winther MP. Myeloid IkappaBalpha deficiency promotes atherogenesis by enhancing leukocyte recruitment to the plaques. PLoS One. 2011;6:e22327.

104. Kanters E, Gijbels MJ, van der Made I, Vergouwe MN, Heeringa P, Kraal G, Hofker MH, de Winther MP. Hematopoietic NF-kappaB1 deficiency results in small atherosclerotic lesions with an inflammatory phenotype. Blood. 2004;103:934-940.

105. Lawrence T, Gilroy DW, Colville-Nash PR, Willoughby DA. Possible new role for NF-kappaB in the resolution of inflammation. Nat Med. 2001;7:1291-1297.

106. Greten FR, Arkan MC, Bollrath J, Hsu LC, Goode J, Miething C, Goktuna SI, Neuenhahn M, Fierer J, Paxian S, Van Rooijen N, Xu Y, O'Cain T, Jaffee BB, Busch DH, Duyster J, Schmid RM, Eckmann L, Karin M. NF-kappaB is a negative regulator of IL-1beta secretion as revealed by genetic and pharmacological inhibition of IKKbeta. Cell. 2007;130:918-931.

107. Pamukcu B, Lip GY, Shantsila E. The nuclear factor--kappa B pathway in atherosclerosis: a potential therapeutic target for atherothrombotic vascular disease. Thromb Res. 2012;128:117-123.

108. Karin M, Yamamoto Y, Wang QM. The IKK NF-kappa B system: a treasure trove for drug development. Nat Rev Drug Discov. 2004;3:17-26.

109. Hacker H, Karin M. Regulation and function of IKK and IKK-related kinases. Sci STKE. 2006;2006:re13.

110. Chen ZJ, Parent L, Maniatis T. Site-specific phosphorylation of IkappaBalpha by a novel ubiquitination-dependent protein kinase activity. Cell. 1996;84:853-862.

111. DiDonato JA, Hayakawa M, Rothwarf DM, Zandi E, Karin M. A cytokine-responsive IkappaB kinase that activates the transcription factor NF-kappaB. Nature. 1997;388:548-554.

112. Yamaoka S, Courtois G, Bessia C, Whiteside ST, Weil R, Agou F, Kirk HE, Kay RJ, Israel A. Complementation cloning of NEMO, a component of the IkappaB kinase complex essential for NF-kappaB activation. Cell. 1998;93:1231-1240.

113. Israel A. The IKK complex, a central regulator of NF-kappaB activation. Cold Spring Harb Perspect Biol. 2010;2:a000158.

114. Mercurio F, Zhu H, Murray BW, Shevchenko A, Bennett BL, Li J, Young DB, Barbosa M, Mann M, Manning A, Rao A. IKK-1 and IKK-2: cytokine-activated IkappaB kinases essential for NF-kappaB activation. Science. 1997;278:860-866.

115. Hinz M, Scheidereit C. The IkappaB kinase complex in NF-kappaB regulation and beyond. EMBO Rep. 2014;15:46-61.

116. Sil AK, Maeda S, Sano Y, Roop DR, Karin M. IkappaB kinase-alpha acts in the epidermis to control skeletal and craniofacial morphogenesis. Nature. 2004;428:660-664.

117. Ling L, Cao Z, Goeddel DV. NF-kappaB-inducing kinase activates IKK-alpha by phosphorylation of Ser-176. Proc Natl Acad Sci U S A. 1998;95:3792-3797.

118. Zhang J, Clark K, Lawrence T, Peggie MW, Cohen P. An unexpected twist to the activation of IKKbeta: TAK1 primes IKKbeta for activation by autophosphorylation. Biochem J. 2014;461:531-537.

119. Tang ED, Inohara N, Wang CY, Nunez G, Guan KL. Roles for homotypic interactions and transautophosphorylation in IkappaB kinase beta IKKbeta) activation [corrected]. J Biol Chem. 2003;278:38566-38570.

120. Solt LA, May MJ. The IkappaB kinase complex: master regulator of NF-kappaB signaling. Immunol Res. 2008;42:3-18.

121. Liu S, Misquitta YR, Olland A, Johnson MA, Kelleher KS, Kriz R, Lin LL, Stahl M, Mosyak L. Crystal structure of a human IkappaB kinase beta asymmetric dimer. J Biol Chem. 2013;288:22758-22767.

122. Liu F, Xia Y, Parker AS, Verma IM. IKK biology. Immunol Rev. 2012;246:239-253.

123. Huang TT, Feinberg SL, Suryanarayanan S, Miyamoto S. The zinc finger domain of NEMO is selectively required for NF-kappa B activation by UV radiation and topoisomerase inhibitors. Mol Cell Biol. 2002;22:5813-5825.

124. Shifera AS. The zinc finger domain of IKKgamma (NEMO) protein in health and disease. J Cell Mol Med. 2010;14:2404-2414.

125. Schrofelbauer B, Polley S, Behar M, Ghosh G, Hoffmann A. NEMO ensures signaling specificity of the pleiotropic IKKbeta by directing its kinase activity toward IkappaBalpha. Mol Cell. 2012;47:111-121.

126. Schmid JA, Birbach A. IkappaB kinase beta (IKKbeta/IKK2/IKBKB)--a key molecule in signaling to the transcription factor NF-kappaB. Cytokine Growth Factor Rev. 2008;19:157-165.

127. Kanters E, Pasparakis M, Gijbels MJ, Vergouwe MN, Partouns-Hendriks I, Fijneman RJ, Clausen BE, Forster I, Kockx MM, Rajewsky K, Kraal G, Hofker MH, de Winther MP. Inhibition of NF-kappaB activation in macrophages increases atherosclerosis in LDL receptor-deficient mice. J Clin Invest. 2003;112:1176-1185.

128. Fong CH, Bebien M, Didierlaurent A, Nebauer R, Hussell T, Broide D, Karin M, Lawrence T. An antiinflammatory role for IKKbeta through the inhibition of "classical" macrophage activation. J Exp Med. 2008;205:1269-1276.

129. Park SH, Sui Y, Gizard F, Xu J, Rios-Pilier J, Helsley RN, Han SS, Zhou C. Myeloid-specific IkappaB kinase beta deficiency decreases atherosclerosis in low-density lipoprotein receptor-deficient mice. Arterioscler Thromb Vasc Biol. 2012;32:2869-2876.

130. Mohan S, Koyoma K, Thangasamy A, Nakano H, Glickman RD, Mohan N. Low shear stress preferentially enhances IKK activity through selective sources of ROS for persistent activation of NF-kappaB in endothelial cells. Am J Physiol Cell Physiol. 2007;292:C362-371.

131. Pathak R, Shao L, Chafekar SM, Feng W, Ponnappan U, Fink LM, Zhou D, Hauer-Jensen M. IKKbeta regulates endothelial thrombomodulin in a Klf2-dependent manner. J Thromb Haemost. 2014;12:1533-1544.

132. Ashida N, Senbanerjee S, Kodama S, Foo SY, Coggins M, Spencer JA, Zamiri P, Shen D, Li L, Sciuto T, Dvorak A, Gerszten RE, Lin CP, Karin M, Rosenzweig A. IKKbeta regulates essential functions of the vascular endothelium through kinase-dependent and -independent pathways. Nat Commun. 2011;2:318.

133. Sui Y, Park SH, Xu J, Monette S, Helsley RN, Han SS, Zhou C. IKKbeta links vascular inflammation to obesity and atherosclerosis. J Exp Med. 2014;211:869-886.

134. Gareus R, Kotsaki E, Xanthoulea S, van der Made I, Gijbels MJ, Kardakaris R, Polykratis A, Kollias G, de Winther MP, Pasparakis M. Endothelial cell-specific NF-kappaB inhibition protects mice from atherosclerosis. Cell Metab. 2008;8:372-383.

135. Lam LT, Davis RE, Ngo VN, Lenz G, Wright G, Xu W, Zhao H, Yu X, Dang L, Staudt LM. Compensatory IKKalpha activation of classical NF-kappaB signaling during IKKbeta inhibition identified by an RNA interference sensitization screen. Proc Natl Acad Sci U S A. 2008;105:20798-20803.

136. Adli M, Merkhofer E, Cogswell P, Baldwin AS. IKKalpha and IKKbeta each function to regulate NF-kappaB activation in the TNF-induced/canonical pathway. PLoS One. 2010;5:e9428.

137. Lawrence T, Bebien M, Liu GY, Nizet V, Karin M. IKKalpha limits macrophage NF-kappaB activation and contributes to the resolution of inflammation. Nature. 2005;434:1138-1143.

138. Huang WC, Hung MC. Beyond NF-kappaB activation: nuclear functions of IkappaB kinase alpha. J Biomed Sci. 2013;20:3.

139. Yamamoto Y, Verma UN, Prajapati S, Kwak YT, Gaynor RB. Histone H3 phosphorylation by IKK-alpha is critical for cytokine-induced gene expression. Nature. 2003;423:655-659.

140. Anest V, Hanson JL, Cogswell PC, Steinbrecher KA, Strahl BD, Baldwin AS. A nucleosomal function for IkappaB kinase-alpha in NF-kappaB-dependent gene expression. Nature. 2003;423:659-663.

141. Liu B, Yang Y, Chernishof V, Loo RR, Jang H, Tahk S, Yang R, Mink S, Shultz D, Bellone CJ, Loo JA, Shuai K. Proinflammatory stimuli induce IKKalpha-mediated phosphorylation of PIAS1 to restrict inflammation and immunity. Cell. 2007;129:903-914.

142. Shembade N, Pujari R, Harhaj NS, Abbott DW, Harhaj EW. The kinase IKKalpha inhibits activation of the transcription factor NF-kappaB by phosphorylating the regulatory molecule TAX1BP1. Nat Immunol. 2011.

143. Olivotto EO, M.; Astolfi, A.; Platano, D.; Facchini, A.; Pagani, S.; Flamigni, F.; Facchini, A.; Goldring, M.B.; Borzì, R.M.; Marcu, K.B. IKKα/CHUK regulates

extracellular matrix remodeling independent of its kinase activity to facilitate articular chondrocyte differentiation. PLoS One. 2013;8.

144. Cao Y, Bonizzi G, Seagroves TN, Greten FR, Johnson R, Schmidt EV, Karin M. IKKalpha provides an essential link between RANK signaling and cyclin D1 expression during mammary gland development. Cell. 2001;107:763-775.

145. Goel R, Schrank BR, Arora S, Boylan B, Fleming B, Miura H, Newman PJ, Molthen RC, Newman DK. Site-specific effects of PECAM-1 on atherosclerosis in LDL receptor-deficient mice. Arterioscler Thromb Vasc Biol. 2008;28:1996-2002.

146. Teupser D, Pavlides S, Tan M, Gutierrez-Ramos JC, Kolbeck R, Breslow JL. Major reduction of atherosclerosis in fractalkine (CX3CL1)-deficient mice is at the brachiocephalic artery, not the aortic root. Proc Natl Acad Sci U S A. 2004;101:17795-17800.

147. Fuster JJ, Castillo AI, Zaragoza C, Ibanez B, Andres V. Animal models of atherosclerosis. Prog Mol Biol Transl Sci. 2012;105:1-23.

148. Nam D, Ni CW, Rezvan A, Suo J, Budzyn K, Llanos A, Harrison D, Giddens D, Jo H. Partial carotid ligation is a model of acutely induced disturbed flow, leading to rapid endothelial dysfunction and atherosclerosis. Am J Physiol Heart Circ Physiol. 2009;297:H1535-1543.

149. Marim FM, Silveira TN, Lima DS, Jr., Zamboni DS. A method for generation of bone marrow-derived macrophages from cryopreserved mouse bone marrow cells. PLoS One. 2010;5:e15263.

150. Heid CA, Stevens J, Livak KJ, Williams PM. Real time quantitative PCR. Genome Res. 1996;6:986-994.

151. Wei Y, Nazari-Jahantigh M, Chan L, Zhu M, Heyll K, Corbalan-Campos J, Hartmann P, Thiemann A, Weber C, Schober A. The microRNA-342-5p fosters inflammatory macrophage activation through an Akt1- and microRNA-155-dependent pathway during atherosclerosis. Circulation. 2013;127:1609-1619.

152. Arya M, Shergill IS, Williamson M, Gommersall L, Arya N, Patel HR. Basic principles of real-time quantitative PCR. Expert Rev Mol Diagn. 2005;5:209-219.

153. Matos LL, Trufelli DC, de Matos MG, da Silva Pinhal MA. Immunohistochemistry as an important tool in biomarkers detection and clinical practice. Biomark Insights. 2010;5:9-20.

154. Xu S, Huang Y, Xie Y, Lan T, Le K, Chen J, Chen S, Gao S, Xu X, Shen X, Huang H, Liu P. Evaluation of foam cell formation in cultured macrophages: an improved method with Oil Red O staining and DiI-oxLDL uptake. Cytotechnology. 2010;62:473-481.

155. Kaisho T, Takeda K, Tsujimura T, Kawai T, Nomura F, Terada N, Akira S. IkappaB kinase alpha is essential for mature B cell development and function. J Exp Med. 2001;193:417-426.

156. Vandesompele J. dPK, Pattyn F., Poppe B., Van Roy N., de Paepe A., Speleman F. Accurate normalization of real-time quantitative RT-PCR data by geometric averaging of multiple internal control genes. Genome Biology. 2002;3.

157. Kawasaki T, Dewerchin M, Lijnen HR, Vreys I, Vermylen J, Hoylaerts MF. Mouse carotid artery ligation induces platelet-leukocyte-dependent luminal fibrin, required for neointima development. Circ Res. 2001;88:159-166.

158. Lawrence T, Bebien M. IKKalpha in the regulation of inflammation and adaptive immunity. Biochem Soc Trans. 2007;35:270-272.

159. Bonizzi G, Bebien M, Otero DC, Johnson-Vroom KE, Cao Y, Vu D, Jegga AG, Aronow BJ, Ghosh G, Rickert RC, Karin M. Activation of IKKalpha target genes

depends on recognition of specific kappaB binding sites by RelB:p52 dimers. Embo J. 2004;23:4202-4210.

160.	Mburu YK, Egloff AM, Walker WH, Wang L, Seethala RR, van Waes C, Ferris RL. Chemokine receptor 7 (CCR7) gene expression is regulated by NF-kappaB and activator protein 1 (AP1) in metastatic squamous cell carcinoma of head and neck (SCCHN). J Biol Chem. 2012;287:3581-3590.

161.	Schiemann B, Gommerman JL, Vora K, Cachero TG, Shulga-Morskaya S, Dobles M, Frew E, Scott ML. An essential role for BAFF in the normal development of B cells through a BCMA-independent pathway. Science. 2001;293:2111-2114.

162.	Balkhi MY, Willette-Brown J, Zhu F, Chen Z, Liu S, Guttridge DC, Karin M, Hu Y. IKKalpha-mediated signaling circuitry regulates early B lymphopoiesis during hematopoiesis. Blood. 2012;119:5467-5477.

163.	Tse K, Tse H, Sidney J, Sette A, Ley K. T cells in atherosclerosis. Int Immunol. 2013;25:615-622.

164.	Ammirati E, Cianflone D, Vecchio V, Banfi M, Vermi AC, De Metrio M, Grigore L, Pellegatta F, Pirillo A, Garlaschelli K, Manfredi AA, Catapano AL, Maseri A, Palini AG, Norata GD. Effector Memory T cells Are Associated With Atherosclerosis in Humans and Animal Models. J Am Heart Assoc. 2013;1:27-41.

165.	Mancino A, Habbeddine M, Johnson E, Luron L, Bebien M, Memet S, Fong C, Bajenoff M, Wu X, Karin M, Caamano J, Chi H, Seed M, Lawrence T. I kappa B kinase alpha (IKKalpha) activity is required for functional maturation of dendritic cells and acquired immunity to infection. EMBO J. 2013;32:816-828.

166.	Hacker H, Chi L, Rehg JE, Redecke V. NIK prevents the development of hypereosinophilic syndrome-like disease in mice independent of IKKalpha activation. J Immunol. 2012;188:4602-4610.

167.	Murray SE. Cell-intrinsic role for NF-kappa B-inducing kinase in peripheral maintenance but not thymic development of Foxp3+ regulatory T cells in mice. PLoS One. 2013;8:e76216.

168.	Fagarasan S, Shinkura R, Kamata T, Nogaki F, Ikuta K, Tashiro K, Honjo T. Alymphoplasia (aly)-type nuclear factor kappaB-inducing kinase (NIK) causes defects in secondary lymphoid tissue chemokine receptor signaling and homing of peritoneal cells to the gut-associated lymphatic tissue system. J Exp Med. 2000;191:1477-1486.

169.	Xiao G, Harhaj EW, Sun SC. NF-kappaB-inducing kinase regulates the processing of NF-kappaB2 p100. Mol Cell. 2001;7:401-409.

170.	Tamura C, Nakazawa M, Kasahara M, Hotta C, Yoshinari M, Sato F, Minami M. Impaired function of dendritic cells in alymphoplasia (aly/aly) mice for expansion of CD25+CD4+ regulatory T cells. Autoimmunity. 2006;39:445-453.

171.	Hofmann J, Mair F, Greter M, Schmidt-Supprian M, Becher B. NIK signaling in dendritic cells but not in T cells is required for the development of effector T cells and cell-mediated immune responses. J Exp Med. 2011;208:1917-1929.

172.	Kajiura F, Sun S, Nomura T, Izumi K, Ueno T, Bando Y, Kuroda N, Han H, Li Y, Matsushima A, Takahama Y, Sakaguchi S, Mitani T, Matsumoto M. NF-kappa B-inducing kinase establishes self-tolerance in a thymic stroma-dependent manner. J Immunol. 2004;172:2067-2075.

173.	Tas SW, Vervoordeldonk MJ, Hajji N, Schuitemaker JH, van der Sluijs KF, May MJ, Ghosh S, Kapsenberg ML, Tak PP, de Jong EC. Noncanonical NF-kappaB signaling in dendritic cells is required for indoleamine 2,3-dioxygenase (IDO) induction and immune regulation. Blood. 2007;110:1540-1549.

174. Puccetti P, Grohmann U. IDO and regulatory T cells: a role for reverse signalling and non-canonical NF-kappaB activation. Nat Rev Immunol. 2007;7:817-823.

175. Chen W, Liang X, Peterson AJ, Munn DH, Blazar BR. The indoleamine 2,3-dioxygenase pathway is essential for human plasmacytoid dendritic cell-induced adaptive T regulatory cell generation. J Immunol. 2008;181:5396-5404.

176. Proietto AI, van Dommelen S, Zhou P, Rizzitelli A, D'Amico A, Steptoe RJ, Naik SH, Lahoud MH, Liu Y, Zheng P, Shortman K, Wu L. Dendritic cells in the thymus contribute to T-regulatory cell induction. Proc Natl Acad Sci U S A. 2008;105:19869-19874.

177. Klingenberg R, Gerdes N, Badeau RM, Gistera A, Strodthoff D, Ketelhuth DF, Lundberg AM, Rudling M, Nilsson SK, Olivecrona G, Zoller S, Lohmann C, Luscher TF, Jauhiainen M, Sparwasser T, Hansson GK. Depletion of FOXP3+ regulatory T cells promotes hypercholesterolemia and atherosclerosis. J Clin Invest. 2013;123:1323-1334.

178. Major AS, Fazio S, Linton MF. B-lymphocyte deficiency increases atherosclerosis in LDL receptor-null mice. Arterioscler Thromb Vasc Biol. 2002;22:1892-1898.

179. Kyaw T, Tipping P, Toh BH, Bobik A. Current understanding of the role of B cell subsets and intimal and adventitial B cells in atherosclerosis. Curr Opin Lipidol. 2011;22:373-379.

180. Kyaw T, Tay C, Krishnamurthi S, Kanellakis P, Agrotis A, Tipping P, Bobik A, Toh BH. B1a B lymphocytes are atheroprotective by secreting natural IgM that increases IgM deposits and reduces necrotic cores in atherosclerotic lesions. Circ Res. 2011;109:830-840.

181. Sasaki Y, Casola S, Kutok JL, Rajewsky K, Schmidt-Supprian M. TNF family member B cell-activating factor (BAFF) receptor-dependent and -independent roles for BAFF in B cell physiology. J Immunol. 2004;173:2245-2252.

182. Sage AP, Tsiantoulas D, Baker L, Harrison J, Masters L, Murphy D, Loinard C, Binder CJ, Mallat Z. BAFF receptor deficiency reduces the development of atherosclerosis in mice--brief report. Arterioscler Thromb Vasc Biol. 2012;32:1573-1576.

183. Kyaw T, Tay C, Hosseini H, Kanellakis P, Gadowski T, MacKay F, Tipping P, Bobik A, Toh BH. Depletion of B2 but not B1a B cells in BAFF receptor-deficient ApoE mice attenuates atherosclerosis by potently ameliorating arterial inflammation. PLoS One. 2012;7:e29371.

184. Kyaw T, Cui P, Tay C, Kanellakis P, Hosseini H, Liu E, Rolink AG, Tipping P, Bobik A, Toh BH. BAFF receptor mAb treatment ameliorates development and progression of atherosclerosis in hyperlipidemic ApoE(-/-) mice. PLoS One. 2013;8:e60430.

185. Sage AP, Mallat Z. Multiple potential roles for B cells in atherosclerosis. Ann Med. 2014;46:297-303.

186. Pastrana JL, Sha X, Virtue A, Mai J, Cueto R, Lee IA, Wang H, Yang XF. Regulatory T cells and Atherosclerosis. J Clin Exp Cardiolog. 2012;2012:2.

187. Lutgens E, Lievens D, Beckers L, Wijnands E, Soehnlein O, Zernecke A, Seijkens T, Engel D, Cleutjens J, Keller AM, Naik SH, Boon L, Oufella HA, Mallat Z, Ahonen CL, Noelle RJ, de Winther MP, Daemen MJ, Biessen EA, Weber C. Deficient CD40-TRAF6 signaling in leukocytes prevents atherosclerosis by skewing the immune response toward an antiinflammatory profile. J Exp Med. 2010;207:391-404.

References

188. Li Q, Lu Q, Bottero V, Estepa G, Morrison L, Mercurio F, Verma IM. Enhanced NF-kappaB activation and cellular function in macrophages lacking IkappaB kinase 1 (IKK1). Proc Natl Acad Sci U S A. 2005;102:12425-12430.

189. Correa RG, Matsui T, Tergaonkar V, Rodriguez-Esteban C, Izpisua-Belmonte JC, Verma IM. Zebrafish IkappaB kinase 1 negatively regulates NF-kappaB activity. Curr Biol. 2005;15:1291-1295.

190. Miller YI, Choi SH, Fang L, Tsimikas S. Lipoprotein modification and macrophage uptake: role of pathologic cholesterol transport in atherogenesis. Subcell Biochem. 2010;51:229-251.

191. Karaflou M, Lambrinoudaki I, Christodoulakos G. Apoptosis in atherosclerosis: a mini-review. Mini Rev Med Chem. 2008;8:912-918.

192. Tabas I. Macrophage apoptosis in atherosclerosis: consequences on plaque progression and the role of endoplasmic reticulum stress. Antioxid Redox Signal. 2009;11:2333-2339.

193. Whitman SC. A practical approach to using mice in atherosclerosis research. Clin Biochem Rev. 2004;25:81-93.

194. Getz GS, Reardon CA. Animal models of atherosclerosis. Arterioscler Thromb Vasc Biol. 2012;32:1104-1115.

195. Baitsch D, Bock HH, Engel T, Telgmann R, Muller-Tidow C, Varga G, Bot M, Herz J, Robenek H, von Eckardstein A, Nofer JR. Apolipoprotein E induces antiinflammatory phenotype in macrophages. Arterioscler Thromb Vasc Biol. 2011;31:1160-1168.

196. Sen R, Smale ST. Selectivity of the NF-{kappa}B response. Cold Spring Harb Perspect Biol. 2010;2:a000257.

197. Penzo M, Molteni R, Suda T, Samaniego S, Raucci A, Habiel DM, Miller F, Jiang HP, Li J, Pardi R, Palumbo R, Olivotto E, Kew RR, Bianchi ME, Marcu KB. Inhibitor of NF-kappa B kinases alpha and beta are both essential for high mobility group box 1-mediated chemotaxis [corrected]. J Immunol. 2010;184:4497-4509.

198. Warboys CM, Amini N, de Luca A, Evans PC. The role of blood flow in determining the sites of atherosclerotic plaques. F1000 Med Rep. 2011;3:5.

199. Witting PK, Pettersson K, Letters J, Stocker R. Site-specific antiatherogenic effect of probucol in apolipoprotein E-deficient mice. Arterioscler Thromb Vasc Biol. 2000;20:E26-33.

200. Chew P, Yuen DY, Koh P, Stefanovic N, Febbraio MA, Kola I, Cooper ME, de Haan JB. Site-specific antiatherogenic effect of the antioxidant ebselen in the diabetic apolipoprotein E-deficient mouse. Arterioscler Thromb Vasc Biol. 2009;29:823-830.

201. Steinman DA. Image-based computational fluid dynamics: a new paradigm for monitoring hemodynamics and atherosclerosis. Curr Drug Targets Cardiovasc Haematol Disord. 2004;4:183-197.

202. VanderLaan PA, Reardon CA, Getz GS. Site specificity of atherosclerosis: site-selective responses to atherosclerotic modulators. Arterioscler Thromb Vasc Biol. 2004;24:12-22.

203. Bhullar IS, Li YS, Miao H, Zandi E, Kim M, Shyy JY, Chien S. Fluid shear stress activation of IkappaB kinase is integrin-dependent. J Biol Chem. 1998;273:30544-30549.

204. Illi B, Nanni S, Scopece A, Farsetti A, Biglioli P, Capogrossi MC, Gaetano C. Shear stress-mediated chromatin remodeling provides molecular basis for flow-dependent regulation of gene expression. Circ Res. 2003;93:155-161.

205. Li M, Tan Y, Stenmark KR, Tan W. High Pulsatility Flow Induces Acute Endothelial Inflammation through Overpolarizing Cells to Activate NF-kappaB. Cardiovasc Eng Technol. 2013;4:26-38.

206. Vogel C, Marcotte EM. Insights into the regulation of protein abundance from proteomic and transcriptomic analyses. Nat Rev Genet. 2012;13:227-232.

207. Back M, Gasser TC, Michel JB, Caligiuri G. Biomechanical factors in the biology of aortic wall and aortic valve diseases. Cardiovasc Res. 2013;99:232-241.

208. Hoffman GS, Calabrese LH. Vasculitis: determinants of disease patterns. Nat Rev Rheumatol. 2014;10:454-462.

209. McCall MN, Kent OA, Yu J, Fox-Talbot K, Zaiman AL, Halushka MK. MicroRNA profiling of diverse endothelial cell types. BMC Med Genomics. 2011;4:78.

210. Ma X, Becker Buscaglia LE, Barker JR, Li Y. MicroRNAs in NF-kappaB signaling. J Mol Cell Biol. 2011;3:159-166.

211. Li T, Morgan MJ, Choksi S, Zhang Y, Kim YS, Liu ZG. MicroRNAs modulate the noncanonical transcription factor NF-kappaB pathway by regulating expression of the kinase IKKalpha during macrophage differentiation. Nat Immunol. 2010;11:799-805.

212. Brooks AR, Lelkes PI, Rubanyi GM. Gene expression profiling of human aortic endothelial cells exposed to disturbed flow and steady laminar flow. Physiol Genomics. 2002;9:27-41.

213. Lawrence T. The nuclear factor NF-kappaB pathway in inflammation. Cold Spring Harb Perspect Biol. 2009;1:a001651.

214. Zernecke A, Shagdarsuren E, Weber C. Chemokines in atherosclerosis: an update. Arterioscler Thromb Vasc Biol. 2008;28:1897-1908.

215. Damas JK, Smith C, Oie E, Fevang B, Halvorsen B, Waehre T, Boullier A, Breland U, Yndestad A, Ovchinnikova O, Robertson AK, Sandberg WJ, Kjekshus J, Tasken K, Froland SS, Gullestad L, Hansson GK, Quehenberger O, Aukrust P. Enhanced expression of the homeostatic chemokines CCL19 and CCL21 in clinical and experimental atherosclerosis: possible pathogenic role in plaque destabilization. Arterioscler Thromb Vasc Biol. 2007;27:614-620.

216. Halvorsen B, Dahl TB, Smedbakken LM, Singh A, Michelsen AE, Skjelland M, Krohg-Sorensen K, Russell D, Hopken UE, Lipp M, Damas JK, Holm S, Yndestad A, Biessen EA, Aukrust P. Increased levels of CCR7 ligands in carotid atherosclerosis: different effects in macrophages and smooth muscle cells. Cardiovasc Res. 2013;102:148-156.

217. Cai W, Tao J, Zhang X, Tian X, Liu T, Feng X, Bai J, Yan C, Han Y. Contribution of homeostatic chemokines CCL19 and CCL21 and their receptor CCR7 to coronary artery disease. Arterioscler Thromb Vasc Biol. 2014;34:1933-1941.

218. Trogan E, Feig JE, Dogan S, Rothblat GH, Angeli V, Tacke F, Randolph GJ, Fisher EA. Gene expression changes in foam cells and the role of chemokine receptor CCR7 during atherosclerosis regression in ApoE-deficient mice. Proc Natl Acad Sci U S A. 2006;103:3781-3786.

219. Wan W, Lionakis MS, Liu Q, Roffe E, Murphy PM. Genetic deletion of chemokine receptor Ccr7 exacerbates atherogenesis in ApoE-deficient mice. Cardiovasc Res. 2013;97:580-588.

220. Reardon CA, Blachowicz L, Lukens J, Nissenbaum M, Getz GS. Genetic background selectively influences innominate artery atherosclerosis: immune system deficiency as a probe. Arterioscler Thromb Vasc Biol. 2003;23:1449-1454.

221. Paigen B, Morrow A, Holmes PA, Mitchell D, Williams RA. Quantitative assessment of atherosclerotic lesions in mice. Atherosclerosis. 1987;68:231-240.

References

222. Aird WC. Phenotypic heterogeneity of the endothelium: II. Representative vascular beds. Circ Res. 2007;100:174-190.

223. Bhasin M, Yuan L, Keskin DB, Otu HH, Libermann TA, Oettgen P. Bioinformatic identification and characterization of human endothelial cell-restricted genes. BMC Genomics. 2010;11:342.

9.   Appendix

125

Acknowledgements

Acknowledgements

Danke auch an meine Freunde außerhalb des Labors für Eure Unterstützung und Geduld. Danke an Helene für den Zuspruch, Motivation und unsere großartige, brillante Freundschaft. Ich bin sehr froh, dass es dich gibt. Robert- ein riesiges Dankeschön für Deine Unterstützung dieser Arbeit, für Deine Geduld mit mir und für die vielen freudigen und schönen Momente der letzten Jahre.

Last, but not least möchte ich einen herzlichen Dank an meine Eltern und meine Familie aussprechen. Ich danke meinen Eltern für den fortwährenden Rückhalt, das Vertrauen in mir und meinen Fähigkeiten, den Zuspruch und die Geduld mit mir. Ich danke meinen Bruder, dafür dass er mich stets in meinen Zielen bestärkt und immer an mich glaubt. Anita und Per danke ich ebenfalls für den unendlichen Beistand und für den Glauben an mich und meine Arbeit. Ich bin sehr dankbar, eine so wundervolle, unterstützende Familie zu haben.